Novel Applications of Chirp Managed Laser in Optical Fiber Communication Systems

JIA, Wei

A Thesis Submitted in Partial Fulfillment
of the Requirements for the Degree of
Doctor of Philosophy
in
Information Engineering

The Chinese University of Hong Kong
August 2013

Acknowledgment

During my childhood, I was always trying to capture the light with a bottle and release it again in the dark. The experimental results proved that the light was unwilling to cooperate with me.

However, many years later, I began to contact with Professor Calvin, Chun-Kit Chan to start postgraduate study in optical area. He instructed me that the character of self-motivation was important as a researcher in the first class. This saying contains a positive attitude towards academic career and has a great influence on me. Here I would like to express the deep gratitude to my supervisor Professor Chan. Thanks for your trust, guidance, and support.

I would also like to thank Professor Lian-Kuan Chen. I appreciate his continuous encouragement and enlightening discussion about my research. I also acknowledge Professor Chester Shu and Professor Chao Lu for kindly supporting experimental facilities.

As a PhD candidate, I am surrounded by equations, equipments, and experiments for most of the time. Sometimes you even need to test data in the midnight. Yet, it is lucky for me to be acquainted with a lot of friends in the lab. We share viewpoints, deal with problem and have fun together. It is such a wonderful life experience with you guys. Thanks for your tolerance, care and help. Besides, it is a pleasant surprise to encounter my girlfriend in this beautiful university. Thanks for your accompanying.

This thesis is dedicated to my family. It is the home where we get the original power to fight. My parents should never believe such a naughty boy would become a doctor, who even failed in the entrance exam of primary school. Thanks for your nurture these years.

Abstract

Nowadays, with the dramatically growing bandwidth requirement of Internet, the number of wavelength division multiplexing (WDM) channels of the optical fiber communication systems is increasing rapidly. Hence, optical transmitters with cost effectiveness, high power efficiency, and excellent transmission performance are necessary. Especially, for access and metropolitan applications, simple configuration is the essential factor. The conventional optical transmitter is composed of a laser as continuous-wave (CW) source and one or more external modulators for modulation. However, the high insertion loss, large driving voltage, and extra cost of external modulator make it relatively bulky and power-hungry.

Chirp managed laser (CML), comprising a directly modulated semiconductor laser (DML) and a passive optical filter, is an alternative promising transmitter candidate. It has the merits of smaller device size, lower cost, less power consumption, and higher fiber chromatic dispersion (CD) tolerance, compared with that based on external modulator. In this thesis, we have investigated several novel applications of CML in optical fiber communication systems, taking advantage of its unique phase modulating and spectral reshaping properties. These topics include optical return-to-zero (RZ) pulses generation using CML, *M*-ary RZ differential phase-shift-keying (RZ-DPSK) signals generation using CML, and enhanced CD tolerance of CML with pre-emphasis. These CML-based designs consume low power for less electrical pre-coding, require reduced or no external modulator, and show notable transmission performances.

Optical RZ pulses generation using CML: RZ pulses have been widely used in optical fiber communication systems together with on-off-keying (OOK) and DPSK modulation formats,

for its high robustness towards inter symbol interference (ISI) and nonlinear distortions. In this thesis, we propose and experimentally demonstrate the technique of 10-Gb/s optical RZ pulses generation using CML. No external modulator is used for pulse carving. The frequency of the sinusoidal driving signal is half the output RZ pulse rate. 70-km and 50-km error-free SSMF transmissions have been achieved for the 10-Gb/s 33%-duty-cycle and 67%-duty-cycle CML-RZ-pulses based RZ-DPSK signals, respectively. Later, we extend to demonstrate the scheme of 20-Gb/s RZ pulses generation using CML driven at one-fourth the output pulse rate and investigate the transmission performance of the 20-Gb/s CML-RZ-pulses based RZ-OOK signal.

***M*-ary RZ-DPSK signals generation using CML**: *M*-ary RZ-DPSK is an attractive modulation format in optical fiber long-haul transmission systems, due to the advantages of high receiver sensitivity, increased spectral efficiency, and strong robustness against fiber nonlinearities. In this thesis, we propose and experimentally demonstrate the techniques of RZ-DPSK, ¾-RZ-DQPSK, and RZ-DQPSK signals generation using CML. First, we generate the 10-Gb/s RZ-DPSK signal using CML and pulse carver. It does not require any differential encoder or phase modulator (PM). The CML-based RZ-DPSK signal shows 3-dB higher receiver sensitivity after 70-km SSMF transmission without dispersion compensation and comparable nonlinear tolerance performance, compared with that generated by PM. Next, this proposal is generalized to generate the 10-Gbaud RZ-DQPSK signal using CML and pulse carver. Compared with the complex pre-coding required for the MZM-based RZ-DQPSK transmitter, only a simple exclusive-or (XOR) encoder is needed for that based on CML. Later, we demonstrate the scheme of 10-Gbaud ¾-RZ-DQPSK signal generation using single CML, without the need for external pulse carver. In this new signal format, the symbols with a differential phase shift of 0 remain non-return-to-zero (NRZ), while those with differential phase shifts of 0.5π, π, and 1.5π are RZ.

Error-free transmission is realized over 60-km SSMF without optical signal-noise-ratio (OSNR) penalty. Finally, we demonstrate the technique of 10.709-Gbaud RZ-DQPSK signal generation using single CML, without the need for differential encoder, external modulator, or pulse carver. The full RZ-shape is orientated from the combined effect of the designated driving signal and the narrow-bandwidth filter in CML. It realizes 40-km SSMF transmission at bit-error-rate (BER) of 10^{-9}.

Enhanced CD tolerance of CML with pre-emphasis: For optical access and metropolitan networks, CML is a promising transmitter for its low cost, compact footprint, low power consumption, and high CD tolerance. In this thesis, we propose and experimentally realize the 10-Gb/s 300-km SSMF transmission at BER of 10^{-9} using CML with a simple and passive pre-emphasis driver. The 10-Gb/s standard CML signal without pre-emphasis can only be transmitted up to 220 km, in comparison. No expensive optical dispersion compensation module (DCM) or power-hungry electronic dispersion compensation (EDC) technique is used. Later, we further demonstrate the 20-Gb/s 100-km SSMF transmission at BER of 10^{-9}, using CML with pre-emphasis.

摘要

當今，隨著互聯網帶寬需求的急劇增長， 光纖通訊系統的波分複用信道數量正在快速增加。因此，具有良好成本效益、高功率效率和優秀傳輸性能的光發射機是極為必要的。特別是在接入網和城域網應用中，設備簡單化是必不可少的考量因素。傳統光發射機是由作為連續波的激光器和用於調製的外部調製器組成。然而，外部調製器的高插入損耗、大驅動電壓和額外成本使得傳統光發射機的體積較大和能耗較高。

啁啾管理激光器，包括一個直接調製的半導體激光器和一個無源光濾波器，是另外一種很有前途的發射機。與基於外部調製器的發射機相比，它具有較小設備尺寸，較低成本，較少能耗，和較高光纖色散容限的優點。在這篇論文中，我們利用啁啾管理激光器獨特的相位調製和频谱再整形特性，研究了其在光線通信系統中的一些創新應用。它们包括使用啁啾管理激光器产生光歸零碼脉衝、使用啁啾管理激光器产生 M 進制歸零差分相移鍵控信號和利用預加重提高啁啾管理激光器的色散容限。這些基於啁啾管理激光器的設計需要較少的預編碼故消耗較低的能量、需要较少或者不需要外部調製器，并展現出了矚目的傳輸性能。

使用啁啾管理激光器产生光歸零碼脉衝：歸零碼脉衝連同開關鍵控及差分相移鍵控調製格式，由於其良好的抗碼間串擾和抗非線性損傷的特性，已經被廣泛應用於光纖通信系統。在這篇論文中，我們提出并展示了利用啁啾管理激光器產生 10-Gb/s 光歸零碼脉衝的技術。沒有外部調製器用來做脉衝雕刻。正弦驅動信號的頻率是輸出歸零脉衝速率的一

半。10-Gb/s 具有 33% 占空比和 67% 占空比的基於啁啾管理激光器歸零脉衝的歸零差分相移鍵控信號，分別實現了 70 公里和 50 公里標準單模光纖的無誤碼傳輸。隨後，我們進一步展示了使用被四分之一輸出脉衝速率驅動的啁啾管理激光器產生 20-Gb/s 歸零碼脉的方案，并研究了 20-Gb/s 基於啁啾管理激光器歸零脉衝的歸零開關鍵控信號的傳輸性能。

使用啁啾管理激光器产生 *M* 進制歸零差分相移鍵控信號：*M* 進制歸零差分相移鍵控，由於其高接收靈敏度、高頻譜效率和強光纖非線性魯棒性的優勢，在光纖長途傳輸系統中是一種很有吸引力的調製格式。在這篇論文中，我們提出并展示了利用啁啾管理激光器產生歸零差分相移鍵控、四分之三歸零差分正交相移鍵控和歸零差分正交相移鍵控信號的產生技術。首先，我們利用啁啾管理激光器和脉衝雕刻器產生了 10-Gb/s 歸零差分相移鍵控信號。這個方案不需要任何差分編碼器或者相位調製器。與相位調製器產生的信號相比，基於啁啾管理激光器的歸零差分相移鍵控信號，經過 70 公里無色散補償的標準單模光纖傳輸，表現了高出 3-dB 的接收靈敏度和具有可比性的非線性容限性能。緊接著，這個方案被拓展至利用啁啾管理激光器和脉衝雕刻器產生 10-Gbaud 歸零正交相移鍵控信號。與基於馬赫曾德調製器的歸零正交相移鍵控信號發射機複雜的預編碼相比，基於啁啾管理激光器的發射機只需要一個簡單的異或編碼器。後來，我們展示了利用單一啁啾管理激光器產生 10-Gbaud 四分之三歸零差分相移鍵控信號的方案，並且不需要外部脉衝雕刻器。在這個新的信號碼型里，無差分相移的符號保持非歸零碼，而那些具有 0.5π、π 和 1.5π 差分相移的符號為歸零碼。在沒有光信噪比損傷的情況下，這種信號實現了 60 公里的標準單模光纖無誤碼傳輸。最後，我們展示了利用單一啁啾管理激光器產生 10.709-Gbaud 歸零差分相移鍵控信號的技術，並且不需要差分編碼器、外部調製器及脉衝雕刻器。這種完整

的歸零碼形態來源于特定的驅動信號和啁啾管理激光器內的窄帶濾波器的綜合效應。這種信號在具有 10^{-9} 誤碼率的情況下，實現了 40 公里標準單模光纖的傳輸。

利用預加重提高啁啾管理激光器的色散容限：對於光接入網和局域網而言，直接調製的啁啾管理激光器，由於成本低、體積緊湊、能耗小和色散容限高，是一種很有潛力的發射機。在這篇論文中，我們提出利用具有一個簡單無源預加重驅動器的啁啾管理激光器，通過實驗實現了 10-Gb/s 300 公里具有 10^{-9} 誤碼率的標准單模光纖傳輸。作為對照，10-Gb/s 無預加重的標準啁啾管理激光器信號只能傳輸 220 公里。系統沒有使用昂貴的光色散補償模塊和高能耗的電色散補償技術。隨後，我們利用具有預加重的啁啾管理激光器，進一步展示了 20-Gb/s 100 公里具有 10^{-9} 誤碼率的標準單模光纖傳輸。

Table of Contents

List of figures and tables

Chapter 1 Introduction

1.1 Optical fiber communication systems

Communication is the basic need of human beings. Everyone wants to deliver emotion, viewpoint and information to others and gets response. It makes us connected. This instinct of human beings has given birth to many kinds of great communication inventions such as language, letter, and telegraph. Optical fiber communication technique is one of the most shining stars among them. We will review its origin and development in this section.

1.1.1 Origin

The light used for communication can be traced back to the beacon towers on the Great Wall, which were applied specifically for transmitting military information about two thousand years ago. The whole system had already contained the basic optical transmission concepts including fire and smoke as transmitter, “on and off” as signal format, atmosphere as transmission medium, tower as repeater, and human eye as receiver.

Nevertheless, light was not considered as an efficient tool to transfer massive information, until in 1960s Dr. A. Javan introduced the first steady helium-neon laser to convert electrical energy to laser light output and Dr. K. Kao discovered that the huge light loss in glass arose from the impurities in material which could be removed. Their innovative demonstrations were recognized as the two essential milestones for the development of fiber optic communication

systems. With their work kept as a reference, research activities expanded and a new industry was born, leading to the production of the most advanced cabling solutions that are in use today as a commodity [1].

To this day, optical fiber transmission systems have been deployed widely around the world to take the place of copper wire communications for the advantages of higher bandwidth, lower cost, longer spanning distance, and so on. They have revolutionized the telecommunication industry with the efforts of numerous scientists and engineers and brought people into the Information Age. They are greatly promoting the advance of human civilization by changing the state of economy, military, and politics in society. However, the whole evolution process of fiber optical communication systems is not always plain sailing, with the unprecedented information capacity as a double-edged sword.

1.1.2 System capacity and traffic demand

In 1970, Corning Corporation developed the optical fiber successfully with attenuation of 20 dB/km, low enough for communication purpose. Meanwhile, the compact GaAs semiconductor laser was developed and therefore suitable for transmitting light through optical fiber to long distance. These achievements paved the way for the operation of commercial optical fiber transmission systems.

After a period of research starting around 1975, the first generation of optical fiber communication system was developed and operated at the wavelength of 0.8 μm and the bit rate of 45 Mb/s, with the repeater spacing of 10 km [2]. By 1987, the second generation commercial

lightwave system was built up on the single mode fiber (SMF) and operated in the wavelength region near 1.3 μm, where the fiber loss was below 1 dB/km and exhibited the minimum dispersion. It could support the bit rate of 1.7 Gb/s and the repeater spacing of 50 km. In 1990, the technology development made the third generation of commercially available fiber optic communication system to be operated at the data rate of 2.5 Gb/s and the wavelength of 1.5 μm, where the fiber loss is minimum, with the repeater spacing in excess of 100 km. Until that time, the fiber optic techniques showed a steady development and brought a slow increase of bit rate in the single channel.

However, the use of wavelength division multiplexing (WDM) technique enabled the capacity of the fourth generation lightwave system to expand rapidly, increasing from a few gigabits per second to several terabits per second in 1990s. Fig. 1.1 shows the capacity of optical fiber communication systems and the total network traffic in North America by year over the period from 1985 through 2008 and some forecasts through 2020 [3]. The points on the figure are the total capacities of a single optical fiber for both the commercial systems and the research demonstrations. The black square points represent the capacity of time division multiplexing (TDM) technology in the laboratory. The purple diamond points represent the capacity of TDM technology in the market. The red round points represent the capacity of WDM technology in the laboratory. The blue triangular points represent the capacity of WDM technology in the market. The solid brown line extrapolates the commercial system capacity in a single optical fiber using the progress rate of research system. The solid green line denotes the total North American network traffic. The latest forecasted global Internet traffic in 2013 is 21.4 Tb/s and will grow twofold by 2017, to reach 46.5 Tb/s [4].

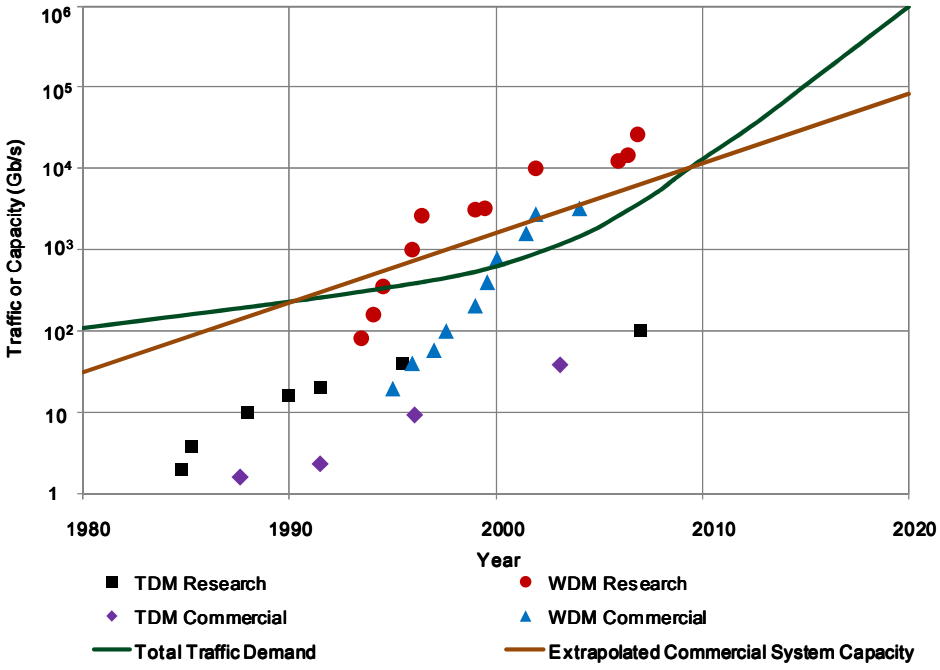

Fig. 1.1 Capacity of optical fiber communication systems and total North American network traffic by year [3]

There was an initial fast increment of capacity in single channel TDM laboratory demonstrations. It began to saturate when the optical system speed became limited by the bottleneck of electronic components. In 1993, another sharp rise in capacity appeared with the application of WDM enabled by optical amplifiers, dispersion management technology, and gain equalization approach. It started a revolution that resulted in doubling the system capacity every half year or so. When the C band wavelength window of 1.53-1.57 μm was nearly filled with multiple channels in 1996, the first 1 Tb/s experiments were reported [5]-[6]. The present highest field capacity is 54.2 Tb/s, with a spectral efficiency of 6.6 b/s/Hz, by tightly packing the optical channels in C band and L band [7].

By 2000, the dramatic increase in the system capacity brought by the technological revolutions attracted a lot of investments from various vendors, which strongly stimulated the

network service providers to lay down large scale of fiber infrastructure. However, a severe market shrink and a significant investment diminution to build new system happened in the following years. The optical fiber communication industry slid from prosperity to depression. There are many interpretations for this bubble burst at the beginning of millennium. The imbalance between system capacity supply and traffic demand should be the main reason. It is clearly shown in Fig. 1.1 that the capacity of single fiber commercial system exceeded the total network traffic in 2000. It means that a system could carry the whole network traffic on one link. Then the need for the network service providers to deploy additional new systems disappeared. Actually, even for now, there is no light running in part of fiber systems laid during that decade.

This lesson tells the related scientists, engineers, customers, and network service providers that the optical fiber communication industry also follows the universal economic law of market, though its underlying techniques are fantastic and amazing. The traffic demand of human beings promotes the birth and development of optical fiber communication techniques. At the same time, the expansion of system capacity enabled by lightwave techniques supports human beings to pursue more plentiful information applications. Compared with the continuously enhancing speed of traffic demand, the technologies sometimes move faster or slower, but they will be in the dynamic equilibrium in the long run.

At present, 13 years have passed after the bubble burst in the optical communication industry. The fiber optic market is gradually recovering with numerous unexampled Internet applications and intelligent electronic devices including Internet social network, video conference, real-time interactive game, smart phone, three-dimensional television, and others. These emerging services steer and greatly boost the traffic need of human beings. In 2013, the

forecasted global Internet traffic [4] is approaching the reported highest field capacity [7]. In the near future, when the old lightwave systems are filled up with the data streams, the network service providers have to choose whether to deploy extra new systems or add more WDM channels with narrower grid and extended band. The increasing cost for infrastructure and consequently higher price for Internet service may level off or even depress the demand for data traffic, whatever the choice is. Also, the added systems and channels will consume huge power. Thus, though the high capacity and reliable transmission performance are the primary goals for the design of next generation of optical fiber communication system, the footprint, cost, and power consumption for each bit are sensitive and important parameters to be considered.

1.2 Transmission impairments and mitigation

Various impairments of fiber can bring serious signal degradation and significantly limit the performance of photonic system, when the designer would like to improve the total capacity and transmission distance. We will briefly present several key impairments in standard single mode fiber (SSMF), including chromatic dispersion (CD), polarization mode dispersion (PMD), and nonlinearity. Conceptually, they could be classified as linear or nonlinear effects. Besides fiber, a lot of noises will be produced when the optical signal is generated, amplified and detected in the fiber optic transmission system. These noises will also induce impairments to the transmit signal. Several main optical and electrical impairment-mitigation techniques are also described, among which advanced modulation formats play a key role.

1.2.1 Chromatic dispersion

CD is a serious issue when the optical link is operated at 10 Gb/s and beyond. The underlying physical phenomenon of CD is that the group velocity associated with the fundamental mode is frequency dependent. This means that different frequency components of an optical pulse travel at different velocities, leading to the spreading of the pulse [8].

The field distribution of the fundamental fiber mode can be approximated by a Gaussian distribution [2]. Different spectral components of an optical pulse propagate inside the fiber according to a simple relation of

$$A(z,\omega) = A(0,\omega)e^{\frac{i(\omega-\omega_0)^2\beta_2 z}{2}} \tag{1.1}$$

Where $A(z,\omega)$ and $A(0,\omega)$ are the spectral amplitudes of the optical output and input signals. ω_0 is the carrier's central frequency. β_2 is the group velocity dispersion (GVD) coefficient, which determines how much an optical pulse would broaden on propagation inside the fiber. z is the transmission fiber distance. CD is commonly characterized by the dispersion parameter D=-2 $\pi c\beta_2/\lambda^2$ expressed in units of ps/(km-nm).The extent of pulse broadening due to CD with a fiber length L is governed by

$$\Delta T = DL\Delta\lambda \tag{1.2}$$

where $\Delta\lambda$ represents the wavelength width of the pulse. The dispersed pulses broaden into the adjacent bits, causing errors at the receiver. The effect of dispersion on the bit rate B can be estimated by using the criterion of

$$B|D|L\Delta\lambda < 1 \tag{1.3}$$

Several optical techniques have been proposed to manage CD. The use of lasers in the wavelength region around 1310 nm can minimize the CD. However, the current fiber optic transmission systems prefer to employ lasers in 1550 nm region, where the fiber attenuation reaches a minimum. Dispersion compensating fiber (DCF) is an all-optical and fiber-based scheme to compensate CD [9]-[10]. Compared with SSMF, it has an opposite slope of delay versus wavelength curves at 1550 nm. Accurate length of DCF must be chosen to completely compensate fiber GVD. Since the GVD affects the optical signal through the spectral phase of $e^{\frac{i(\omega-\omega_0)^2\beta_2 z}{2}}$, an optical filter which has similar but reverse transfer function can also partially restore the original signal [11]. Generally, optical dispersion compensation (ODC) techniques will bring extra insertion loss and cost to the fiber link.

Electronic pre-distortion at the transmitter and post-compensation at the receiver are other more adaptive methods for CD compensation in electrical domain. Electronic pre-distortion technique requires the precise knowledge of the transmitter and fiber link. Together with the feedback information from the receiver, it could calculate and generate the pre-distorted real and imaginary parts of the optical signal to remove GVD, by multiplying the desired received signal spectrum and spectral phase $e^{\frac{-i(\omega-\omega_0)^2\beta_2 z}{2}}$ [12]. Electronic post-compensation techniques such as feedforward equalization (FFE), decision feedback equalization (DFE), and maximum likelihood sequence estimation (MLSE) can increase the CD tolerance by a factor of two or so in direct detection system [13]. Since coherent detection can retrieve both the optical intensity and phase information of the received signal, the following electronic dispersion compensation (EDC) is able to greatly mitigate the accumulated CD in the long haul transmission link [14]. However, EDC techniques typically depend on fast digital signal processing (DSP) technology and will

increase power consumption heavily.

Generation of advanced modulation formats at the transmitter is another attractive way to enhance the CD tolerance. Optical duobinary signal with special phase relation between bits and more compact spectrum had realized 252-km uncompensated SSMF transmission at 10 Gb/s, leading to a reach improvement by a factor of 3, compared with the conventional non-return-to-zero (NRZ) on-off-keying (OOK) signal [15]-[16]. High spectral-efficient modulation formats including differential quadrature phase-shift-keying (DQPSK) and quadrature amplitude modulation (QAM) had demonstrated increased tolerance to CD due to the reduced symbol rate [17]-[18]. The main drawback of these advanced modulation formats is the enhanced complexity of transceiver. Complicated electronic pre-coders and more external modulators are required at the transmitter, imposing heavy burden of cost and power on the system. Moreover, self-coherent or local-oscillator (LO) based coherent detection is necessary at the receiver for DQPSK and QAM signals.

1.2.2 Polarization mode dispersion

Fiber birefringence is another potential source to induce pulse broadening. Small departures from perfect cylindrical symmetry lead to birefringence because of different mode indices associated with the orthogonally polarized components of the fundamental fiber mode. If the input pulse excites both polarization components, it becomes broader as the two components disperse along the fiber because of their different group velocities. This phenomenon is called PMD [2]. One of the intrinsic causes of PMD is due to the asymmetry of the fiber core. The other causes are derived from fiber deformation, including stress applied on the fiber, fiber aging, variation of

temperature over time, or effects from a vibration source. These processes randomly result in the dynamic of PMD [8].

The polarization state of light propagating in fibers with randomly varying birefringence would change stochastically along the fiber during propagation. The polarization state will also be unequal for different spectral components of the optical pulse. Since the statistical nature of PMD, it is complex to build up the analytical model. After averaging over random birefringence changes, the approximated differential group delay (DGD) between two principal orthogonal states of polarization (PSPs) is characterized by

$$\sigma_T = D_p\sqrt{L} \tag{1.4}$$

where σ_T is the root-mean-square (RMS) value of DGD. D_p is the PMD parameter measured in $\mathrm{ps}/\sqrt{\mathrm{km}}$. L is the fiber length. PMD induces relatively smaller pulse broadening than CD. However, it will become a serious issue and limiting factor for ultra-long haul optical transmission at 10-Gb/s or higher bit rate.

Several optical and electronic adaptive techniques have been developed for PDM compensation. A delay line can be used for an optical PMD compensator [19]. The PMD-distorted signal is separated into two waveforms polarized along the two PSPs using a polarization controller (PC) followed by a polarization beam splitter. The two components are combined after removing their delay through a variable delay line in one branch. Electronic compensation methods including FFE, DFE and MLSE can also help to mitigate PMD distortions [20]-[21]. A single PMD compensator cannot be used for all WDM channels. Rather, a separate PMD compensator is required for each channel. This problem makes these PMD

compensation techniques expensive for WDM system [2].

From the modulation format point of view, we can choose signals robust to PMD. Return-to-zero (RZ) pulses based OOK signals show superior PMD tolerance than those using NRZ format [22]. The main reason is that the energy is confined in the center of each bit-slot in the RZ case and that more DGD is required before the energy leaks out of the bit-slot to result in inter symbol interference (ISI). Under reasonable conditions, the RZ pulses with shorter duty cycle (the ratio of full-width at half maximum to bit duration) have better performance [23]. Studies further demonstrated differential binary phase-shift-keying (DBPSK, or simply DPSK) signals always have smaller PMD penalties than OOK signals with the same duty cycle. Especially, RZ-DPSK signals with duty cycles of 33% and 67% perform better than that with duty cycle of 50% [24]. The 67%-duty-cycle RZ pulse is also named as carrier-suppressed RZ (CSRZ) pulse. Similar to CD compensation, advanced multilevel formats such as DQPSK, characterized by a larger number of bits per-symbol at lower symbol rate, show narrower optical spectrum and higher PMD robustness with respect to binary modulation at the same bit rate [25].

1.2.3 Nonlinearity

The response of any dielectric to light becomes nonlinear for intense electromagnetic fields, and optical fiber is no exception. On a fundamental level, the origin of non-linear response is related to aharmonic motion of bound electrons under the influence of an applied field [26]. Fiber nonlinearities are classified by two categories depending on whether there is energy exchange between the electromagnetic field and the dielectric medium.

The first one originates from the third-order susceptibility without energy exchange between the electromagnetic field and the dielectric medium. The third-order susceptibility is responsible for phenomena such as third-harmonic generation, four-wave mixing (FWM), and nonlinear refraction. If the phase matching condition is achieved, the third-harmonic generation and FWM will generate new frequency components. The nonlinear effects including self-phase modulation (SPM) and cross-phase modulation (XPM) is induced by nonlinear refraction, a phenomenon referring to the intensity dependence of the refractive index. SPM refers to the self-induced phase shift experienced by an optical field during propagation. XPM means the nonlinear phase shift of an optical field induced by another one with different wavelength, direction, or polarization state. Both SPM and XPM effects will lead to the spectral broadening of propagating optical pulses.

The second one results from stimulated inelastic scattering in which the optical field transfers part of its energy to the nonlinear medium, including stimulated Raman scattering (SRS) and stimulated Brillouin scattering (SBS). SRS can transfer a small fraction of power from one optical field to another field, whose frequency is downshifted by an amount determined by the vibrational modes of the optical fiber. SBS is another nonlinear process that can occur in optical fibers at input power levels much lower than those needed for SRS. The downshifted wave propagates backward for SBS, in contrast to SRS that can occur in both directions. Their differences stem from a fundamental distinctive, which is acoustical phonons participate in SBS whereas optical phonons are involved in SRS.

These nonlinear effects in fiber can be beneficially used for optical amplifiers, lasers, all-optical regenerators, and wavelength converters. However, FWM will generate new frequency

components, inducing crosstalk to WDM system. SPM and XPM will broaden spectrum, creating signal distortion and increasing CD penalty. SBS and SRS will induce power transferring, limiting the input signal power to the fiber. Specifically, if the number of WDM channels is increased or the channel spacing is decreased to improve the fiber capacity, the nonlinear penalties will be higher.

There are several methods to mitigate nonlinear distortions. Optical techniques of managing fiber dispersion [27]-[29], polarization interleaving [30]-[31], optical phase conjugation [32]-[33], and nonlinear post processing [34]-[35] have been investigated to reduce nonlinear effects. Digital post compensation [36] and digital backward propagation [37] are the other useful electrical ways to remove nonlinear impairments, together with coherent detection to access the complete electric field of signal. In respect of modulation techniques, DPSK signal exhibits constant power flow, diminishing nonlinear effects [38]-[40]. Alternate-mark inversion (AMI) is another kind of nonlinearity tolerant signal format [41]. Furthermore, RZ pulse shape, particular for CSRZ, with less optical peak power, shows higher robustness towards nonlinearity than NRZ [42]-[44]. Therefore, RZ-DPSK, RZ-DQPSK, and RZ-AMI modulation formats are always used to enhance the fiber nonlinearity tolerance of WDM system, together with other optical and electrical compensation techniques.

1.2.4 Noise

In addition to the impairments from fiber, there are many noise sources in the optical transmission system. The noises basically originate from the transmitter containing laser intensity and phase noises, the optical amplifier induced amplified spontaneous emission (ASE)

noise, and two kinds of noises at the receiver composed of shot noise and thermal noise.

The optical amplifier such as erbium-doped fiber amplifier (EDFA) degrades the optical signal-to-noise ratio (OSNR) of the amplified signal because of spontaneous emission that adds noise to the signal during its amplification [2]. The spectral density of ASE noise is nearly constant (white noise) and expressed by

$$S_{sp}(v) = (G-1)n_{sp}hv \tag{1.5}$$

where v is the optical frequency. G is the gain. n_{sp} is the spontaneous-emission factor. h is the Planck constant. The beating of ASE with the signal produces noise current at the receiver.

The shot noise and thermal noise are the two fundamental noise mechanisms responsible for current fluctuations in all optical receivers even when the incident optical power is constant [2]. Shot noise is a manifestation of the fact that an electric current consists of a stream of electrons that are generated at random times. It has its origin in the particle nature of electrons. Thermal noise is due to the electrons moving randomly in any conductor at a finite temperature. Random thermal motion of electrons in a resistor manifests as a fluctuating current even in the absence of an applied voltage. The load resistor in the front end of an optical receiver adds such fluctuations to the current generated by the photo-detector (PD).

The various noises will corrupt the signal received and degrade the OSNR. The OSNR determines the receiver sensitivity defined as the minimum average optical power required to realize a fixed bit-error-rate (BER). Signal formats play an important role in the OSNR and receiver sensitivity requirements of the noise-limited transmission system. The RZ formats in general require 1-3 dB less OSNR for identical BER than the NRZ equivalents, due to the

reduced ISI impact [45]-[46]. OSNR requirement can be significantly reduced when DPSK is used. The receiver sensitivity improvement of DPSK over OOK is around 3 dB. Therefore, RZ-DPSK is the most sensitive modulation format known today [47]. DQPSK requires 1-1.5 dB higher OSNR than DPSK at BER of 10^{-3}, due to the more closed constellation space [48].

1.3 Modulation techniques

Since advanced modulation formats such as optical RZ pulses, duobinary, AMI, RZ-DPSK and RZ-DQPSK provide a lot of benefits to reduce the fiber impairments and noise distortions in optical fiber transmission systems, we will review their generation using traditional transmitter and detection in this section.

1.3.1 Transmitters

In SSMF, there are three physical attributes in optical field that can be used to carry information, comprising intensity, phase, and polarization. As a degree of freedom, orthogonal polarization multiplexing is able to double the system capacity, with the advent of coherent receiver. However, due to random polarization change of fiber, polarization shift keying (Pol-SK) format is rarely used. But modulation formats using intensity and phase to encode information are popular. To convert the electronic data onto light, optical transmitters using directly modulated laser (DML), electro-absorption modulator (EAM), Mach-Zehnder modulator (MZM) are necessary components.

Direct modulation of distributed-feedback (DFB) or distributed-Bragg-reflector (DBR) semiconductor laser is the simplest way to impose information on optical carrier. The laser driving current is modulated with the data, generating the intensity modulated binary OOK signal, as shown in Fig. 1.2. Usually, the bias is set near the threshold for large extinction ratio (ER). DML is compact, cost-effective, power-efficient, and suitable for dense integration in small form factor pluggable (XFP) transponder. The modulation speed of DML can reach 40 Gb/s [49]. The main problem of DML operating at high speed for long reach transmission is that two kinds of residual chirp will broaden the signal spectrum and increase CD distortion. Chirp which occurs at bit transitions is known as transient chirp, while chirp that causes mark bits to blue-shift relative to space bits is referred to as adiabatic chirp. Transient chirp makes the leading edge of the pulse to advance over the main body, and adiabatic chirp induces signal compression [50]. The SSMF transmission distance of 10-Gb/s DML signal is usually less than 10 km. Besides, there is rare experimental report on DML to generate the above mentioned advanced modulation formats, since its intensity and phase modulating properties are not easy to be decoupled.

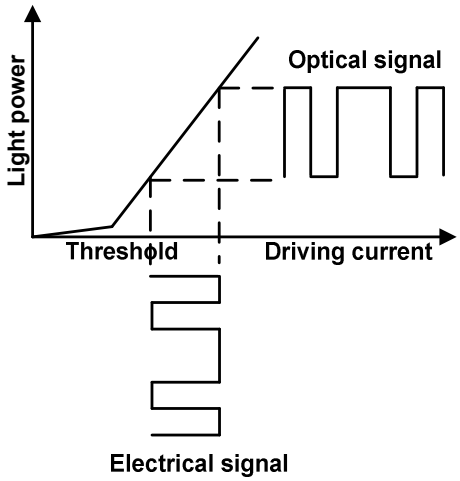

Fig. 1.2 Transmission function of DML

EAM makes use of the Franz-Keldysh effect, according to which the band-gap of a semiconductor decreases when an electric field is applied across it [2]. Thus, a transparent semiconductor layer begins to absorb light when its band-gap is reduced electronically by applying an external voltage. The typical attenuation characteristic of EAM as a function of driving voltage is shown in Fig. 1.3 [51]. The EAM can exhibit a modulation speed of 80 Gb/s [52]. An advantage of EAM is that it is made of the same semiconductor material that is used for laser, and thus the two can be easily integrated on the same chip to form the electro-absorption modulated laser (EML). However, it will also generate some residual chirp like DML. The fiber-to-fiber insertion loss of EAM is about 10 dB. The typical output power of EML is around 0 dBm. More important, it has wavelength-dependent absorption characteristic, which makes it hard to cover all WDM wavelengths with good performance.

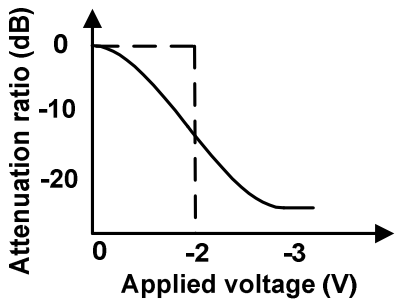

Fig. 1.3 Attenuation characteristic of EAM [51]

MZM works by the principle of interference, controlled by modulating the optical phase [48]. The transmission function and modulator structure are shown in Fig. 1.4. The incoming light is split into two paths by an input coupler. Both paths are equipped with phase modulators (PMs) that let the two optical fields acquire some phase difference relative to each other,

controlled by the applied phase modulation voltages V_1 and V_2. Finally, the two fields interfere at an output coupler. Depending on the applied electrical voltage, the interference varies from destructive to constructive, thereby producing the intensity modulation.

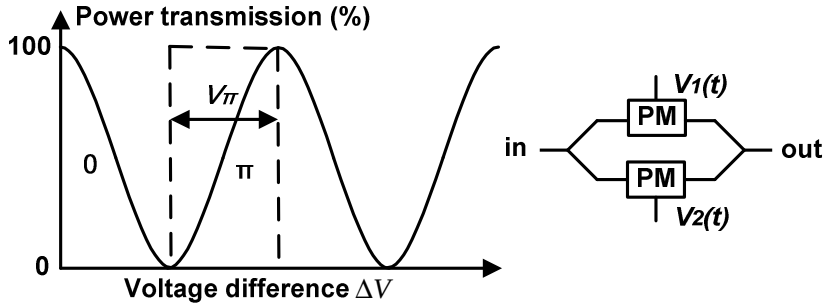

Fig. 1.4 Transmission function and structure of MZM [48]

The optical field transfer function $T_E\ (V_1, V_2)$ of the MZM is governed by

$$T_E\ (V_1, V_2) = \frac{1}{2}\left\{e^{i\phi(V_1)} + e^{i\phi(V_2)+i\psi}\right\}$$

$$= e^{\frac{i(\phi(V_1)+\phi(V_1)+\psi)}{2}} \cos\left[\frac{\phi(V_1)-\phi(V_1)}{2} - \frac{\psi}{2}\right] \quad (1.6)$$

where $\phi(V_1)$ and $\phi(V_2)$ are the voltage-modulated optical phases of the two MZM arms, and ψ is an additional, temporally constant phase shift in one of the arms, referred to as the modulator bias. Since the phase modulation depends linearly on the driving voltage for most materials used for MZM such as $LiNbO_3$, its power transfer function depends only on the driving voltage difference between the two arms ΔV. The driving voltage required to change the phase difference between the two arms by π, thereby letting MZM switch from full transmission to full extinction, is called switching voltage V_π. If MZM is symmetrically driven around zero transmission, it will produce π phase jumps at the expense of residual intensity dips and result in phase modulation.

$LiNbO_3$-based MZM features the characteristics of wavelength-independent modulation and high ER performance. Several combined MZMs can also realize independent intensity and phase modulating of the optical field, which forms the basis of many advanced modulation formats. Today, MZM is widely available for modulation up to 40 Gb/s. However, MZM has significant insertion loss (> 7 dB) and large length (> 44 mm), requiring high driving voltage (V_π > 3.5 V). It brings extra footprint, cost, and power consumption to the optical transmitter. Usually, more than one MZM and complex electronic pre-coder are needed to generate the above mentioned advanced modulation formats.

1.3.2 Optical RZ pulses

RZ shape is commonly formed by carving pulses out of continuous-wave (CW) light using MZM driven by clock, named pulse carver, as shown in Fig. 1.5. Then the data are printed on the optical RZ pulses using another MZM or PM to generate the RZ-OOK or RZ-DPSK signals.

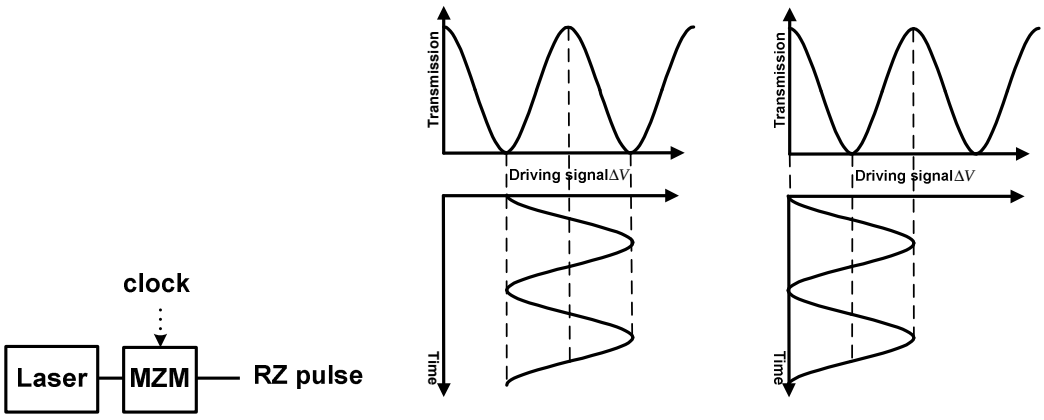

(a) Structure (b) 33% RZ pulses (c) 67% RZ pulses

Fig. 1.5 Structure and operation principle of RZ pulses generator using MZM

When the MZM is sinusoidally driven at the pulse rate between the minimum and maximum transmission, it results in RZ pulses with a duty cycle of 50%. When the MZM is sinusoidally driven at the half pulse rate between the transmission minima, it produces RZ pulses with a duty cycle of 33%. When the MZM is sinusoidally driven at the half pulse rate between the transmission maxima, it generates RZ pulses with a duty cycle of 67%. For the 67%-duty-cycle RZ pulses, the carrier at the optical center frequency vanishes due to the alternating phases for the adjacent pulses, giving the name CSRZ.

There are other schemes to generate optical RZ pulses. An alternative method is based on an optical PM followed by an optical delay interferometer (DI) [53]. Mode-locked laser using EAM as a mode locker is another candidate [54]. However, all the schemes require external modulator.

1.3.3 Duobinary and AMI

Optical duobinary and AMI belong to the general class of correlative coding format, a subclass of which being referred to as partial response signaling [48]. Correlative coding introduces a distinct correlation between the optical phase and the data information. A π phase change occurs whenever there is odd number of 0 bits between two successive 1 bits for duobinary, whereas for AMI, the π phase change for each 1 bit is independent of the number of 0 bits in between.

The reason of high tolerance to CD for duobinary can be explained using “101” bit pattern. The dispersed two 1 bit pulses spread into the 0 bit time slot between them, leading to destructive interference due to the opposite phase. The structure and operation principle of one common duobinary transmitter using MZM are shown Fig. 1.6 [55]-[56].

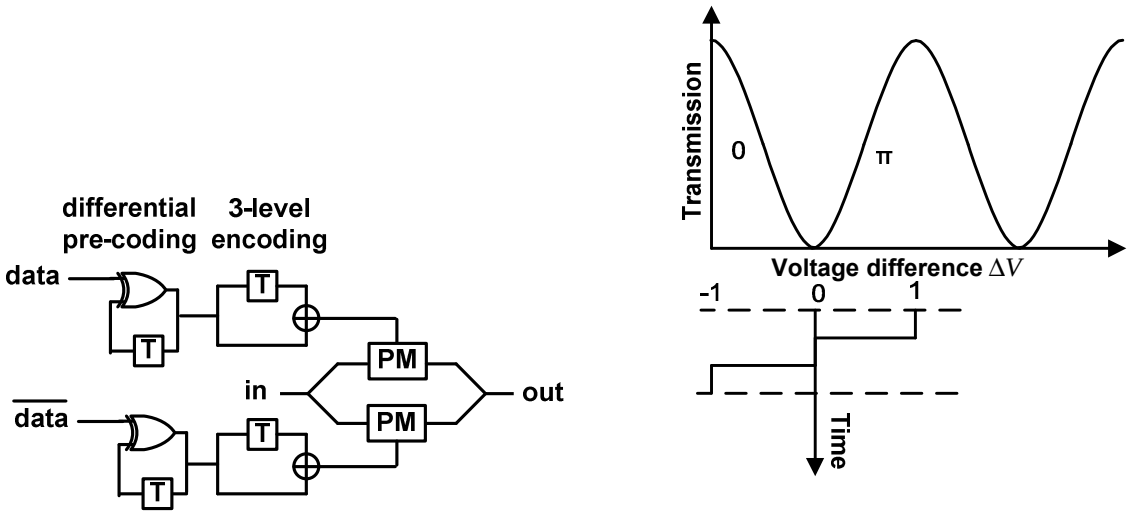

(a) Structure (b) Operation principle

Fig. 1.6 Structure and operation principle of duobinary transmitter using MZM [55]-[56]

Duobinary transmitter uses the differentially pre-coded non-inverting data and inverting data as the inputs. Then the two pre-coded data streams are converted into two three-level electrical signals by means of delay-and-add operation or low-pass filter. The two three-level electrical signals are then used to drive the MZM for push-pull operation between its transmission maxima to produce the optical duobinary signal.

One typical AMI transmitter implementation is identical to the duobinary transmitter in Fig. 1.6, except that it uses an electrical delay-and-subtract circuit or high-pass-filter [48]. The data modulator is usually followed by a pulse carver to obtain RZ-AMI signal.

1.3.4 RZ-DPSK and RZ-DQPSK

In the DPSK format, optical power appears in each bit slot, with the binary data encoded as

either 0 or π optical phase shift between adjacent bits. The optical power in each bit can occupy the entire bit slot (NRZ-DPSK) or can appear as an optical pulse (RZ-DPSK) [57]. One commonly used RZ-DPSK transmitter setup is shown in Fig. 1.7.

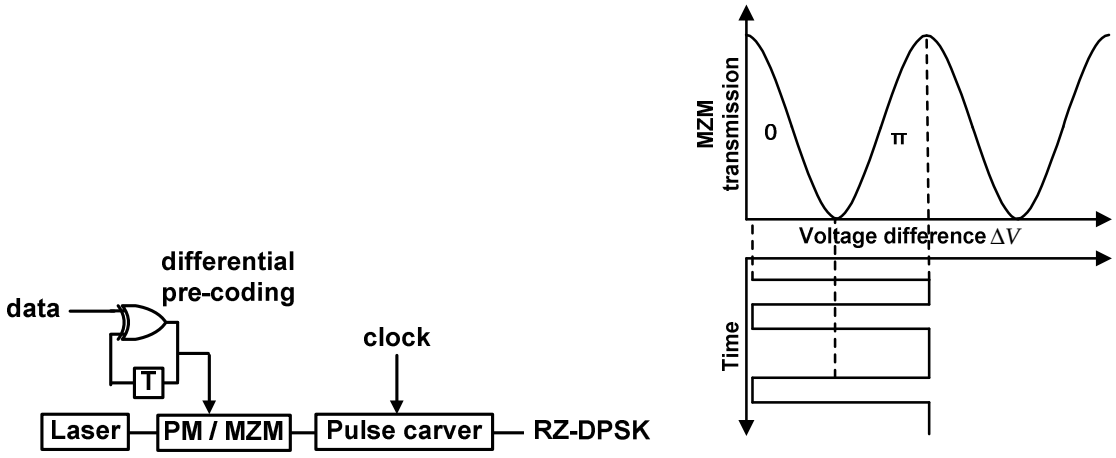

(a) Structure (b) Operation principle using MZM

Fig. 1.7 Structure and operation principle of RZ-DPSK transmitter using PM/MZM [57]

The transmitter consists of a continuously oscillating laser followed by two external modulators. Phase modulation can either be performed by straight-line PM or MZM. A PM only modulates the phase of the optical field, resulting constant envelope optical DPSK signal. Since phase modulation does not occur instantaneously, the PM inevitably introduces residual chirp across bit transitions. When using MZM for phase modulation, the modulator is biased at its transmission null, and is driven with a switching voltage of 2 V_π. The operation principle of phase modulation using MZM is also visualized in Fig. 1.7. Since the phase of the optical field changes its sign upon transitioning through a minimum in the MZM power transmission curve, two neighboring intensity transmission maxima have opposite phase, and a near perfect 180^o phase shift for DPSK signal is obtained, independent of the drive voltage swing. The benefit of

highly accurate phase modulation comes at the expense of some residual amplitude modulation at the transition of two bits, with the width of the resulting intensity dips depending on the driving signal's bandwidth and voltage. A pulse carver is used to carve pulses out of the DPSK signal, thus generating RZ-DPSK signal. The pulse carver cuts out the center portions of the bits only, and thus largely eliminates any residual chirp or intensity modulation.

A typical balanced DPSK receiver is shown in Fig. 1.8. The DPSK signal is first passed through a Mach-Zehnder delay interferometer (DI), whose differential delay is equal to the bit period. This optical preprocessing is necessary using direct detection receiver to accomplish demodulation, since PD is inherently insensitive to the optical phase. The DI lets two adjacent bits interfere constructively or destructively with each other, leading to the presence or absence of power at an output port. The preceding bit in DPSK signal acts as the phase reference for demodulating the current bit. Thus, the differential pre-coding is necessary at the transmitter. Note that in coherent detection, a local oscillator can be used to provide the phase reference. Ideally, one of the DI output port is adjusted for destructive interference, while the other output port then automatically exhibits constructive interference. The two DI output ports will carry identical, but logically inverted data streams with full information. Therefore, either single-ended detection or balanced detection with 3-dB higher receiver sensitivity can be performed.

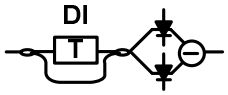

Fig. 1.8 Structure of a typical DPSK receiver

The benefit of DQPSK is that, for the same data rate, the symbol rate is reduced by a factor of two. Consequently, the spectral efficiency is enhanced and the transceiver bandwidth

requirement is reduced, which make DQPSK a very promising candidate for long-haul transmission. Nevertheless, the frequency offset tolerance between the laser and the DI is about six times less than for DPSK [58]. The most widely used implementation of RZ-DQPSK transmitter using MZM and receiver is shown in Fig. 1.9 [57]. The transmitter consists of two parallel DPSK modulators, a π/2 phase shifter, and a pulse carver. Two independent data streams are pre-coded before driving the two MZMs. They will introduce four kinds of phase shifts in the DQPSK signal including 0, π/2, π, and 3π/4 to represent four kinds of symbols comprising 11, 01, 00, and 10. A pulse carver is needed to convert the DQPSK signal into RZ-DQPSK signal. The structure of electrical pre-coder for DQPSK transmitter using MZM is very complicated, as shown in Fig. 1.10 [59]. It needs many electrical logical gates and precise lengths of delay lines to realize differential and gray pre-coding of the two data streams. These electrical logical gates consume much power and cost a lot for the MZM-based RZ-DQPSK transmitter. The receiver essentially consists of two DPSK receivers, and the phase difference between the arms of each DI is set to be +π/4 and -π/4. The two DPSK receivers with different phase differences between the arms of the DI will recover the original two data streams independently.

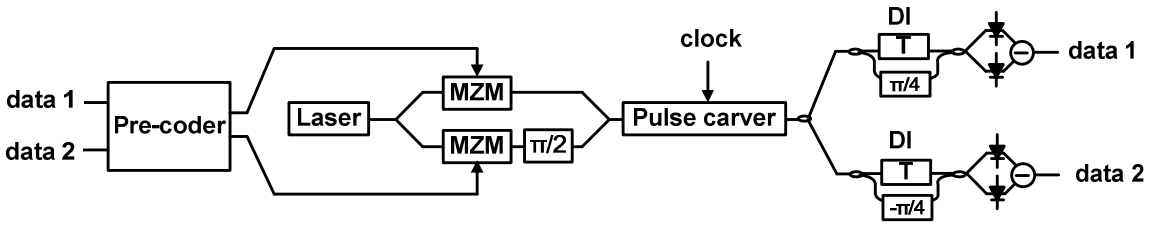

Fig. 1.9 Structure of typical DQPSK transmitter using MZM and receiver [57]

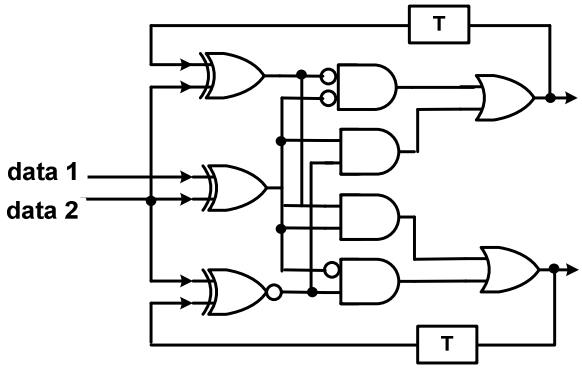

Fig. 1.10 Structure of electrical pre-coder for typical DQPSK transmitter using MZM [59]

Except MZM, there are other methods to generate DPSK and DQPSK using EAM taking the advantage of the interference between the TE and TM modes of a polarization-sensitive EAM [60]-[61].

1.4 Research challenges of transmitter design

With the explosively growing bandwidth requirement, new optical fiber communication systems with more WDM channels are needed. Hence, a huge number of optical transmitters are needed. To avoid the heavy burden on the customer and earth, these transmitters should be cost-effective, compact, and power-efficient. Meanwhile, to combat the distortions imposed on the transmission system by the fiber impairments involving CD, PMD, and nonlinearity and various noises, the transmitters should be capable of generating advanced modulation formats including optical RZ pulses, duobinary, AMI, RZ-DPSK, and RZ-DQPSK. In general, compact footprint, low cost, low power consumption, and excellent transmission performances are the essential parameters in the design of the optical transmitter.

Nevertheless, the conventional transmitters using DML, EAM, and MZM cannot entirely possess these characteristics. DML can produce high output power with low cost, but it cannot generate high-performance modulation formats. EAM is suitable for integration with semiconductor laser. However, it is not wavelength transparent and is traditionally used as OOK element. MZM is a great invention with the capability to engender advanced modulation formats, yet usually several external modulators and complex power-hungry electrical pre-coders are required for each scheme. Also, MZM brings extra cost, huge size, and large insertion loss. Therefore, the work to make innovative designs of the optical transmitter to satisfy the above requirements is challenging but meaningful.

1.5 Major contributions of this thesis

In this thesis, we propose and experimentally demonstrate several novel optical transmitter designs using chirp managed laser (CML), composed of a DML and an optical filter. These designs preserve the merits of DML such as low cost, high output power, and small package size. At the same time, contrast to the previous views towards the residual chirp in DML, we utilize its unique adiabatic chirp property to realize the phase modulating of optical field for advanced modulation formats generation and dispersion tolerant transmission. The following filter provides an additional degree of freedom to perform signal intensity manipulation by spectral reshaping. This filter also greatly enhances the CD tolerance of DML.

Therefore, we generate advanced modulation formats such as optical RZ pulse, RZ-DPSK, and RZ-DQPSK, using CML. No or very few electrical pre-coding is required thanks to the

natural differential encoding feature of the adiabatic chirp. These CML-based formats show remarkable transmission performances comparable with those equivalents using MZM.

In addition, we employ a simple and passive electrical pre-emphasis driver to further extend the CD tolerance of CML. Compared with the other power-consuming electronic pre-compensation schemes, it is more adaptable to the elegant designing concept of CML. The detailed original contributions of this thesis are listed in the following subsections.

1.5.1 Optical RZ pulses generation using CML

We propose and experimentally demonstrate the technique of 10-Gb/s optical RZ pulses generation using CML. No external modulator is used for pulse carving. The frequency of the sinusoidal driving signal is half the output pulse rate. 70-km and 50-km error-free SSMF transmissions have been achieved for the 10-Gb/s 33%-duty-cycle and 67%-duty-cycle CML-RZ-pulses based RZ-DPSK signals, respectively.

Later, we extend to demonstrate the scheme of 20-Gb/s RZ pulses generation using CML driven at one-fourth the pulse rate and investigate the transmission performance of the 20-Gb/s CML-RZ-pulses based RZ-OOK signal.

1.5.2 *M*-ary RZ-DPSK signals generation using CML

We propose and experimentally demonstrate the techniques of RZ-DPSK, ¾-RZ-DQPSK, and RZ-DQPSK signals generation using CML.

First, we generate the 10-Gb/s RZ-DPSK signal using CML and pulse carver. It does not require any differential encoder or PM. The CML-based RZ-DPSK signal shows 3-dB higher receiver sensitivity after 70-km SSMF transmission without dispersion compensation and comparable nonlinear tolerance performance, compared with that generated by PM.

Next, this proposal is generalized to generate the 10-Gbaud RZ-DQPSK signal using CML and pulse carver. Compared with the complex pre-coding required for the MZM-based RZ-DQPSK transmitter, only a simple exclusive-or (XOR) encoder is needed for that based on CML.

Later, we demonstrate the scheme of 10-Gbaud ¾-RZ-DQPSK signal generation using single CML, without the need for external pulse carver. In this new signal format, the symbols with a differential phase shift of 0 remain NRZ, while those with differential phase shifts of 0.5π, π, and 1.5π are RZ. Error-free transmission is realized over 60-km SSMF without OSNR penalty.

Finally, we demonstrate the technique of 10.709-Gbaud RZ-DQPSK signal generation using single CML, without any differential pre-coder, PM, or pulse carver. It realizes 40-km SSMF transmission at BER of 10^{-9}.

1.5.3 Enhanced CD tolerance of CML with pre-emphasis

We propose and experimentally realize the 10-Gb/s 300-km SSMF transmission at BER of 10^{-9} using CML with a simple and passive pre-emphasis driver. The 10-Gb/s standard CML signal without pre-emphasis can only be transmitted up to 220 km, in comparison. No expensive DCF or power-hungry EDC technique is used.

Later, we further demonstrate the 20-Gb/s 100-km SSMF transmission at BER of 10^{-9}, using

CML with pre-emphasis.

1.6 Outline of this thesis

The chapters of this thesis are organized as follow.

Chapter 1 reviews the origin of optical fiber communication systems, transmission impairments, modulation techniques, and challenges for transmitter design.

Chapter 2 talks about the basic knowledge of CML such as history and device structure, and analyzes the chirp origin and modulation bandwidth of DML. Then, the previous works using CML done by other groups are discussed.

Chapter 3 demonstrates the techniques of 10-Gb/s optical RZ pulses generation using CML driven at half pulse rate and 20-Gb/s optical RZ pulses generation using CML driven at one-fourth pulse rate.

Chapter 4 investigates the schemes of 10-Gb/s RZ-DPSK signal generation using CML and pulse carver, 10-Gbaud RZ-DQPSK signal generation using CML and pulse carver, 10-Gbaud ¾-RZ-DQPSK signal generation using single CML, and 10.709-Gbaud RZ-DQPSK signal generation using single CML.

Chapter 5 presents the operations of 10-Gb/s 300-km and 20-Gb/s 100-km SSMF transmissions at BER of 10^{-9} using CML with a simple and passive pre-emphasis driver.

Chapter 6 gives the summary of this thesis and suggestions on the future work.

Chapter 2 Chirp Managed Laser

2.1 Introduction

The concept of CML, comprising a DML biased high above the threshold and a narrow passive optical filter, was proposed by D. Mahgerefteh *et al.* and became popular around 2005 [62]-[63]. Due to its excellent transmission performance of CD robustness and simplicity, the inventors of CML co-founded a corporation to commercialize the product in 2002. Actually, much effort had been made to improve the CD tolerance of DML by narrowing the spectral or reducing the residual chirp in 1990s.

2.1.1 History

In 1993, M. Blez *et al.* surprisingly found that the best chirp value of DML was even below the information bandwidth in the experiment. Then, their calculated spectrum evolution suggested that an optimum but low chirping would obtain a reduced spectrum with strong one-side modulation band suppression on the long wavelength side [64]. Nevertheless, a clear relation between the simultaneous amplitude modulation (AM) and frequency modulation (FM) in DML for this optimum condition was not given.

In 1994, J. Binder *et al.* analyzed that one spectral sideband would be suppressed with a particular balance between the simultaneous AM and FM in DML, when it was dominated by adiabatic chirp [65]. The balance is governed by

$$\Delta f_{\mathrm{pp}} = \frac{B}{2} \cdot m_{\mathrm{IM}} = \frac{B}{2} \cdot \frac{\mathrm{EXT}-1}{\mathrm{EXT}+1} \tag{2.1}$$

where Δf_{pp} is the peak-to-peak frequency deviation caused by adiabatic chirp, *B* is the data rate, m_{IM} is the AM modulation index, and EXT is the signal ER. It predicted that the DML would have better CD tolerance with high signal ER and less than or equal to half-data-rate adiabatic chirp. However, to get high signal ER, the DML needs to be operated near threshold, where harmful transient chirp instead of adiabatic chirp is dominated. S. Mohrdiek *et al*. showed by calculation that, with increased laser bias for adiabatic chirp and lower ER as trade-off, 70-km SSMF transmission was possible with a 3-dB penalty for 10-Gb/s DML signal [66]. B. Wedding *et al*. experimentally reported 253-km SSMF transmission of 10-Gb/s DML signal, using dispersion-supported FM-to-AM conversion [67], which was a remarkable advancement in manipulating the chirp in DML. Yet, the drawbacks of this scheme were that the transmitter chirp need to be adjusted for given fiber length and an uncommon receiver with integrator was used.

In 1995, C.-H. Lee *et al.* proposed to use a 12-GHz optical Fabry-Perot (FP) filter to reduce the spectral width of 2.5-Gb/s DML signal, increase the signal ER, and decrease the chirping-induced penalty. Thus, 250-km non-dispersion-shifted fiber (NDSF) transmission was demonstrated [68]-[69]. This was the first time when the model of DML followed by an optical filter was built up. However, the DML was modulated with huge transient chirp and the optimum relation between AM and FM was also neglected.

In 1997, P. A. Morton *et al.* realized that the bias of DML could be increased to eliminate the ringing or overshoot during transition induced by transient chirp and the poor signal ER could be improved using a narrow spectral filter. 38.5-km SSMF transmission at 10 Gb/s was achieved [70]. This work was approaching nearly the optimum operating condition of CML, except that the large driving voltage of 4 V_{pp} covered the full potential advantage of adiabatic

chirp. M. McAdams *et al.* presented that the modulation response of DML or its magnitude of AM would be greatly improved by the FM-to-AM conversion using any frequency discriminator, such as an optical filter or resonant cavity [71].

In 1999, D. Mahgerefteh *et al.* demonstrated the propagation over 600-km NDSF at 2.5 Gb/s using a fiber-grating high-pass filter after DML [72]. The scheme especially mentioned that the laser need to be biased high (100 mA) and modulated with moderate depth (20%-40%) to minimize transient chirp, leaving adiabatic chirp which made ones and zeros had different frequencies. A fiber Bragg grating with a sharp and step-line response (7 GHz) passed the ones and blocks the zeros, resulting in signal with 12-dB ER. Hence, most of the remaining energy had the same optical frequency. The authors practically used a feed-back loop to keep the laser frequency at the transmission edge of the grating and maintain the high ER over time. They also pointed out the pattern dependent problem of DML because of the non-uniform frequency response, which could be remedied by using low-frequency circuitry to equalize the response. These simple but useful thinking paved the way for the model of DML plus filter in the lab to be a CML product in the market. However, the driving voltage was set to be 1.8 V_{pp} in the experiment, which was yet not the best value for the balance of AM and FM in DML signal, implying that there was still room for improvement.

In 2001, T. Niemi developed a tunable optical etalon filter for simultaneous spectral filtering and wavelength monitoring of the output of DML [73]. The FP filter was fabricated by depositing dielectric mirrors on a double-side polished silicon wafer, which was transparent in the wavelength rage of 1.2-1.7 μm. Moreover, the refractive index of silicon was sensitive to temperature, allowing the transmission of the filter to be tuned and locked to a preselected value

on the slope of the filter transmission spectrum by controlling the optical thickness of the etalon via temperature. By tracking the temperature of the etalon locked to a constant transmission value, changes in the wavelength of the transmitter was conveniently be monitored. These features made the etalon filter to be a good candidate for the spectral reshaping of DML signal.

In 2002, D. Mahgerefteh *et al.* demonstrated a simple and wavelength-locked directly modulated RZ transmitter [74]. The packaged device comprised a 10-Gb/s DML and a fiber Bragg grating (FBG) filter with tap monitors, which was the miniature of CML. The thermoelectric cooler (TEC) for temperature stabilization and electronic control circuit for wavelength locking had been applied with good performance. So far, the theory investigation and device structure design had been mature for CML.

In 2005, D. Mahgerefteh *et al.* proposed and demonstrated the error-free 250-km SSMF transmission using 10-Gb/s CML driven with an optimal voltage of 0.8 V at 1550 nm, which had already been a popular product in the market. It set a transmission record for DML without any CD compensation [62].

In 2006, Y. Matsui *et al.* explained the model and operation principle of CML systematically [63], which indeed generated phase correlated optical duobinary signal and also agreed with the balance of AM and FM mentioned in equation of (2.1). Since then, much research has been performed to demonstrate a wide range of applications using CML.

In the following subsections, we will concisely introduce the device structure of CML and analyze the chirp origin and modulation bandwidth of DML.

2.1.2 Device structure

The commercial available CML module uses a 10-Gb/s directly modulated DFB chip co-packaged with a multi-cavity etalon filter for optical spectral reshaping as shown in Fig. 2.1 [75]. The FM efficiency of the DFB laser is 0.24 GHz/mA. The Bessel filter has a 3-dB bandwidth of 11 GHz or 7 GHz and a slope of 1.5 dB/GHz or 2.2 dB/GHz for different models. Sharper filter typically supports better performance. The first optical isolator is included between the DFB and the filter, while a beam-splitter component and two PDs are configured to allow frequency locking. The first lens is used to collimate the DFB laser output and pass the beam through the splitter and filter, prior to coupling into fiber using the second lens. A second isolator is included in the fiber pigtail to minimize the effect of external back-reflections on module performance.

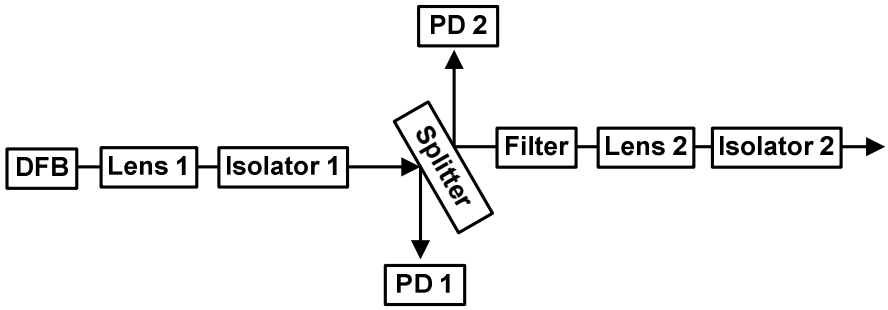

Fig. 2.1 Structure and internal layout of CML module [75]

The schematic in Fig. 2.2 shows the key components and control loops that are used to operate the CML module. The output power of the DFB is monitored by PD 1. PD 2 monitors the back-reflection from the filter. The photocurrent ratio from the two detectors is used to lock the relative spectral locations of the laser and the filter via temperature control of the DFB using TEC 1. TEC 2 controls the temperature of the filter and locates the operating point of the filter on the WDM grid in both C band and L band. The locked frequency deviation on the International

Telecommunication Union (ITU) channel is less than 2.5 GHz.

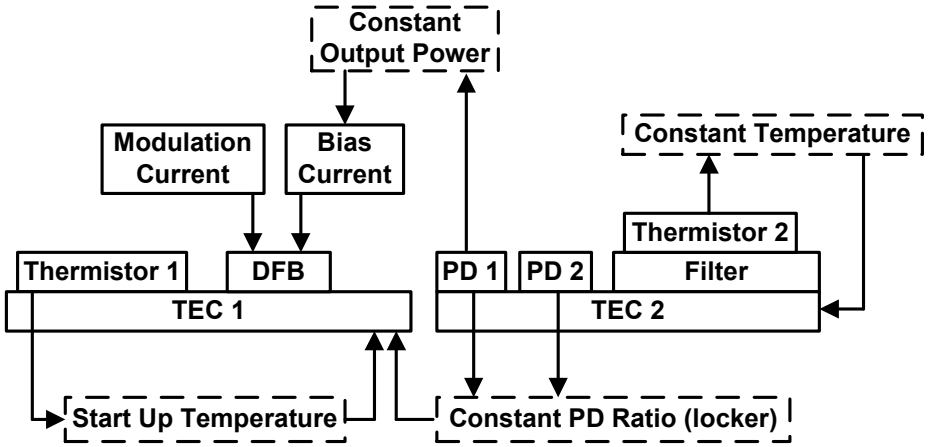

Fig. 2.2 Control schematic for CML module [75]

The CML module offers a reduced footprint which is included in standard butterfly package or transmitter optical sub-assembly (TOSA) package, shown in Fig. 2.3. The miniature size of TOSA (5.5 x 6.5 x 15.5 mm) ensures it suitable for integration into an XFP transceiver module. The typical driving voltage and output power of CML module for dispersion-compensation free transmission is 1 V and 0-7 dBm, respectively. By comparison, the $LiNbO_3$-MZM-based transmitter cannot fit into an XFP module due to its large size and high power consumption.

Fig. 2.3 Butterfly package and TOSA package for CML module [75]

2.1.3 Chirp origin and modulation bandwidth

There are three types of chirp in DML including transient chirp and adiabatic chirp caused by carrier density modulation effect and thermal chirp induced by temperature change effect. The underlying physical phenomenon is that the refractive index of semiconductor material varies with carrier density and temperature.

When the laser is directly modulated, a change in the bias current will lead to a change in the carrier density, which in turn will lead to a change of the refractive index of the semiconductor material. Since the lasing frequency is determined from the feedback condition in the laser cavity, which itself depends on the refractive index, the instantaneous frequency of the emitted signal will be a time varying signal. This effect is known as frequency chirping. The relation between the frequency shift $\Delta\nu$ induced by the chirp and the power waveform P at the laser output needs to be clarified first for chirp management of DML.

Under the laser threshold condition, the lasing frequency of an FP laser ν is given by

$$\nu = mc/2nL \tag{2.2}$$

where m is an integer, corresponding to the mth longitudinal mode of an FP cavity, c is the speed of light in vacuum, n is the real part of the complex refractive index, and L is the laser cavity length. The real part of the complex refractive index varies with frequency due to dispersion in semiconductor material and also depends on the carrier density [76].

The complex refractive index $\tilde{n}$ can be written as

$$\tilde{n} = n + j\,\bar{n} \tag{2.3}$$

where $\bar{n}$ is the imaginary part of the complex refractive index. The real and imaginary parts of the complex refractive index are related through use of Kramers-Kroning relations and verified by C. H. Henry *et al.* in 1981 [77]. In 1982, C. H. Henry pointed out that besides the instantaneous phase change caused by spontaneous emission, there would be a delayed phase change resulting from the instantaneous change in the field intensity for lasing [78]. To restore the steady-state field intensity, the laser will undergo relaxation oscillations, lasting for about 1 ns. During this time, there will be a net gain change Δg, denoted by

$$\Delta g = (-2\omega/\,c)\,\Delta\bar{n} \tag{2.4}$$

where ω is the angular frequency in vacuum. $\Delta\bar{n}$ is the deviation of the imaginary part of the refractive index from its steady-state value. The change in $\bar{n}$ is caused by a change in carrier density, which will also alter the real part of the refractive index *n*. The ratio of these changes is defined by a linewidth enhancement factor α with a typical value of 5, expressed by

$$\alpha = \frac{\Delta n}{\Delta\bar{n}} \tag{2.5}$$

A change in *n* during a limited period of time will result in an additional phase shift of the laser field and in additional line broadening. Insert (2.5) into (2.4), leading to

$$\Delta g = (-2\omega/\,\alpha c)\,\Delta n \tag{2.6}$$

The relation between gain and carrier density *N* is often modeled as below

$$g(N) = a\,(N - N_t)(1 - \epsilon S) \tag{2.7}$$

where a is the gain coefficient. N_t is the carrier density needed for transparency. The first-order effect of a small degree of spectral hole-burning (SHB), namely, strong non-uniformity across the spectral distribution, and other gain nonlinearity is denoted through a reduction or compression in gain by a factor $(1 - \epsilon S)$, where ϵ characterizes the strength of the nonlinearity and *S* is the photon density. Therefore, in semiconductor laser, the changes in the carrier density affect the gain, as well as the real part of the complex refractive index, which results in the frequency chirp.

From 1984 to 1987, T. L. Koch *et al.* derived the expression of the time-dependent frequency deviation in terms of the output power using the following single-longitudinal-mode laser rate equations [79]-[81].

$$\frac{dS}{dt} = a\upsilon_g \, \Gamma \, (N - N_t)(1 - \epsilon S)S - \frac{S}{\tau_{ph}} + \beta \frac{\Gamma N}{\tau_{sp}} \tag{2.8}$$

$$\frac{dN}{dt} = \frac{I(t)}{eV_{act}} - a\upsilon_g(N - N_t)(1 - \epsilon S)S - \frac{N}{\tau_{sp}} \tag{2.9}$$

$$\frac{d\emptyset}{dt} = -\frac{\alpha}{2} a\upsilon_g \Gamma (N - N_{cw}) \tag{2.10}$$

The photon density is defined in terms of the number of photons in the mode N_p or the optical power out one facet *P* as

$$\begin{aligned} S(t) &= \Gamma \frac{N_p(t)}{V_{act}} \\ &= \frac{\Gamma 2\tau_{ph} P(t)}{h\nu\eta V_{act}} \end{aligned} \tag{2.11}$$

where V_{act} is the active layer volume. r is the usual optical modal confinement factor. η is the total differential quantum efficiency assuming no leakage currents. υ_g is the group velocity. β is the fraction of spontaneous emission into the lasing mode. τ_{sp} is the spontaneous emission lifetime. I is the applied current. e is the elementary charge. $\emptyset$ is the optical phase. N_{cw} is the photon density during the steady state. τ_{ph} is the photon lifetime, related with the internal loss α_{int} and the mirror loss α_m in semiconductor laser, governed by

$$\tau_{ph}{}^{-1} = \upsilon_g(\alpha_m + \alpha_{int})$$

$$= \upsilon_g \left[\frac{1}{2L}\ln\left(\frac{1}{R_1 R_2}\right) + \alpha_{int}\right] \qquad (2.12)$$

where L is the laser cavity length. R_1 and R_2 are the facet reflectivities at the two ends of the laser cavity.

On the right-hand side of the photon density rate equation of (2.8) describing the change of photons as a function of time, the first term is the rate at which photon density increases due to stimulated emission. The second term is the rate at which photons leave the cavity, for internal absorption or exiting the mirrors. The third term is the contribution of the spontaneous emission from carrier non-radiative recombination. On the right-hand side of the carrier rate equation of (2.9) describing the change of carriers as a function of time, the first term is the injected electrons rate. The second term is the carrier depletion due to stimulated recombination. The third term is the carrier depletion rate due to non-radiative recombination.

The relation between chirp and output optical power in DML is derived as

$$\Delta\nu(t) = \frac{1}{2\pi}\frac{d\emptyset}{dt}$$

$$= \frac{-\alpha}{4\pi}\left[\frac{1}{P(t)}\frac{dP(t)}{dt} + \kappa.P(t)\right] \quad (2.13)$$

where $\kappa = 2\,r\epsilon/h\nu\eta V_{act}$. The spontaneous emission term is neglected, which contributes to intensity and phase noises. Here the first term is a laser-structure-independent transient chirp, and the second term is a laser-structure-dependent adiabatic chirp.

The transient chirp leads to deleterious chirping during relaxation oscillation at the transition points on the waveform which are of infinitesimal temporal extent. Fortunately, if the laser power is increased to a high level, the transient chirp will be reduced significantly. The change of adiabatic chirp almost instantaneously follows the variation of output power as a function of time, which is a key characteristic for CML to realize phase modulation via driving signal manipulation, generating a wide variety of advanced modulation formats. The adiabatic chirp is induced by the nonlinear gain compression effect, which causes the carrier density to saturate at the peak intensity regions of the mode profile, related with the strong damping of relaxation oscillation in semiconductor laser [82]-[85]. A laser with large damping necessarily has a large adiabatic chirp or frequency offset, and since the oscillations and hence derivatives will be small, the transient chirp term when evaluated on the power waveform will be small [80]. The converse is also true. In 1987, P. J. Corvini and T. L. Koch also pointed out that the moderate ER was optimal for reduced chirp penalty and the transient chirp was more detrimental to system performance, with the adiabatic chirp being more benign or even beneficial [81].

Thermal chirp is the third kind of FM in DML, generally undesirable. The laser frequency

changes with variance in temperature because the refractive index of the semiconductor material is a function of temperature [86]-[87]. Thermal chirp has the opposite sign to adiabatic chirp. An increase in injection current generates a blue-shifted adiabatic chirp, while thermal effect produces a red-shifted thermal chirp. In addition, thermal chirp has a delayed response to the applied current, which increases exponentially in time. Thermal chirp is controlled by several time constants, which are relatively long in duration compared to the typical bit period of high speed digital signals, i.e., 100 ps for 10 Gb/s. The fastest time constant for thermal chirp is on the order of 25 ns for a typical DFB laser chip. Thus, following a sudden increase of the injection current, the continuously increasing temperature results in a continuous exponential-like decrease of the optical frequency (from a new higher value set by the adiabatic chirp) [88]. Specifically saying, FM response in the low modulation frequency region from 0 to 10 MHz, gradually decreasing with modulation frequency, stems from the thermal effect. FM response in the high modulation frequency from 10 MHz to the AM modulation limit of DML is mainly controlled by the carrier effect [89]. The overall FM response is non-uniform and V-shaped due to the transition between the thermal response and carrier density response [90].

Thermal chirp gives rise to severe pattern-dependent effect for DML, limiting the data pattern length [87]. When a DFB laser is modulated by a random sequence, a high density of 1 bit will tend to heat the laser since the average injection current is increased. The temperature of the active region of the laser will decrease for a high density of 0 bit. Hence, the temperature of the laser and its optical frequency tend to wander over time in response to short term changes in the mark density of the random sequence, resulting in phase noise. The phase noise can be converted into intensity noise via FM-to-AM conversion process. This frequency wander can also cause another harmful effect in data links with long lengths of optical fiber. Since the fiber is

dispersive, the frequency wander can cause a little difference in the arrival time of the bits with different mark density at the receiver, inducing timing jitter.

Different approaches have been reported to combat the adverse effects of thermal chirp. The preamplifier with a compensation network can enhance the signal at the laser FM response dip [91]. Modulation formats of AMI and Manchester or line coding can delete the low-frequency spectral content of the signal [92]-[94]. CML designers provide other compensation techniques [87]. Additional correction current can be supplied to the laser chip which generates an additional adiabatic chirp component to compensate for thermal chirp. The correction current is electronically synthesized from the incoming electrical data or determined by monitoring the output optical signal. However, this method affects the output amplitude. In another direct thermal compensation scheme, the correction current is supplied to a heater, which is integrated with the laser chip and functions to change the chip temperature. The correction signal is generated from the digital data modulating the laser.

Modulation bandwidth is another important issue for high-performance CML. The modulation response of a semiconductor laser is strongly affected by the relaxation oscillation frequency Ω_R and the damping rate Γ_R [95]. Essentially, the damping phenomenon results from the nonlinear gain saturation.

In 1990, G. P. Agrawal used a different model for gain nonlinearity to derive modulation response, which is more suitable than the assumptions in [96]-[97] when the laser power is high, governed by

$$g = \frac{g_L}{(1+p)^{\frac{1}{2}}} \tag{2.14}$$

where g_L is the linear gain. The dimensionless parameter p takes into account the effects of intraband carrier relaxation. It can be related to the output power by using the relation

$$p = |E_0|^2/I_s$$

$$= P/P_s \tag{2.15}$$

where $|E_0|^2$ is the intracavity mode intensity, and the saturation intensity I_s is related to the intraband relaxation times. The saturation photon number P_s is related to I_s by the linear relation

$$P_s = \frac{\epsilon_0 n_{eff} c V_{act}}{h\nu \Gamma \upsilon_g} I_s \tag{2.16}$$

where ϵ_0 is the vacuum permittivity. n_{eff} is the effective index.

By solving the laser rate equations and keeping only the dominant term, the frequency and the damping rate of relaxation oscillations are found to depend on the mode intensity through

$$\Omega_R^2 \cong \frac{G_N P_s}{\tau_{ph}} \frac{\left(1+\frac{p}{2}\right)p}{(1+p)^2} \tag{2.17}$$

$$\Gamma_R \cong \frac{1}{\tau_{ph}} \frac{\frac{p}{4}}{(1+p)^{\frac{3}{2}}} \tag{2.18}$$

where G_N is gain derivative by N, given by

$$G_N = \frac{\Gamma \upsilon_g a}{V_{act}} \tag{2.19}$$

The quantity of interest from a practical standpoint is the 3-dB bandwidth $\Delta\,\omega_{3dB}$, defined

as the modulation frequency at which the modulation response drops by a factor of 2 from its zero-frequency value. $\Delta\,\omega_{3\mathrm{dB}}$ is related to the relaxation-oscillation parameters by the relation

$$\Delta\omega_{3dB}^2 = \Omega_R^2 - \Gamma_R^2 + 2[\Omega_R^2(\Omega_R^2 + \Gamma_R^2) + \Gamma_R^4]^{1/2} \tag{2.20}$$

The limiting value of $\Delta\,\omega_{3\mathrm{dB}}$ at saturation due to gain nonlinearity is obtained from (2.20) and given by

$$\Delta\omega_{3dB}^{max} \cong \sqrt{3}\,\Omega_{\max}$$

$$= \left(\frac{3}{2}\frac{G_N P_s}{\tau_{ph}}\right)^{\frac{1}{2}}$$

$$= \left(\frac{3\epsilon_0 c n_{eff} a I_s}{2h\nu\tau_{ph}}\right)^{\frac{1}{2}}$$

$$= \left\{\frac{3\epsilon_0 c n_{eff} a I_s \upsilon_g}{2h\nu}.\left[\frac{1}{2L}\ln\left(\frac{1}{R_1 R_2}\right) + \alpha_{int}\right]\right\}^{\frac{1}{2}} \tag{2.21}$$

where Ω_{max} is the maximum value of Ω_R when p is approaching the infinity and the condition of $\Gamma_R \ll \Omega_R$ is assumed.

For CML applications, both large adiabatic chirp and high modulation bandwidth are desirable, which is challenging for laser design and requires innovation. Equations of (2.13) and (2.21) should be considered simultaneously. First of all, high bias is a working condition for the maximum modulation bandwidth and strongest gain nonlinearity. Secondly, the FM efficiency can be strengthened by enhancing the optical confinement factor. The differential gain is becoming higher too, leading to higher modulation bandwidth, because larger optical

confinement factor results in lower threshold gain [98]. Therefore, the nonlinear gain effect will be increased using quantum-well (QW) design due to the quantum confinement of electrons and proportional optical confinement [99]. The FM efficiency should be roughly doubled, since the saturation intensity controlled by gain nonlinearity is reduced by a factor of 1-2. The differential gain is expected to be increased by a factor of 2-3 with QW. Thus, the limiting 3-dB bandwidth is also expected to be larger for QW laser but by no more than 50% of that of conventional laser [95]. The gain nonlinearity and differential gain will be enhanced further when the thickness of the well is reduced and the number of the well is increased [98]. Last, decreasing the laser cavity length is another effective approach to improve the modulation bandwidth [49]. At the same time, the FM efficiency is also enhanced due to the decreased laser active layer volume. Overall, short-cavity semiconductor laser with large optical confinement factor using QW structure can provide high modulation bandwidth and large adiabatic chirp for CML applications, though the short cavity may limit the laser output power to a poor value.

2.2 Previous works

Since the inception of CML technology, most of the research has been focused on the demonstration of its various applications including extended transmission reach and advanced modulation formats generation [100]. In this section, we will review several representative works using CML such as NRZ-duobinary signal generation, electronic pre- and post- dispersion compensation, RZ-AMI signal generation, and RZ-DPSK signal generation. Their advantages and limitations will also be discussed.

2.2.1 NRZ-duobinary signal generation using CML

To generate NRZ-duobinary signal, the DML in CML is typically biased at 5 x threshold, resulting in a low ER (about 2 dB) intensity modulation [63]. The benefits of high bias for CML compared to conventional DML are high output power, wide modulation bandwidth, stable single-mode operation, low timing jitter, and suppression of transient chirp. Importantly, gain compression in the laser generates the accompanying adiabatic chirp, which follows the intensity waveform; “1” bits are blue shifted relative to “0” bits. The laser wavelength is aligned on the transmission edge of the filter in CML, so as to pass blue-shifted “1” bits and attenuate red-shifted “0” bits. This FM-to-AM conversion increases ER at the output of filter to > 10 dB.

Fig. 2.4 shows operation principle of NRZ-duobinary signal using CML via the intensity, frequency, and phase profiles at the output of driver, laser, and filter.

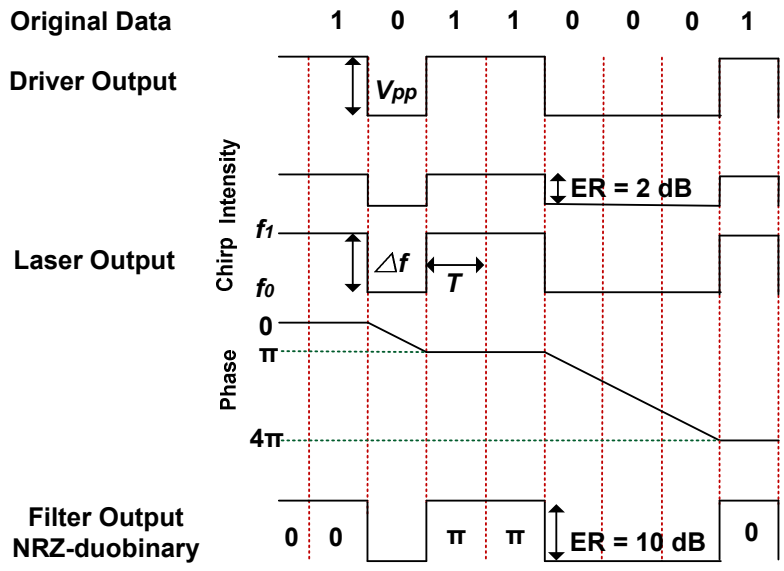

Fig. 2.4 Operation principle of NRZ-duobinary signal generation using CML

The laser is biased at 70 mA and modulated with 10 Gb/s NRZ signal. The modulation current of the laser is 23 mA_{pp} (1 V_{pp}), producing an adiabatic chirp Δf of 5 GHz. The peak-to-peak adiabatic chirp is set to be half the bit rate frequency, satisfying the balanced AM and FM condition in equation of (2.1), together with high signal ER after filter. Hence, the phase varies slowly during each 0-bit with a total shift $\Delta\emptyset$, given by

$$\Delta\emptyset = 2\pi \times \Delta f \times T$$

$$= 2\pi \times 5\ \text{GHz} \times 100\ \text{ps}$$

$$= \pi \tag{2.22}$$

where T is the time duration of bit period. The limited bandwidth and high slope of the filter in CML removes ring in the intensity, converting slowly-varying adiabatically-chirped pulses to flat-topped chirp pulses with abrupt transitions. In other words, the chirp at the rising and falling edges is significantly reduced and the frequency becomes flat-topped over the entire 1 bit pulses. The constant phase envelope with the accompanying abrupt π phase shift during odd number of 0 bits, generating the NRZ-duobinary signal, which is the key to CD tolerance of CML. Note that no electrical differential pre-coding or other encoding is needed.

D. Mahgerefteh *et al.* showed that the dispersion penalty of the 10-Gb/s CML using 2^{31}-1 pseudo-random binary sequence (PRBS) was 0.5 dB for 200-km SSMF and 4.8 dB for 250-km SSMF at BER of 10^{-12} [62]. A compact 10-Gb/s DFB-array-based CML module with 30-nm tuning range across C band for 200-km SSMF reach was reported [101]. Y. Yokoyama *et al.* achieved 300-km SSMF transmission at BER of 10^{-4} using a 10.709-Gb/s CML with a planar lightwave circuit (PLC) based ring resonator filter [102]. S. Chandrasekhar *et al.* transmitted the

10-Gb/s CML signal over 1980-km link, with the dispersion management using DCF [103]. S. Matsuo *et al*. demonstrated the 60-km SSMF transmission using a 20-Gb/s frequency-modulated DBR (FM-DBR) laser combined with a 40-GHz free-spectral-range (FSR) DI filter and a 13.5-GHz etalon filter [104]. Since the laser phase section was directly modulated, there was no residual intensity modulation. A clear eye opening after 40-km SSMF transmission was observed using a 25-Gb/s FM-DBR laser and a DI filter with 20-GHz bandwidth [105]. Error-free operation was achieved for 20-km SSMF using a 40-Gb/s FM-DBR laser and a 13.5-GHz etalon filter [106]. J. Yu *et al.* demonstrated the transmission of a 42.8 Gb/s CML signal over 20-km SSMF and 100-m graded index plastic optical fiber (GI-POF) with BER smaller than 10^{-3} and its application in a centralized WDM passive optical network (PON) [107]-[109]. The 42.8-Gb/s CML signal could be transmitted over 640-km SSMF, with the help of DCF [110].

There is another way for DML to generate NRZ-duobinary signal or obey the relation in equation of (2.1), which is the use of an external EAM to take the place of the filter in CML for ER enhancement. Hoon Kim *et al.* demonstrated the 10-Gb/s transmission using this dual-modulated EML (D-EML) over 200-km SSMF with PRBS of 2^7-1 giving rise to 3.4-dB power penalty and over 175-km SSMF with PRBS of 2^{23}-1 suffering from 6-dB power penalty at BER of 10^{-9} [111]. K. Hasebe *et al.* demonstrated the 10-Gb/s error-free 180-km SSMF transmission using an integrated D-EML with PRBS of 2^{31}-1, by suppressing the thermal effect with a shorter cavity length [112]. K. Kechaou *et al.* demonstrated the 39.7-km SSMF transmission at 20 Gb/s with PRBS of 2^7-1 and 10-km SSMF transmission at 40 Gb/s with PRBS of 2^{31}-1 using a D-EML at BER of 10^{-9} [113]-[114]. In comparison, one advantage of D-EML over CML is the insensitivity to temperature. Nevertheless, the transmission records of D-EML at different data rates are not as good as CML. The main reason should be attributed to the continuous phase

change in D-EML and the sharp phase change in CML over the space bits.

The idea of FM-to-AM conversion behind CML can also be used for other modulation techniques to improve the system performance. J. L. Wei *et al.* demonstrated that the wavelength-offset optical filtering resulted in a 7-dB power budget improvement for DML-based PON system using intensity-modulation and direct-detection (IMDD) orthogonal frequency division multiplexing (OFDM) [115]. Z. X. Liu *et al.* demonstrated the generation of Manchester-duobinary signal using CML and its application in WDM-PON [116]-[117].

2.2.2 Electronic pre- and post- dispersion compensation for CML

To further improve the CD tolerance of CML, many kinds of electronic techniques including pre-EDC at the transmitter and post-EDC at the receiver had been used.

S. Chandrasekhar *et al.* demonstrated the continuous detectability of 10-Gb/s data from 0- to 675-km of SSMF using a combination of a CML and tunable ODC and adaptive EDC at the receiver [118]. The ODC device was made from silica waveguide DI [119] and the EDC incorporated a combination of DFE, FFE and complexity-reduced MLSE [120]. The 285-km repeaterless SSMF transmission at 10.664 Gb/s was reported using a CML with the same receiver [121]. A 10-Gb/s CML in conjunction with MLSE at the receiver achieved transmission over 1200-km nonzero dispersion-shifted fiber (NZDSF) [122]. X. Zheng demonstrated the 10.7-Gb/s 300-km SSMF transmission at BER of 10^{-5} using a CML and FFE/DFE-based EDC at the receiver, which could fit into hot pluggable XFP module [123].

Post-EDC is not an efficient way to correct optical signal distortion caused by CD because

the phase information critical to undoing the distortion is lost in the power law detector at the receiver. Pre-EDC at the transmitter does not suffer from this loss of information.

X. Zheng *et al.* demonstrated the SSMF transmission of 10.709-Gb/s signal from 0 to 360 km at BER of 10^{-4} using a CML and an integrated DSP control driver for pulse shaping at the transmitter [124]. Fig. 2.5 shows the operation principle of the pulse-shaped CML.

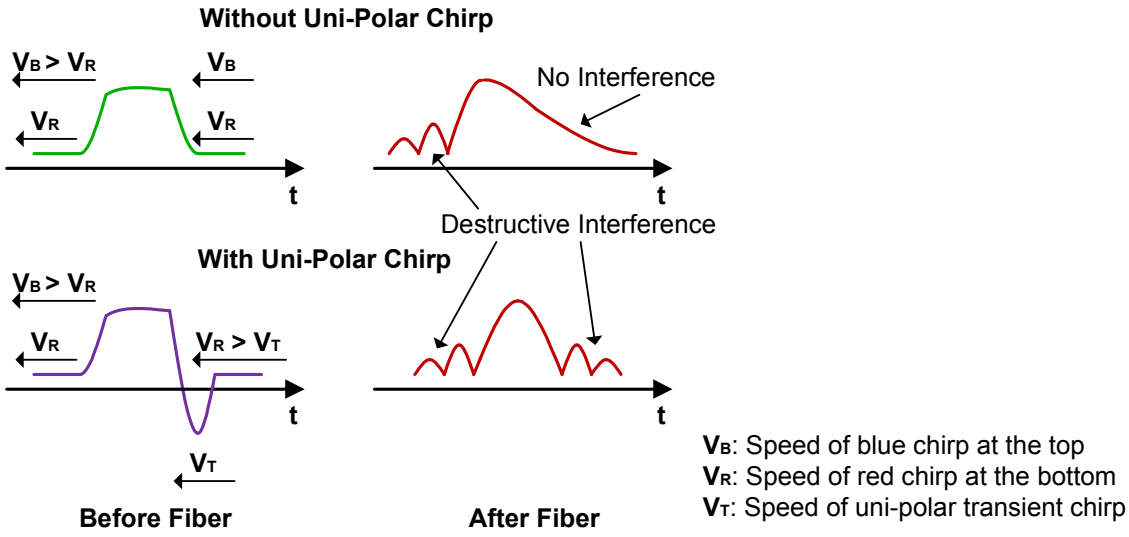

Fig. 2.5 Operation principle of CML with uni-polar transient chirp [124]

For standard CML, the main factor limiting BER at 200 km is the “0 1 0” bit sequence, for which the trailing edge of the pulse spreads into the adjacent “0” bit causing 0 to 1 errors. The rising edge of the pulse does not limit BER at 200 km because of inter-pulse destructive interference. The faster blue chirp at the rising edge of the isolated pulse over-runs the slower red chirp part of the transition causing destructive interference. There is no interference on the trailing edge since the bottom of the transition moves away from the faster top portion. In order to overcome the energy spreading from the trailing edge, a CML driver with uni-polar boosting

function is developed. The integrated DSP control driver adds a transient boost at the trailing edges of the pulses, which generates a large uni-polar red transient chirp at 1-to-0 transitions at the output of the laser. In this case, the bottom of the pulse transition overruns the more red shifted transient portion causing destructive interference in the adjacent “0” bit. This eliminates the 0 to 1 error for that bit and increases the reach of CML.

The structure of the uni-polar driver for CML is shown in Fig. 2.6. About 30 mW extra power was needed for generating the uni-polar function.

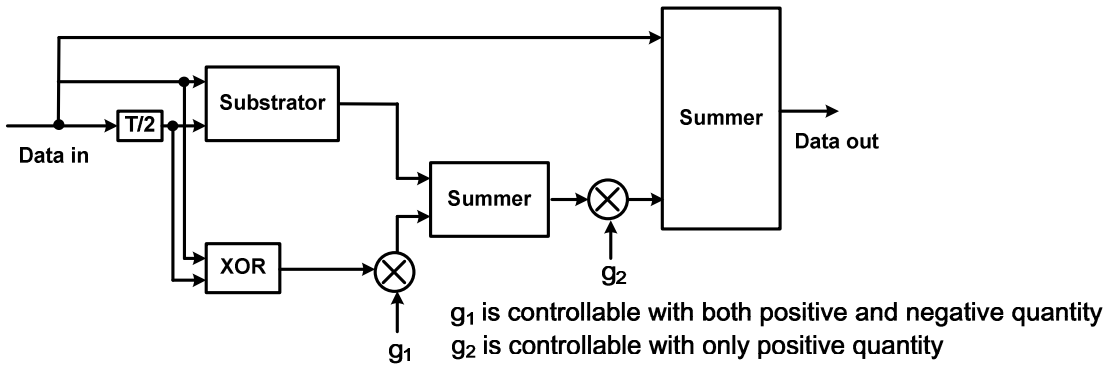

Fig. 2.6 Structure of the uni-polar driver for CML [124]

A. S. Karar *et al.* demonstrated the transmission over 608-km SSMF at BER of 10^{-3} using a 10.709-Gb/s CML and pre-distortion at the transmitter [125]. It involves shaping the drive current through back-calculation which is optimized for a minimum BER at a specified transmission distance. A 6-bit 21.4-GSa/s digital-to-analog converter (DAC) was implemented. The 1-dB dispersion penalty window was 110 km at BER of $1x10^{-3}$. Therefore, the heavily pre-distorted signal is only detectable in the vicinity of the distance which it is pre-distorted for.

Electronic pre- and post- dispersion compensation helps a lot to extend the reach of CML.

However, EDC brings extra cost and high power consumption to CML, whose market position is located at cost and power sensitive access and metropolitan networks.

2.2.3 RZ-AMI signal generation using CML

S. Chandrasekhar *et al.* generated RZ-AMI signal by operating the CML with RZ electrical driving signal [126]. The operation principle is shown in Fig. 2.7.

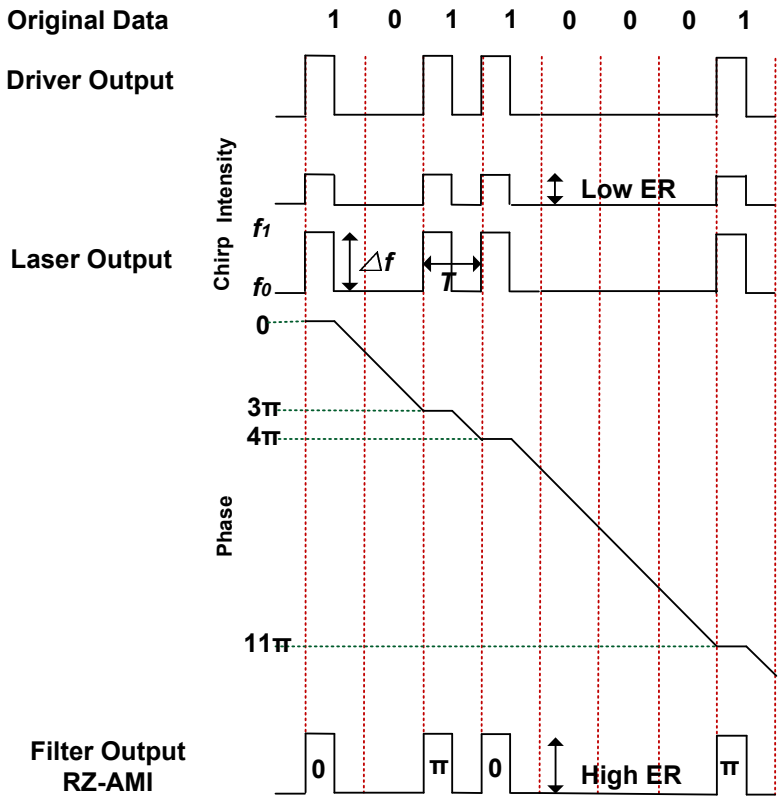

Fig. 2.7 Operation principle of RZ-AMI signal generation using CML

The laser is biased at 80 mA high above its threshold and directly modulated by a RZ

electrical waveform with 50% duty cycle. The peak-to-peak driving voltage of the 10.664-Gb/s RZ signal is 2 V, generating an adiabatic chirp Δf of 10 GHz. Hence, the phase varies slowly during the space of two adjacent 1-bits with a total shift $\Delta\emptyset$, given by

$$\Delta\emptyset = 2\pi \times \Delta f \times T/2$$

$$= 2\pi \times 10\ \text{GHz} \times 50\ \text{ps}$$

$$= \pi \tag{2.23}$$

where *T* is the time duration of bit period. The phase slip during a "0" bit, on the other hand, is 2π, since "0" bit occupies the full bit period. Overall, a phase change of π occurs for each "1" bit, independent of the number of "0" bits in between. The following filter improves the output signal ER and changes slow-FM into fast-FM accompanied with sharp phase transition, generating RZ-AMI signal.

The 10-Gb/s generated RZ-AMI signal using CML showed a reach beyond 9000 km using DCF for CD compensation and high fiber nonlinearity robustness, similar to that generated using traditional MZM [127]. However, the electrical pre-coding procedures are reduced significantly for CML source with small footprint.

2.2.4 RZ-DPSK signal generation using CML

J. Franklin *et al.* demonstrated the generation of 2.67-Gb/s RZ-DPSK signal with PRBS of 2^7-1 using CML, without separate differential pre-coder and pulse carver [128]. The operation principle of RZ-DPSK generation using CML is shown in Fig. 2.8.

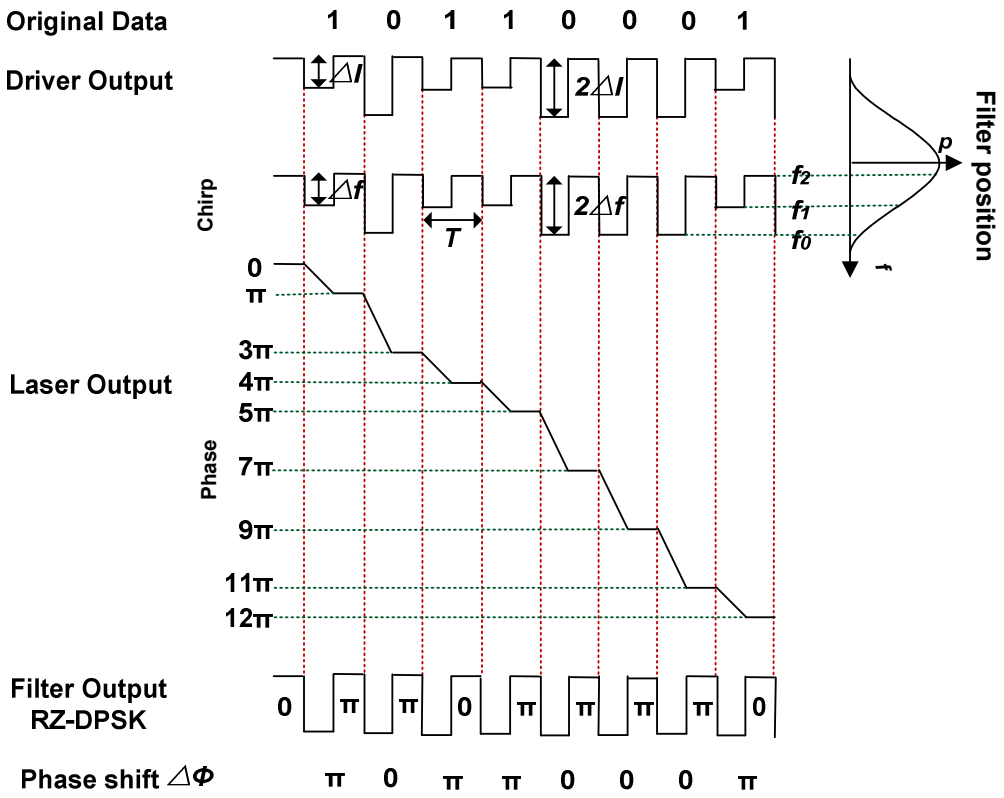

Fig. 2.8 Operation principle of RZ-DPSK signal generation using CML

The laser is biased high above the threshold and modulated with a three level RZ driver with duty cycle of 50%. The driver maps the input two-level digital data into three output levels. The current swings down from a high level to one of the two lower levels by ΔI or $2\Delta I$ for incoming 1 and 0 bits respectively, and returns back to the high level in half the bit period T. The drive amplitude is adjusted to generate adiabatic chirp of $\Delta f = 1/T$ or $2\Delta f = 2/T$ for the input current swings ΔI and $2\Delta I$ respectively. The produced adiabatic chirp shifts the phase of the optical field by

$$\Delta\emptyset = 2\pi \int_0^{T/2} \Delta f(t)dt \qquad (2.24)$$

during the two lower levels, resulting in phase shifts of π or 2π, for input 1 and 0 bits respectively. The three level intensity modulated signal that accompanies the frequency modulation is converted to a two level RZ signal by the following filter. As shown in Fig. 2.8., the laser wavelength is adjusted to the transmission edge of the filter, so that the high level frequency f_2 is near the peak transmission and the lower level frequencies f_1 and f_0 experience high loss. The filter edge also converts the adiabatic chirp into flat-top chirp with abrupt phase transitions at the lower levels. The resulting phase modulation is automatically differentially encoded due to the relationship between carrier phase and adiabatic chirp, eliminating the need for a differential pre-coder.

The present approach is distinguished from the pioneering work of R. S. Vodhanel [129], in which a DML was used to generate DPSK at 5 Gb/s. In that work, a DFB laser was modulated with an incoming signal that was differentially encoded and then differentiated to produce short pulses, a fraction of the bit period. The accompanying amplitude modulation resulted in an undesirable but small BER penalty.

The detected CML-based RZ-DPSK signal using DI had a 0.7-dB back-to-back (BtB) penalty relative to that using MZM transmitter at a BER of 10^{-9}. No differential pre-coder or pulse carver was used in the experiment, showing great simplicity. However, this approach requires the adiabatic chirp value of two times the data rate, which is difficult to obtain with the current relatively low FM efficiency value of standard DFB laser when the data rate goes up to 10 Gb/s or higher. Hence, this scheme is only operated at 2.67 Gb/s. The three level driving

signal also brings pattern dependence problem to this CML-based RZ-DPSK transmitter, limiting the PRBS length to 2^7-1. What's more, it is impossible to suppress the energy with different frequencies of f_0 and f_1 to equal, due to the finite sharpness of the filter. Therefore, the residual intensities on the space levels of the CML-based RZ-PPSK signal in this approach are uneven. They will cause intensity noises on detection. No transmission experiment was operated.

Chapter 3 Optical RZ Pulses Generation using CML

3.1 Optical RZ pulses generation using CML driven at half pulse rate

3.1.1 Introduction

As discussed in chapter one, optical RZ pulses have been widely used in high-speed optical fiber transmission systems with OOK and DPSK modulation formats, with the advantages of high robustness towards ISI, nonlinear distortions and higher receiver sensitivity. Conventionally, a sinusoidally-driven MZM is used as an external pulse carver to generate the optical RZ pulses. An alternative method is based on an optical PM followed by an optical DI. Mode-locked laser using an EAM as a mode locker is another candidate. However, external modulators suffer from the drawbacks of high cost, high insertion loss, and large driving voltage.

In this section, we demonstrate a cost-effective and power-consuming approach to generate high-speed optical RZ pulses using a CML, which integrates a directly modulated DFB laser and a DI periodic filter in a single laser package [130], without any external modulator for pulse carving. It is designed for access and metropolitan network applications. Both 33%-duty-cycle and 67%-duty-cycle optical RZ pulses are generated simultaneously at the two output ports of the DI in the CML. The frequency of the sinusoidal driving signal is half the repetition rate of the output optical RZ pulses. The transmission performances of 10-Gb/s CML-RZ-pulses based RZ-

DPSK signals with duty cycles of 33% and 67% have also been investigated. 70-km and 50-km error-free SSMF transmissions have been achieved for the 10-Gb/s 33%-duty-cycle and 67%-duty-cycle CML-RZ-pulses based RZ-DPSK signals, respectively, while those based on MZM-RZ-pulses generation could be transmitted up to 60 km. The former case also shows comparable fiber nonlinearity robustness in single-channel test, compared with the latter approach. With the development of 40-Gb/s DML technology [131], the proposed technique could generate ultra high-speed optical RZ pulses.

3.1.2 Operation principle

Fig. 3.1 depicts the proposed scheme and the operation principle of optical RZ pulses generation based on CML. Fig. 3.1(d) illustrates the structure of CML consisting of a DML and a DI. RZ pulses at a pulse rate of $2f$ Hz can be generated by directly modulating the built-in DML with a sinusoidal clock at a frequency of f Hz, and carefully set the frequency offset position of the built-in DI, which has a FSR value of $2f$ Hz, as shown in Fig. 3.1(a). The built-in DML is biased high above the threshold with the benefits of high output power, wide modulation bandwidth, single mode operation, and suppression of transient chirp. Fig. 3.1(c) shows the intensity and chirp characteristics of the built-in DML output signal. The laser generates an accompanying adiabatic chirp which follows the intensity waveform change. The peak level is blue shifted relative to the bottom level. The frequency deviation of $2\,\Delta f$ between the peak level and bottom level of the DML output signal equals the FSR of the built-in DI. If the DML output signal is biased at the DI transmission maximum, the 33%-duty-cycle RZ pulses at the pulse rate of $2f$ Hz are produced, as depicted in Fig. 3.1(b). If the DML output signal is biased at the DI transmission

minimum, it generates the 67%-duty-cycle RZ pulses at the pulse rate of 2*f* Hz.

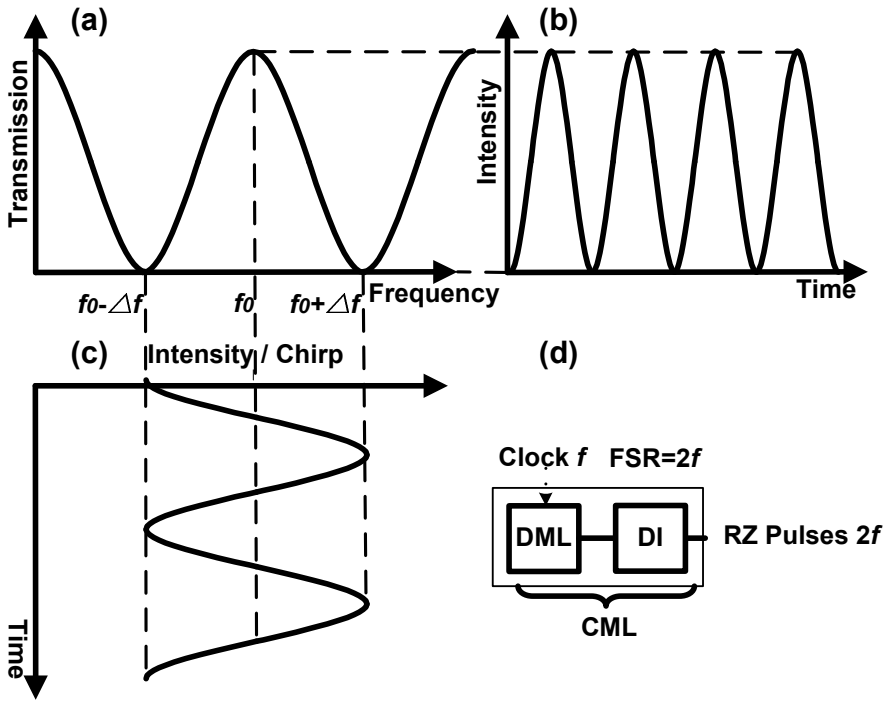

Fig. 3.1 Proposed scheme and operation principle of optical RZ pulses generation based on CML: (a) transmission function of DI, (b) CML output, (c) DML output, and (d) structure of CML

3.1.3 Experiments and results

We have experimentally demonstrated the generation and transmission of the 10-Gb/s RZ-DPSK signal using CML-RZ-pulses, as shown in Fig. 3.2. We employed a commercially available DML module (NEL: NLK5C5EBKA) and a commercially available DI to simulate the CML in the experiment. The input impedance, threshold current, and cut-off frequency of the DML were 50 ohms, 15 mA, and 18 GHz, respectively. The DI had a FSR of 10 GHz. The DML was directly modulated with a 5-GHz sinusoidal signal. The driving voltage V_{pp} was 2.3 V, and the laser was

biased at 80 mA. A $LiNbO_3$ single-waveguide PM was then employed so as to modulate the generated optical RZ pulses using a 10-Gb/s NRZ data with PRBS length of 2^{31}-1. The central wavelength of the generated optical RZ-DPSK signal was around 1551.3 nm. The measured powers of the DML output signal, the 33%-duty-cycle RZ pulses, and the 67%-duty-cycle RZ pulses were 6.7 dBm, 3.0 dBm, and 3.2 dBm, respectively. The linear transmission system was composed of a piece of SSMF. An EDFA was inserted after the fiber to boost up the optical power. A tunable optical band pass filter (OBPF) with ~1.0 nm bandwidth was placed after the EDFA to eliminate the excessive ASE noise. At the receiver, the transmitted RZ-DPSK signal was demodulated by another DI with a FSR of 10 GHz. We used a 12.5-GHz PD for BER measuring and a 40-GHz PD for eye diagrams recording at the same time for convenience.

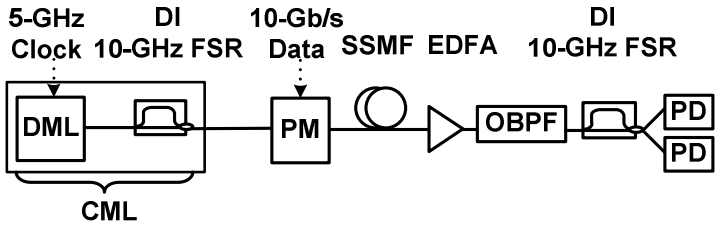

Fig. 3.2 Experimental setup of the 10-Gb/s CML-RZ-pulses based RZ-DPSK transmission system

Fig. 3.3 shows the BtB eye diagrams of the 5-GHz sinusoidal driving signal, the 5-GHz DML output signal, the 10-GHz 33%-duty-cycle RZ pulses, and the 10-GHz 67%-duty-cycle RZ pulses. The ERs of the 33%-duty-cycle RZ pulses and the 67%-duty-cycle RZ pulses were 10.8 dB and 9.8 dB, respectively. The respective ERs of the 33%-duty-cycle RZ pulses and the 67%-duty-cycle RZ pulses were 12.7 dB and 8.3 dB with a higher driving voltage of 2.7 V, while the respective ERs of the 33%-duty-cycle RZ pulses and the 67%-duty-cycle RZ pulses were 4.6 dB and 11.3 dB with a lower driving voltage of 1.7 V.

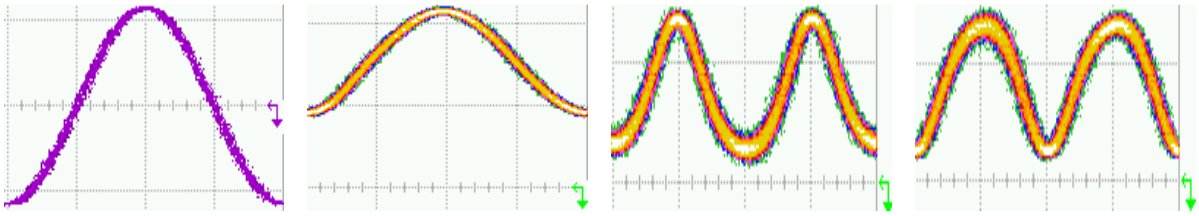

(a) 50 ps/div (b) 50 ps/div (c) 50 ps/div (d) 50 ps/div

Fig. 3.3 BtB eye diagrams of (a) 5-GHz sinusoidal driving signal, (b) 5-GHz DML output signal, (c) 10-GHz 33%-duty-cycle RZ pulses, and (d) 10-GHz 67%-duty-cycle RZ pulses. Time scale: 50 ps/div

Fig. 3.4 shows the BtB eye diagrams of the 20-GHz sinusoidal driving signal, the 20-GHz DML output signal, the 40-GHz 33%-duty-cycle RZ pulses, and the 40-GHz 67%-duty-cycle RZ pulses. The laser was biased at 120 mA and the driving voltage was 5.1 V. The DI here had a FSR of 40 GHz. The ERs of the 33%-duty-cycle RZ pulses and the 67%-duty-cycle RZ pulses were 5.6 dB and 4.1 dB, respectively. The poor ER made the measured duty cycle inaccurate. The ER of CML-RZ-pulses could be further enhanced by using DML with higher FM efficiency and DI with higher ER. Therefore, the proposed scheme could generate 40-Gb/s RZ-DPSK signal or 40-Gbaud RZ-DQPSK signal based on CML-RZ-pulses using the same module.

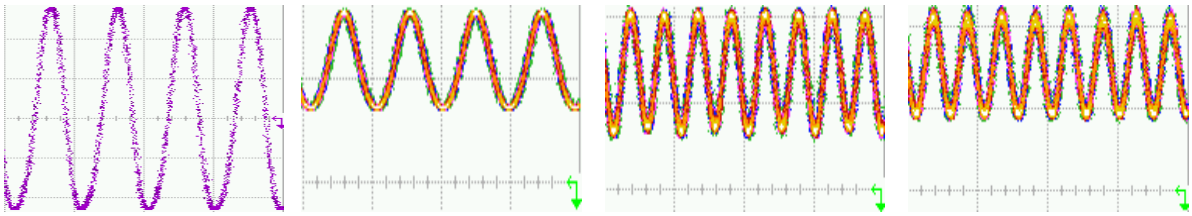

(a) 50 ps/div (b) 50 ps/div (c) 50 ps/div (d) 50 ps/div

Fig. 3.4 BtB eye diagrams of (a) 20-GHz sinusoidal driving signal, (b) 20-GHz DML output signal, ((c) 40-GHz 33%-duty-cycle RZ pulses, and (d) 40-GHz 67%-duty-cycle RZ pulses. Time scale: 50 ps/div

In the control experiment, we employed a DFB laser for CW light and a MZM as the pulse carver to generate the 10-GHz 33%-duty-cycle RZ pulses or 67%-duty-cycle RZ pulses. The

respective driving voltages were 7.6 V and 6.2 V. The insertion loss of the MZM was around 7 dB. The corresponding ERs of the 33%-duty-cycle RZ pulses and 67%-duty-cycle RZ pulses were 6.9 dB and 12.0 dB. The low ER of 33%-duty-cycle RZ pulse was due to the limited dynamic range of the modulator driving amplifier in our laboratory. Fig. 3.5 shows the respective optical spectra of the 10-GHz RZ pulses based on CML and MZM. The 10-GHz 33%-duty-cycle CML-based RZ pulses exhibited slightly more compact spectrum, as compared to that based on MZM. The 10-GHz 67%-duty-cycle CML-based RZ pulses exhibited the carrier-suppressed property with two 10-GHz-separated peaks, similar to that based on MZM, except that the two peaks were unequal in power, due to the residual intensity modulation of the DML output signal.

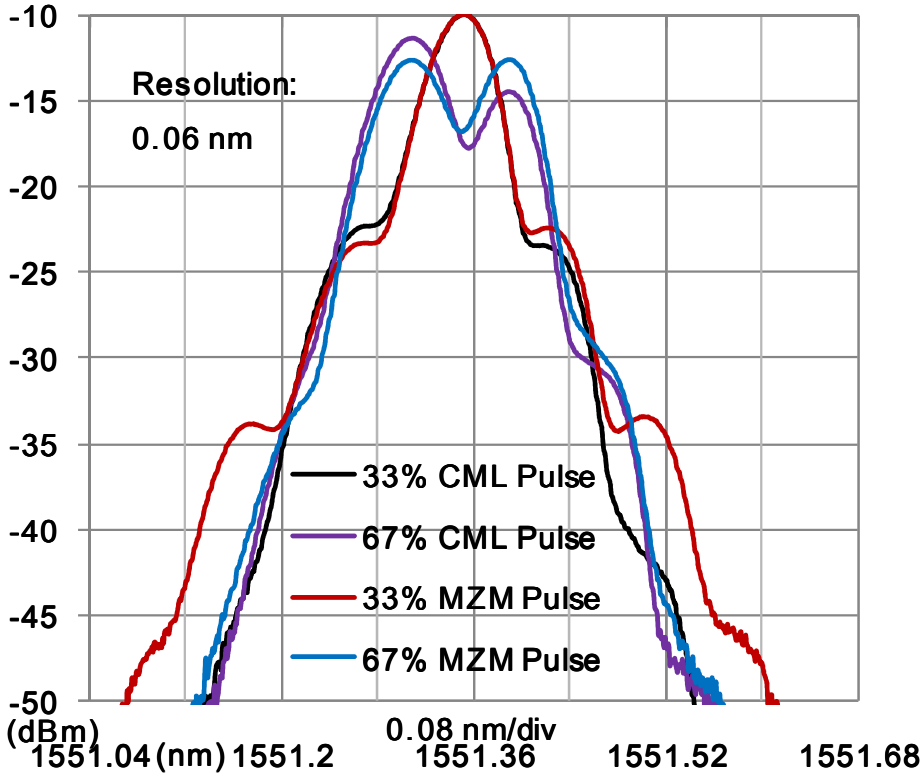

Fig. 3.5 Optical spectra of 10-GHz CML- and MZM-based RZ pulses

We have compared the transmission performances of fiber CD and nonlinearity tolerances between the 10-Gb/s CML-RZ-pulses based RZ-DPSK signal and the MZM-RZ-pulses based RZ-DPSK signal using single detection. The driving voltage of the DML was tuned to generate the 33%-duty-cycle CML-based RZ pulses with ER of 6.8 dB and the 67%-duty-cycle CML-based RZ pulses with ER of 11.3 dB, separately, for fair comparison with MZM cases. The DML bias was set to be 120 mA when generating the 67%-duty-cycle CML-based RZ pulses to suppress the inequality of the two spectral peaks shown in Fig. 3.5. The residual intensity modulation of the DML here could be completely removed by using FM-DBR laser [104]. Fig. 3.6 shows the BtB eye diagrams of demodulated 10-Gb/s CML-RZ-pulses based RZ-DPSK signals with duty cycles of 33% and 67% at the two output ports of the DI at the receiver. The uneven bottom line in Fig. 3.6(b) was attributed to the low ER of 33%-duty-cycle RZ pulses.

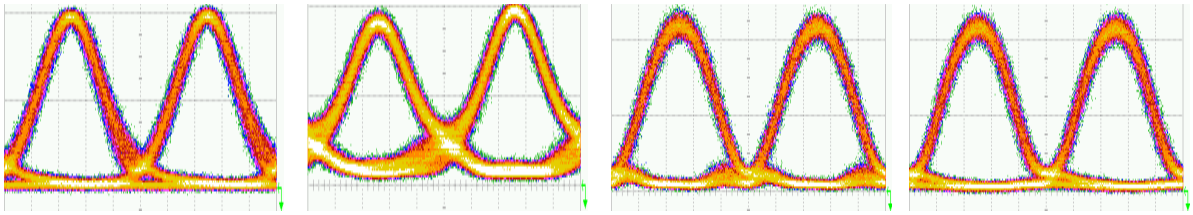

(a) 20 ps/div (b) 20 ps/div (c) 20 ps/div (d) 20 ps/div

Fig. 3.6 BtB eye diagrams of the demodulated 10-Gb/s RZ-DPSK signals with CML-based RZ pulses: (a) 33% at one port of the DI, (b) 33% at the other port of the DI, (c) 67% at one port of the DI, (b) 67% at the other port of the DI. Time scale: 20 ps/div

Fig. 3.7 depicts the receiver sensitivities at BER of 10^{-9} measured after various lengths of SSMF transmission for the 10-Gb/s RZ-DPSK signals based on CML-RZ-pulses and MZM-RZ-pulses. The insets show the respective eye diagrams of RZ-DPSK signals based on CML-RZ-pulses and MZM-RZ-pulses after SSMF transmission using the 40-GHz PD. There were still

reasonable eye openings for the CML-RZ-pulses based RZ-DPSK signals after SSMF transmission. The intensity noises shown in the eye diagrams would be alleviated by using the 12.5-GHz PD.

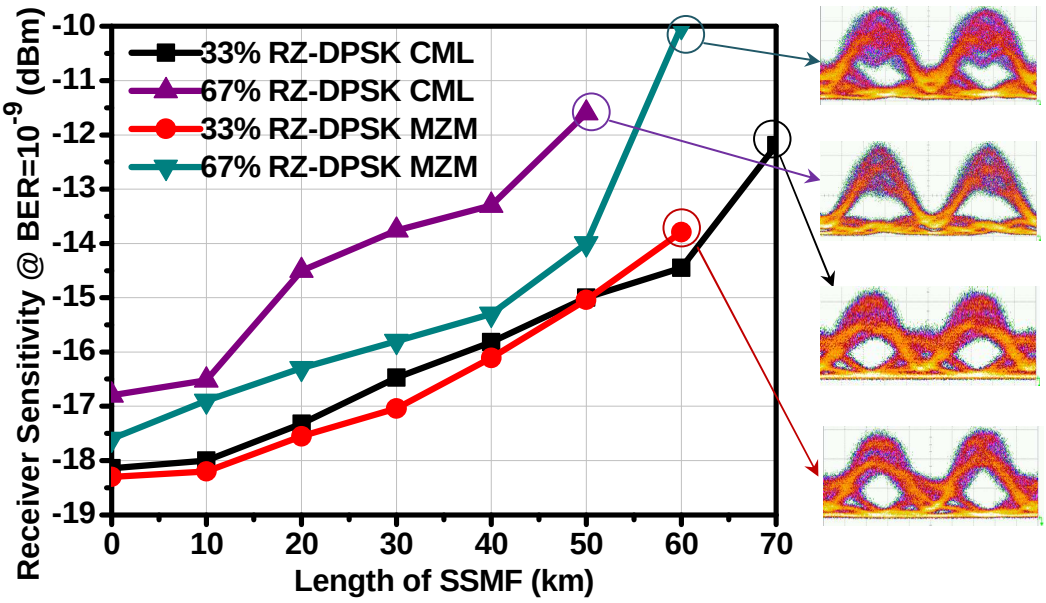

Fig. 3.7 Measured CD tolerance for 10-Gb/s RZ-DPSK signals based on CML and MZM. Insets show the respective eye diagrams after SSMF transmission using 40-GHz PD. Time scale: 20 ps/div.

Fig. 3.8 shows the measured BER performances for the 10-Gb/s RZ-DPSK signals based on CML-RZ-pulses and MZM-RZ-pulses. 70-km and 50-km error-free SSMF transmissions with power penalties of 6.0 dB and 5.2 dB were achieved for the 10-Gb/s CML-RZ-pulses based RZ-DPSK signals with duty cycles of 33% and 67%, respectively, with reference to their BtB receiver sensitivities at BER of 10^{-9}. No BER error floor was observed for the CML-RZ-pulses based RZ-DPSK signals after SSMF transmission. As for comparison, the MZM based ones could be transmitted up to 60-km with power penalties of 4.5 dB and 7.6 dB, respectively, with

reference to their BtB receiver sensitivities at BER of 10^{-9}.

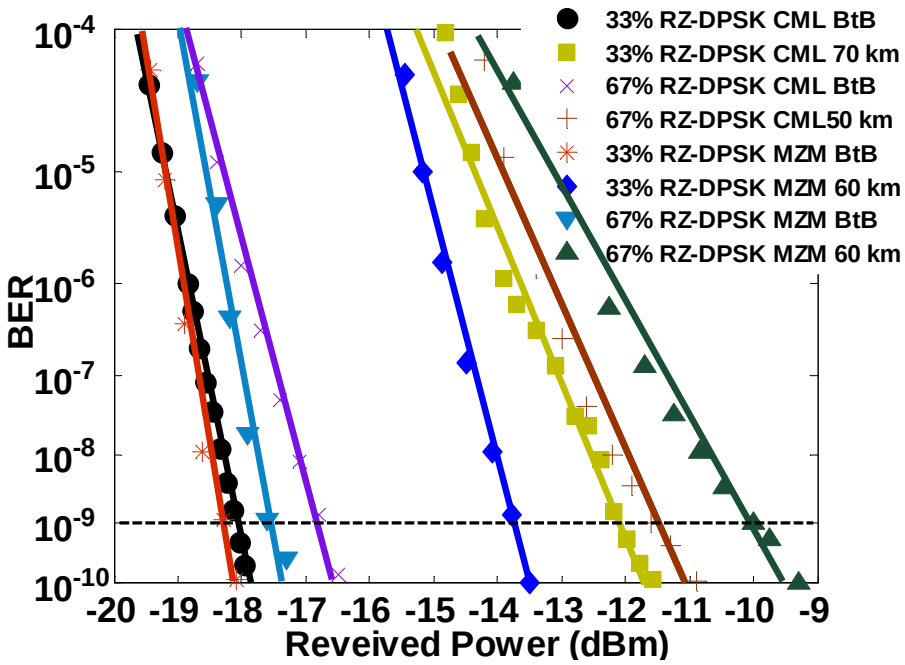

Fig. 3.8 BER measurements for 10-Gb/s RZ-DPSK signals based on CML and MZM.

We have further measured and compared the fiber nonlinearity tolerance of the 10-Gb/s RZ-DPSK signals based on CML-RZ-pulses and MZM-RZ-pulses in single-channel test. One span of 80-km SSMF was used. The CD of the SSMF was compensated with dispersion compensating module (DCM). The power launched into the SSMF was varied from 0 dBm to 16 dBm. The results were shown in Fig. 3.9. The CML-RZ-pulses based RZ-DPSK signals demonstrated comparable tolerance to high launch power, compared with the MZM-RZ-pulses based ones. With reference to their respective receiver sensitivities around BER of 10^{-9} at 0-dBm launch power, the 33%-duty-cycle CML-RZ-pulses based RZ-DPSK signal, 67%-duty-cycle CML-RZ-pulses based RZ-DPSK signal, 33%-duty-cycle MZM-RZ-pulses based RZ-DPSK signal, and 67%-duty-cycle MZM-RZ-pulses based RZ-DPSK signal, suffered from power penalties of 1.1

dB, 2.4 dB, 1.4 dB, and 0.8 dB, respectively, at launch power of 16 dBm. Their respective eye diagrams were shown in the insets of Fig. 3.9, using the 40-GHz PD.

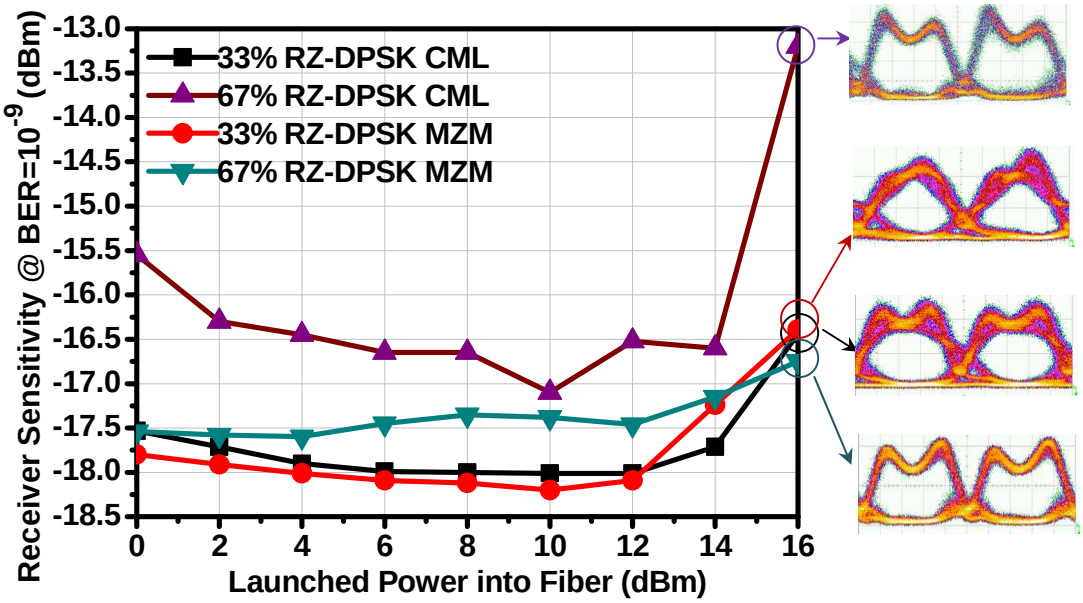

Fig. 3.9 Measured nonlinearity tolerance for 10-Gb/s RZ-DPSK signals based on CML and MZM. Insets show the respective eye diagrams at launch power of 16 dBm using 40-GHz PD. Time scale: 20 ps/div.

3.1.4 Discussion

Fig. 3.10 shows the operation principle of 67%-duty-cycle RZ pulses generation based on CML. The DML output signal is biased at the DI transmission minimum. The phase shift $\Delta\emptyset$ between the peak intensity and bottom intensity of DML output signal is given by

$$\Delta\emptyset = 2\pi \int_{T/4}^{3T/4} \Delta f(t)dt$$

$$= \frac{1}{2} \times 2\pi \times 2\Delta f . \frac{T}{2}$$

$$= \pi \tag{3.1}$$

where T is the time period of the sinusoidal driving signal. Therefore, there will be π phase change for the adjacent RZ pulses at the CML output. This proves that the CML-based 67%-duty-cycle RZ pulses are CSRZ-type.

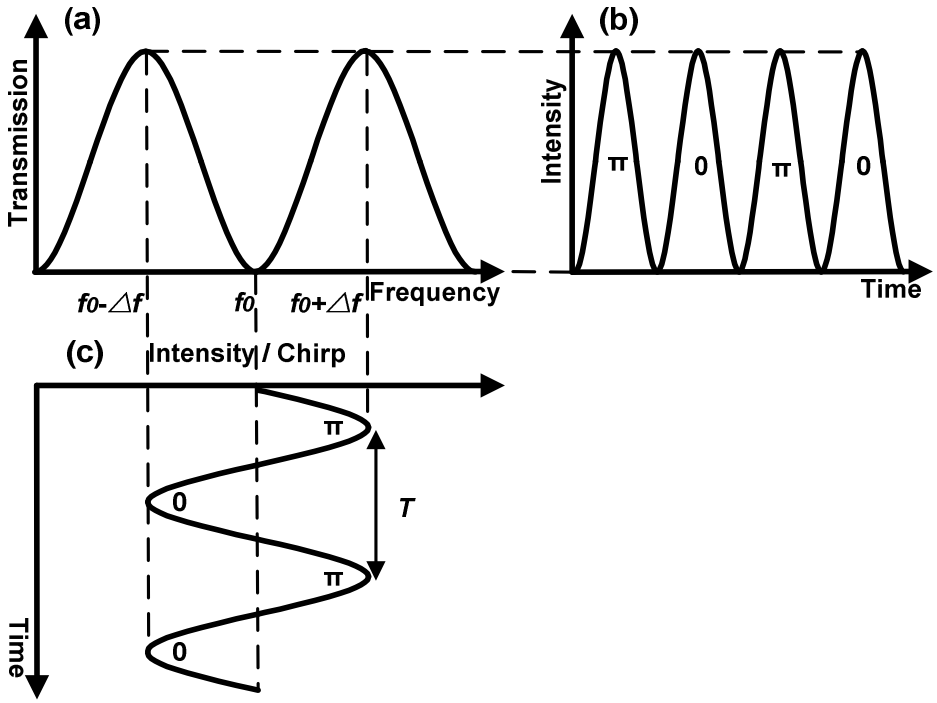

Fig. 3.10 Operation principle of 67%-duty-cycle RZ pulses generation based on CML: (a) transmission function of DI, (b) CML output, and (c) DML output.

3.1.5 Summary

In this section, we have proposed and experimentally demonstrated the generation of 33%-duty-

cycle and 67%-duty-cycle optical RZ pulses using CML, driven by a sinusoidal signal at half pulse rate, without any external pulse carver. The single channel transmission performances of 10-Gb/s RZ-DPSK signals based on CML-RZ-pulses such as tolerances in fiber CD and nonlinearity have been experimentally characterized and compared with the equivalents generated using MZM pulse carver. We have also discussed that the CML-based 67%-duty-cycle RZ pulses are CSRZ-type.

3.2 Optical RZ pulses generation using CML driven at one-fourth pulse rate

3.2.1 Introduction

As mentioned in chapter one, optical RZ pulses together with OOK and DPSK modulations show superior tolerance to the distortions induced by ISI, PMD, and nonlinear effects. These modulation formats also enjoy high receiver sensitivities. With the increased capacity of optical fiber communication systems, high-speed optical RZ pulses are desirable. The common way to generate optical RZ pulses is to use a MZM sinusoidally driven at the same or half pulse rate as an external pulse carver. To produce optical RZ pulses at higher speed, several schemes using external modulators were proposed. The RZ pulses generation at four-fold of the electrical clock was reported using a PM plus two polarization-maintaining fibers (PMFs) and two polarizers [132]. In [133], a RZ pulses generator comprising an overdriven MZM at one-fourth data rate and a following equalizer was investigated theoretically. However, the external modulators suffer from the drawbacks of extra cost, high insertion loss, and large driving voltage.

In the last section, we have demonstrated the generation of 10-GHz optical RZ pulses with duty cycles of 33% and 67% using CML, which integrates a directly modulated DFB laser and an optical DI periodic filter in a single laser package. The output optical RZ pulse rate is two times the frequency of the driving signal.

In this section, we propose and experimentally demonstrate the generation of 20-GHz 33%-duty-cycle and 20-GHz asymmetric-duty-cycle optical RZ pulses using CML driven at one-fourth pulse rate. No external modulator or additional equalizer is required. The transmission performance of 20-Gb/s CML-RZ-pulses based 33%-duty-cycle RZ-OOK signal in SSMF has also been investigated. It shows comparable fiber CD tolerance, compared with that generated via external pulse carver.

3.2.2 Operation principle

Fig. 3.11 depicts the proposed scheme and the operation principle of optical RZ pulses generation based on CML driven at one-fourth pulse rate. Fig. 3.11(d) illustrates the structure of CML consisting of a built-in DML and a built-in DI periodic filter. Optical RZ pulses at a pulse rate of $4f$ Hz can be generated by directly modulating the DML with an electrical clock at a frequency of f Hz, and carefully set the frequency offset position of the DI, which has a FSR value of $2f$ Hz, as shown in Fig. 3.11(a). The DML is biased high above the threshold with the benefits of high output power, single mode operation, wide modulation bandwidth, and suppression of transient chirp and residual intensity modulation. Fig. 3.11(c) shows the intensity and chirp characteristics of the DML output signal. The laser generates an accompanying adiabatic chirp which follows the intensity waveform change. The peak level is blue shifted

relative to the bottom level. The frequency deviation of $2\Delta f$ Hz between the peak level and bottom level of DML output signal equals two times the FSR of the DI. If the peak level and bottom level of DML output signal are set at the minimum of DI transmission function, the optical RZ pulses at the pulse rate of $4f$ Hz with 33% duty cycle will be produced, as depicted in Fig. 3.11(b). If the peak level and bottom level of DML output signal are set at the maximum of DI transmission function, as shown in Fig. 3.12, the optical RZ pulses at the pulse rate of $4f$ Hz with asymmetric duty cycle will be produced. For the latter case, the duty cycles for the adjacent optical RZ pulses are 33% and 67%, respectively. This technique could be generalized to generate the optical RZ pulses at six times the clock rate or even higher using CML with larger driving amplitude or higher FM efficiency.

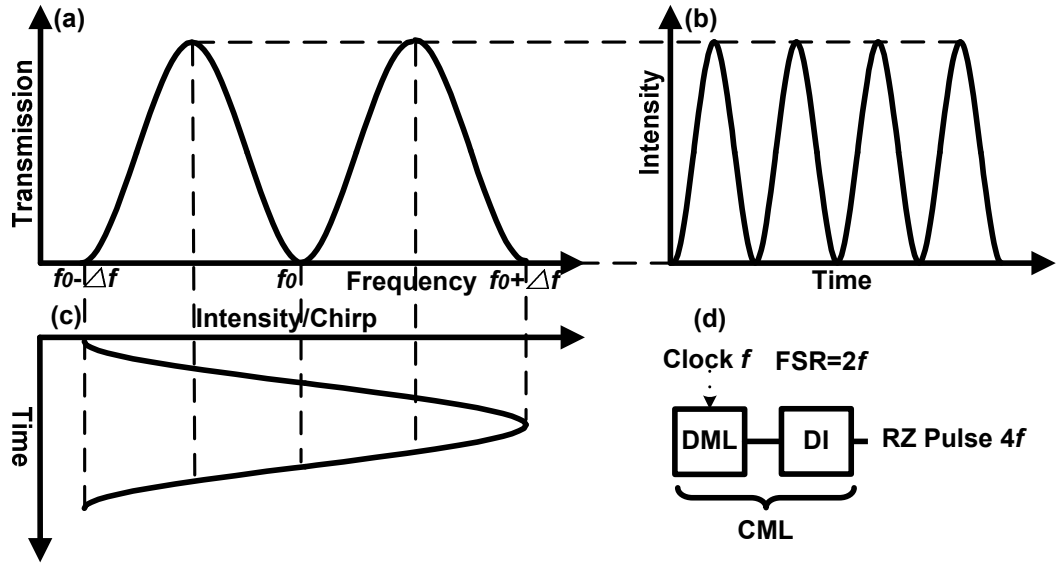

Fig. 3.11 Proposed scheme and operation principle of optical RZ pulses generation based on CML driven at one-fourth pulse rate: (a) transmission function of DI, (b) CML output, (c) DML output, and (d) structure of CML

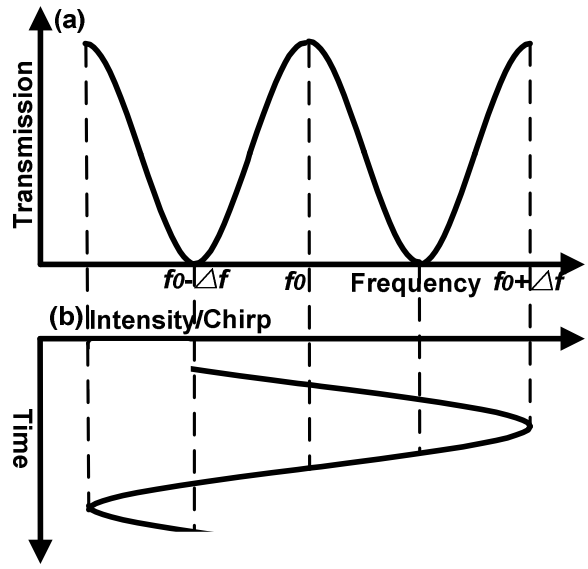

Fig. 3.12 Spectral position of DI for 4*f* asymmetric-duty-cycle optical RZ pulses generation based on CML: (a) transmission function of DI, and (b) DML output

3.2.3 Experiments and results

We have experimentally demonstrated the generation and transmission of the 20-Gb/s RZ-OOK signal using CML-based RZ pulses, as shown in Fig. 3.13. We employed a commercially available DML module (NEL: NLK5C5EBKA) and a commercially available DI to simulate the CML in the experiment. The input impedance, threshold current, FM efficiency, and cut-off frequency of the DML were 50 ohms, 15 mA, ~0.2 GHz/mA and 18 GHz, respectively. The DI had a FSR of 10.6 GHz. The DML biased at 180 mA was directly modulated with a 5-GHz electrical clock. The driving voltage was amplified to 4.9 V using an electrical amplifier (Amp.). An intensity modulator (IM) was then employed so as to modulate the generated optical RZ pulses with a 20-Gb/s 2^{31}-1 PRBS data. The central wavelength of the generated RZ-OOK signal

was around 1553.1 nm. The measured powers of the DML output signal, the 33%-duty-cycle RZ pulses, and the asymmetric-duty-cycle RZ pulses were 11.0 dBm, 6.7 dBm, and 7.9 dBm, respectively. The linear transmission system was composed of a piece of 10-km SSMF. An EDFA was inserted after fiber to boost up the optical power. A tunable OBPF with ~1.0 nm bandwidth was placed after the EDFA to eliminate the ASE noise. At the receiver, the transmitted RZ-OOK signal was detected using a 35-GHz photoreceiver containing a waveguide-integrated pin-photodiode and a transimpedance amplifier (TIA). The detected signal was demultiplexed by a 1:4 electrical demultiplexer (DEMUX) and then sent to the BER-tester (BERT) for BER measuring. In the control experiment, we employed a DFB laser for CW light and a MZM driven by 20-GHz clock as external pulse carver to generate the 20-GHz optical RZ pulses. The driving voltage and insertion loss of the MZM were 4.1 V and 8.2 dB, respectively.

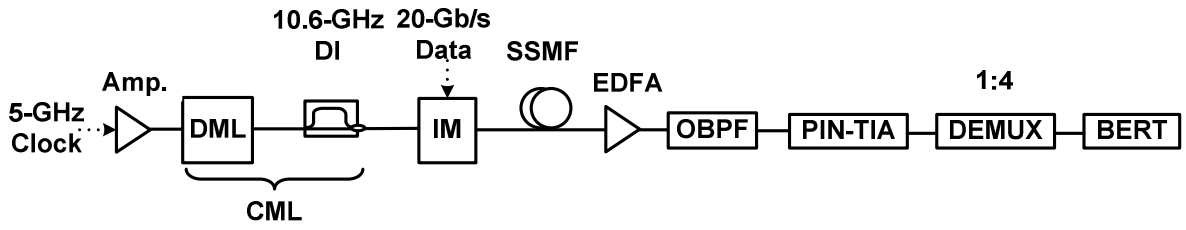

Fig. 3.13 Experimental setup of the 20-Gb/s CML-RZ-pulses based RZ-OOK transmission system

Fig. 3.14(a)-(e) show the BtB eye diagrams of the 5-GHz electrical clock, the 5-GHz DML output signal, the 20-GHz CML-based 33%-duty-cycle RZ pulses, the 20-GHz CML-based asymmetric-duty-cycle RZ pulses, and the 20-GHz MZM-based RZ pulses. The ERs of the 20-GHz CML-based 33%-duty-cycle RZ pulses, the CML-based asymmetric-duty-cycle RZ pulses, and the MZM-based RZ pulses were 9.4 dB, 7.8 dB and 11.1 dB, respectively. When the driving voltage of DML was improved to 8.0 V, the 30-GHz CML-based RZ pulses would be produced, which was six times the clock rate. Fig. 3.14(f)-(g) show the BtB eye diagrams of the 30-GHz

CML-based 33%-duty-cycle RZ pulses and the asymmetric-duty-cycle RZ pulses with ERs of ~6.0 dB. The intensity fluctuations of the 30-GHz CML-based RZ pulses could be eliminated by using a DI with a FSR of 10 GHz and further suppressing the residual intensity modulation of the DML output signal. On the other hand, the ER of the CML-based RZ pulses could be further enhanced by using DML with larger FM efficiency and DI with higher ER.

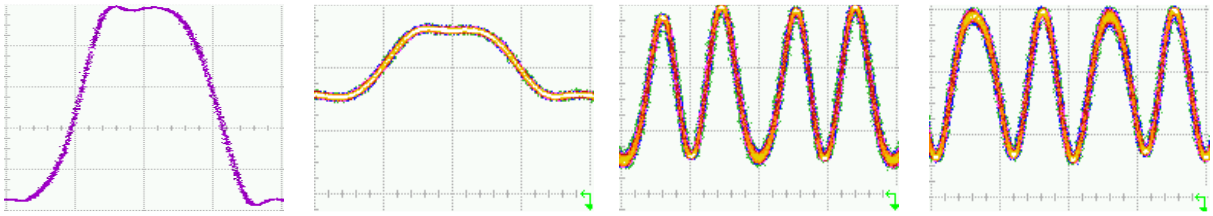

(a) 50 ps/div (b) 50 ps/div (c) 50 ps/div (d) 50 ps/div

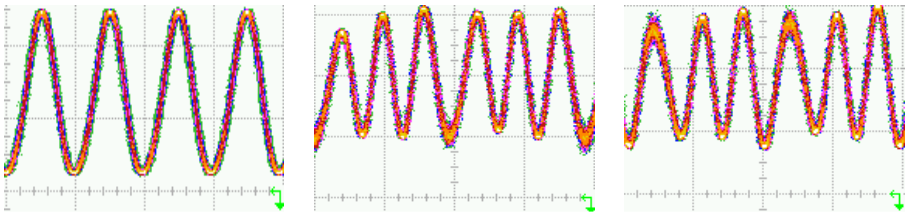

(e) 50 ps/div (f) 50 ps/div (g) 50 ps/div

Fig. 3.14 Eye diagrams of the (a) 5-GHz electrical clock, (b) 5-GHz DML output signal, (c) 20-GHz CML-based 33%-duty-cycle RZ pulses, (d) 20-GHz CML-based asymmetric-duty-cycle RZ pulses, (e) 20-GHz MZM-based RZ pulses, (f) 30-GHz CML-based 33%-duty-cycle RZ pulses, and (g) 30-GHz CML-based asymmetric-duty-cycle RZ pulses. Time scale: 50 ps/div

Fig. 3.15 shows the respective optical spectra of the 5-GHz DML output signal and 20-GHz CML-based RZ pulses. The spectrum of the 5-GHz DML output signal shows that 20-GHz adiabatic chirp was generated by directly modulating the DFB laser. The spectrum of the 20-GHz CML-based 33%-duty-cycle RZ pulses denotes that the DI worked as a periodic filter to extract spectral components spaced by 10 GHz. The 20-GHz CML-based asymmetric-duty-cycle RZ pulses exhibited carrier-suppressed property with two 20-GHz-separated peaks.

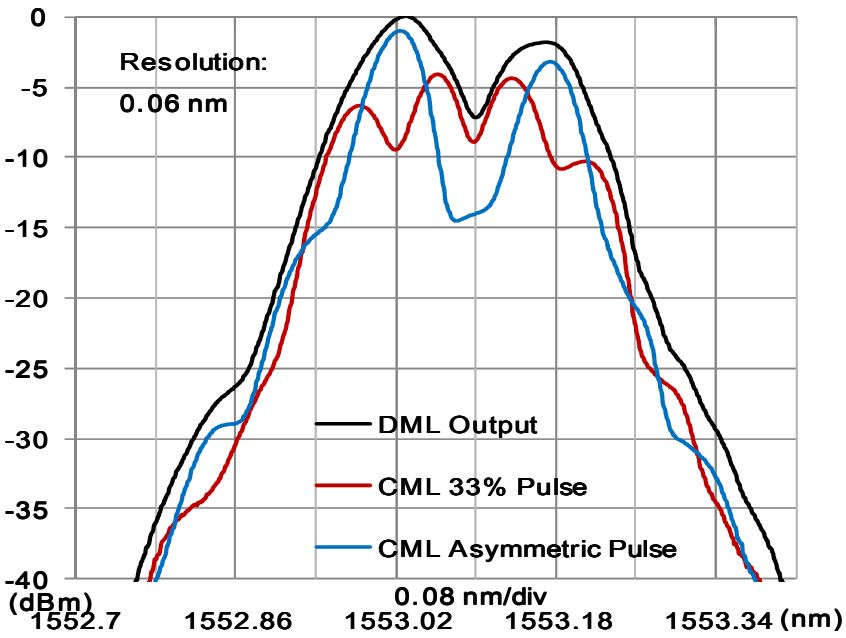

Fig. 3.15 Optical spectrum of the 5-GHz DML output signal and 20-GHz CML-based RZ pulses

We have compared the transmission performance of fiber CD tolerance between the 20-Gb/s CML-RZ-pulses based and MZM-RZ-pulses based RZ-OOK signals. Fig. 3.16 shows the eye diagrams of 20-Gb/s CML-based and MZM-based signals before and after 10-km SSMF. The 20-Gb/s CML-based 33%-duty-cycle RZ-OOK signal showed comparable eye opening after 10-km SSMF, compared with that based on MZM. However, the 20-Gb/s CML-based asymmetric-duty-cycle RZ-OOK signal showed uneven intensities for adjacent bits after 10-km SSMF. Fig. 3.17 shows the measured BER performances for the 20-Gb/s CML-based and MZM-based RZ-OOK signals before and after 10-km SSMF. The 20-Gb/s CML-based 33%-duty-cycle RZ-OOK signal suffered a power penalty of 0.44 dB at BER of 10^{-9} after transmission, with reference to its BtB receiver sensitivity of -10.86 dBm. The BtB receiver sensitivity at BER of 10^{-9} of the 20-Gb/s CML-based asymmetric-duty-cycle RZ-OOK signal was -11.17 dBm. As a reference, the 20-Gb/s MZM-based RZ-OOK signal suffered a power penalty of 1.56 dB at BER

of 10^{-9} after transmission, compared with its BtB receiver sensitivity of -12.16 dBm

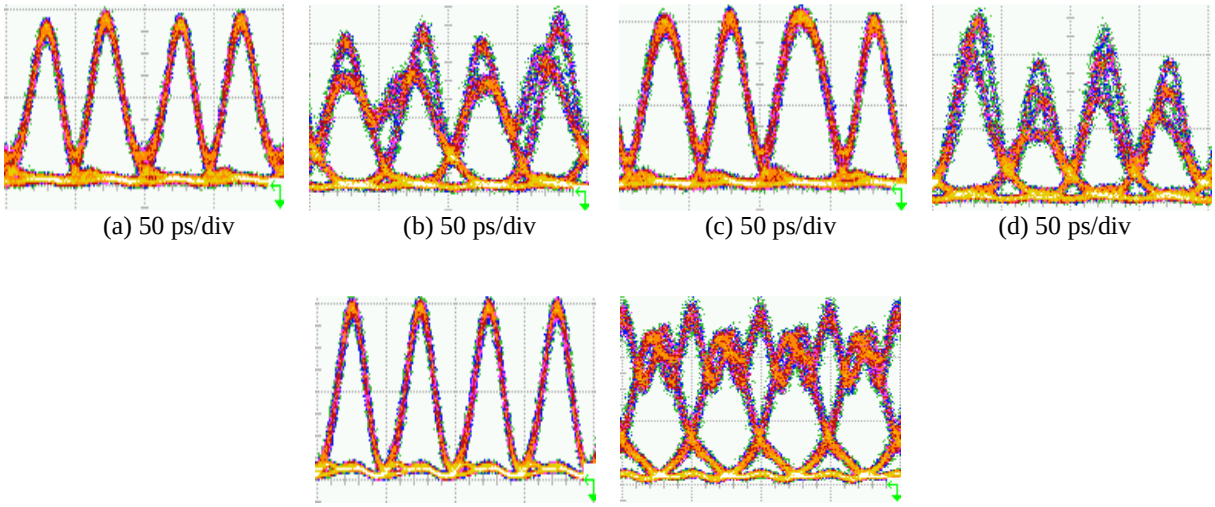

(a) 50 ps/div (b) 50 ps/div (c) 50 ps/div (d) 50 ps/div

(e) 50 ps/div (f) 50 ps/div

Fig. 3.16 Eye diagrams of the 20-Gb/s (a)-(b) CML-based 33%-duty-cycle RZ-OOK signal, (c)-(d) CML-based asymmetric-duty-cycle RZ-OOK signal, and (e)-(f) MZM-based RZ-OOK signal before and after 10-km SSMF. Time scale: 50 ps/div

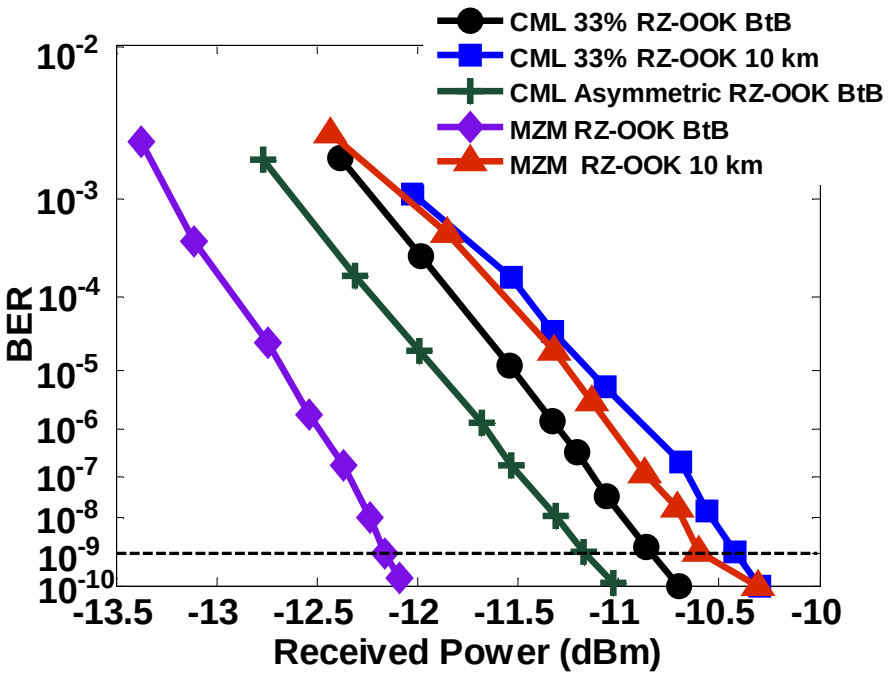

Fig. 3.17 BER performances for 20-Gb/s CML- and MZM-based RZ-OOK signals before and after 10-km SSMF

3.2.4 Summary

In this section, we have proposed and experimentally demonstrated the generation of 20-GHz 33%-duty-cycle and asymmetric-duty-cycle optical RZ pulses using CML driven by 5-GHz clock. No external modulator or additional equalizer is needed. The tolerance in fiber CD of the 20-Gb/s RZ-OOK signals based on CML has been experimentally characterized and compared with that generated using MZM. The extension to optical RZ pulses generation at even higher fold rate using CML is also investigated preliminarily.

3.3 Summary and discussion

In this chapter, we have proposed and experimentally demonstrated the generation of 10-GHz optical RZ pulses using CML driven by half pulse rate and 20-GHz optical RZ pulses using CML driven one-fourth pulse rate. The working rule is established on the designed adiabatic chirp with sinusoidal shape, which is further reshaped with a DI periodic filter. The RZ-DPSK and RZ-OOK signals based on the CML-RZ-pulses with different duty cycles show good transmission performances of CD and nonlinearity tolerance, comparable with the equivalents using MZM. Moreover, CML occupies smaller device space, takes lower cost, and consumes less power than MZM transmitter.

The laser bias plays an important role in generation of optical RZ pulses using CML. Higher bias would further suppress the residual intensity modulation of DML, though it could not be completely suppressed. To further improve the quality of CML-based RZ-pulses, FM-

DBR laser which has constant output power can be used to suppress the residual intensity modulation of DML.

The inherent transfer curve of CML-based RZ-pulse transmitter is similar to that using MZM, governed by the trigonometric function, resulting in the same duty-cycle RZ pulses. Nevertheless, the obtained ER will affect the actual duty cycle of RZ pulses achieved in the experiment, especially when the ER is poor. Therefore, the ER enhancement of DI is another important technical aspect for consideration to improve the performance of CML-based RZ-pulses.

For the generation of optical RZ pulses with higher pulse rate using CML, either driven by the higher-frequency sinusoidal signal or driven by the larger-amplitude sinusoidal signal, the laser with large modulation bandwidth and high FM efficiency is essential.

Chapter 4 *M*-ary RZ-DPSK Signals Generation using CML

4.1 RZ-DPSK signal generation using CML and pulse carver

4.1.1 Introduction

As described in chapter one, RZ-DPSK is a promising modulation format in long-haul WDM transmission system due to the advantages of 3-dB higher receiver sensitivity than OOK when using balanced detection and robustness against fiber PMD and nonlinearities. The typical RZ-DPSK transmitter is based on MZM or PM for external phase modulation and electrical pre-coder for differential encoding. Nevertheless, external modulators suffer from the drawbacks of high cost, high insertion loss, and large driving voltage. What's more, electrical pre-coder increases extra cost, footprint, and power consumption for the transmitter.

In chapter two, 2.67-Gb/s RZ-DPSK signal was obtained using CML [128]. No external modulator or differential pre-coder was used. The CML showed comparable BtB receiver sensitivity to a $LiNbO_3$ MZM transmitter with separate phase coding. However, the operation speed of that scheme is hardly scalable to 10 Gb/s due to the required high adiabatic chirp value, which is two times the modulation frequency. The PRBS length of the driving signal was limited to 2^7-1 for the three-level driving signal. No transmission performance was studied.

In this section, we demonstrate a new approach to generate RZ-DPSK signal using CML and pulse carver at higher date rate (10 Gb/s) and with longer PRBS data (2^{31}-1). We employ a

commercially available 10-Gb/s CML (Finisar DM80-01), which is the same as the one used in [128]. No differential encoder or PM is required. The driving signal for the CML is in two-level Inverse-RZ (IRZ) format, instead of three-level RZ format. The required adiabatic chirp value is the same as the data rate. After 70-km transmission on SSMF without CD compensation, the proposed CML-based 10-Gb/s RZ-DPSK signal shows about 3-dB higher receiver sensitivity and comparable nonlinear tolerance performance, compared with that generated by a conventional $LiNbO_3$ PM.

4.1.2 Operation principle

Fig. 4.1 depicts the proposed scheme of 10-Gb/s RZ-DPSK transmission system based on CML and pulse carver. The transmitter consists of an IRZ driver, a CML, and a pulse carver.

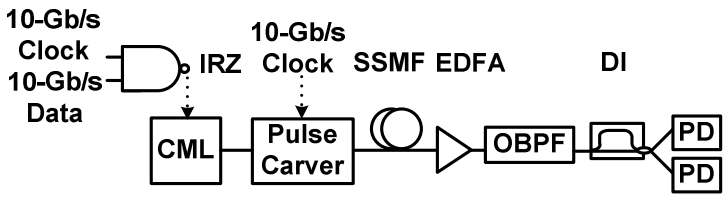

Fig. 4.1 Proposed scheme of 10-Gb/s RZ-DPSK transmission system based on CML and pulse carver

Fig. 4.2 illustrates the operation principle through intensity, frequency and phase characteristics of output signals of the driver, DFB laser (inside CML), filter (inside CML), and pulse carver. The IRZ-shaped data sequence 10111001 with a duty cycle of 50% is generated, via a commercial logic NAND gate with power consumption of 275 mW, before being used to directly modulate the CML. The laser is biased high above the threshold with the benefits of high output power, single mode operation, wide modulation bandwidth, and suppression of transient

chirp. The driving voltage V_{pp} is adjusted to induce adiabatic chirp Δf given by

$$\Delta f = 1/T \tag{4.1}$$

where T is time period of the driving signal. The adiabatic chirp generates phase shift $\Delta\emptyset$, which is governed by

$$\Delta\emptyset = 2\pi \int_0^{\frac{T}{2}} \Delta f(t)dt$$

$$= 2\pi \times 1/T \times T/2$$

$$= \pi \tag{4.2}$$

during low level period. Here, the adiabatic chirp value required for the 10-Gb/s RZ-DPSK is 10 GHz while 20 GHz would be necessary in [128]. The relative spectral locations of the DFB laser and filter in CML are detuned to pass the signal component with high level frequency f_1 and suppress the signal component with the low level frequency f_0 to increase the ER of the optical signal. This filter also helps to change the slowly changing phase shifts into abrupt phase transitions. The output of the filter is an IRZ-DPSK signal, in which both the intensity and differentially encoded phase carry the same data information. The pulse carver carves the second half-bit of the phase-modulated signal, thus generating the RZ-DPSK signal with a duty cycle of 50%. The phase modulation is intrinsically differentially encoded, similar to [128]. No differential encoder or PM is needed. This scheme could be generalized to generate RZ-DQPSK signal, where the two input data streams are in IRZ format with different V_{pp} and are combined by a passive RF combiner to drive the CML.

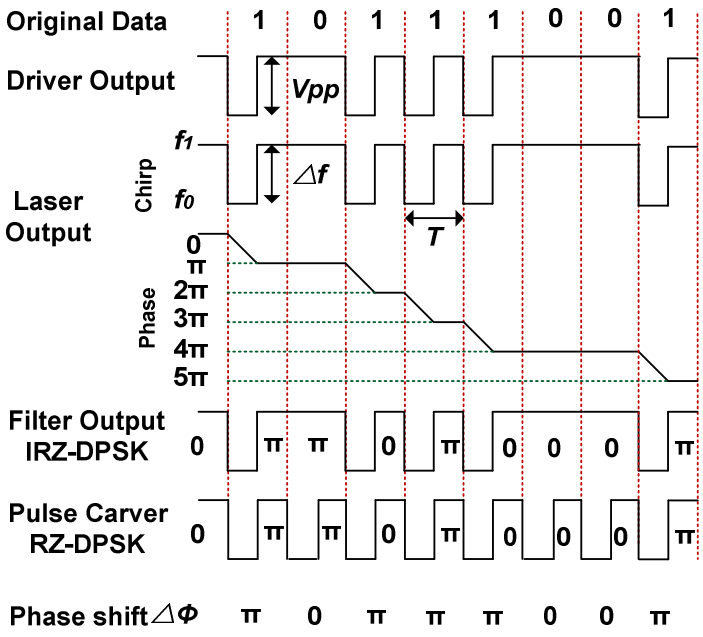

Fig. 4.2 Operation principle of RZ-DPSK signal generation based on CML and pulse carver

4.1.3 Experiments and results

We have experimentally demonstrated the proposed 10-Gb/s RZ-DPSK transmission system based on CML and pulse carver, as shown in Fig. 4.1. We used a standard CML module (Finisar DM80-01) in the experiment. The input impedance, threshold current, and FM efficiency of the DFB laser were 50 ohms, 25 mA, and 0.24 GHz/mA, respectively. The filter in DM80-01 had a 3-dB bandwidth of 11 GHz and an average slope of 1.5 dB/GHz. The DFB laser was directly modulated with a 10-Gb/s 2^{31}-1 PRBS IRZ data. The driving voltage V_{pp} was ~2.0 V. The laser was biased at 80 mA. The central wavelength of signal after the filter was 1555.48 nm. A MZM driven by 10-Gb/s clock was used as the pulse carver. The output power after the pulse carver

was ~0.2 dBm. The linear transmission system was composed of SSMF. An EDFA was inserted after fiber to boost up the optical power. A tunable OBPF with ~1.0 nm bandwidth was placed after the EDFA to eliminate the ASE noise. At the receiver, the transmitted RZ-DPSK was demodulated by a 1-bit optical DI before being detected by the PD.

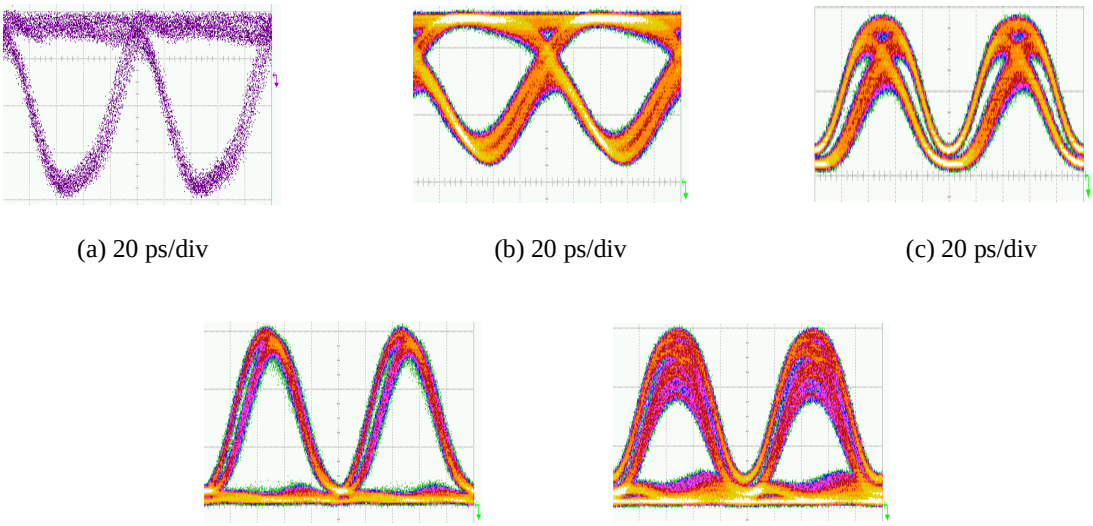

(a) 20 ps/div (b) 20 ps/div (c) 20 ps/div

(d) 20 ps/div (e) 20 ps/div

Fig. 4.3 Eye diagrams of (a) IRZ driving signal, (b) IRZ-DPSK signal, (c) RZ-DPSK signal, (d) demodulated RZ-DPSK signal at the destructive port of DI, and (e) demodulated RZ-DPSK signal at the constructive port of DI.

Fig. 4.3 shows the BtB eye diagrams of the IRZ driving signal after the driver, IRZ-DPSK signal after CML, RZ-DPSK signal after the pulse carver, and demodulated RZ-DPSK signals at the two output ports of the DI. The double line of the RZ-DPSK signal, as shown in Fig. 4.3(c), was due to the wide bandwidth of IRZ driving signal and the limited bandwidth of the DFB laser and filter in CML [134], as denoted in Fig. 4.3(b). Demodulated RZ-DPSK signal at the destructive port of the DI, as shown in Fig. 4.3(d), had better performance than the one at the constructive port of DI, as shown in Fig. 4.3(e). This phenomenon was mainly attributed to the asymmetric shape and noise of the driving signal as shown in Fig. 4.3(a) and the limited

bandwidth of DFB laser and filter in the CML. The CML based RZ-DPSK signal would have better performance using a CML with high modulation bandwidth and a periodic DI filter [130].

Fig. 4.4(a) shows the waveform traces at the IRZ driver output measured by a real-time oscilloscope. The 10111001 bit sequence was applied to the transmitter. Fig. 4.4 (b) show the detected outputs of the two ports of DI without transmission, respectively. The subtraction of the top and bottom demodulated waveforms, as shown in Fig. 4.4(b), would regenerate the input bit sequence correctly. It illustrated that no differential encoding of the original data was required for the CML-based RZ-DPSK signal.

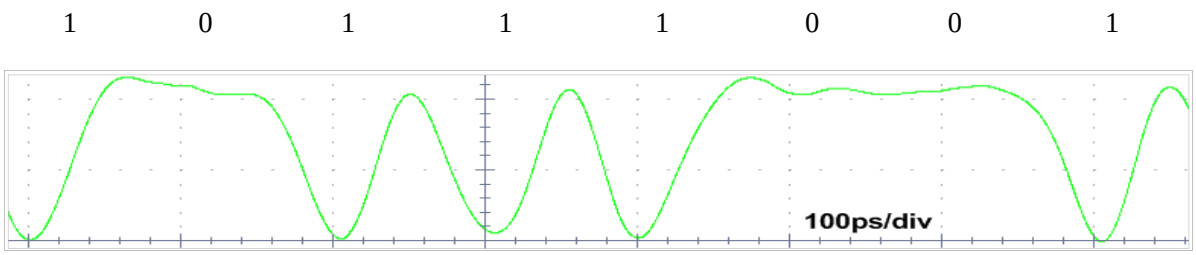

(a) 100 ps/div

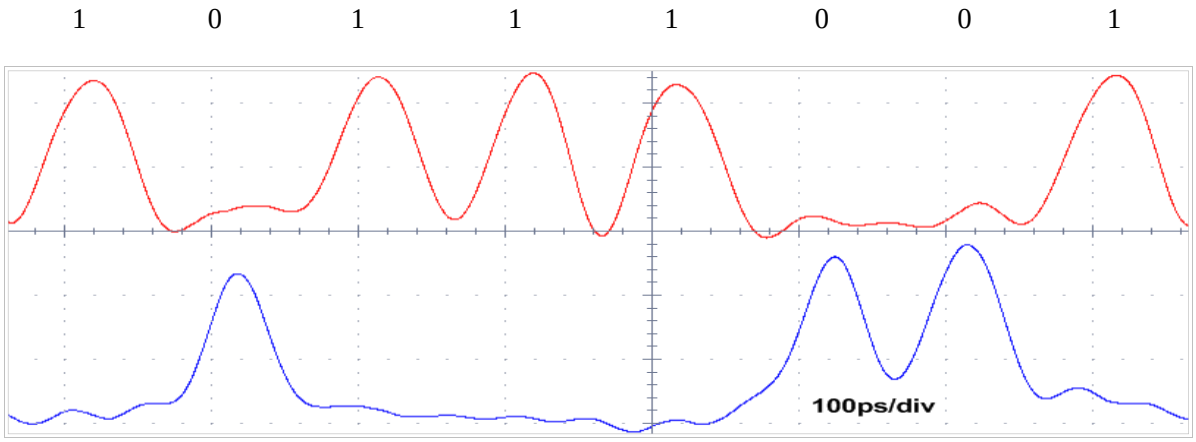

(b) 100 ps/div

Fig. 4.4(a) IRZ driving waveform for 10111001 bit sequence after the IRZ driver, and (b) demodulated waveforms for 10111001 bit sequence at the two output ports of DI. Time scale: 100 ps/div.

We compared the BtB tolerances in fiber CD and nonlinearity between the proposed CML-based RZ-DPSK transmitter and the $LiNbO_3$-PM-based RZ-DPSK transmitter, using 2^{31}-1 PRBS data. The PM-based RZ-DPSK transmitter was composed of a wavelength tunable DFB laser for CW light, a $LiNbO_3$ PM for external phase modulation, and a pulse carver for signal carving. Due to the lack of balanced detector, only the demodulated RZ-DPSK signal at the destructive port of DI was detected for comparison.

Fig. 4.5 shows the optical spectrum of the CML-based RZ-DPSK signal. It exhibited relatively more compact spectrum, as compared to that of PM-based RZ-DPSK signal. Thus it had better tolerance in fiber CD.

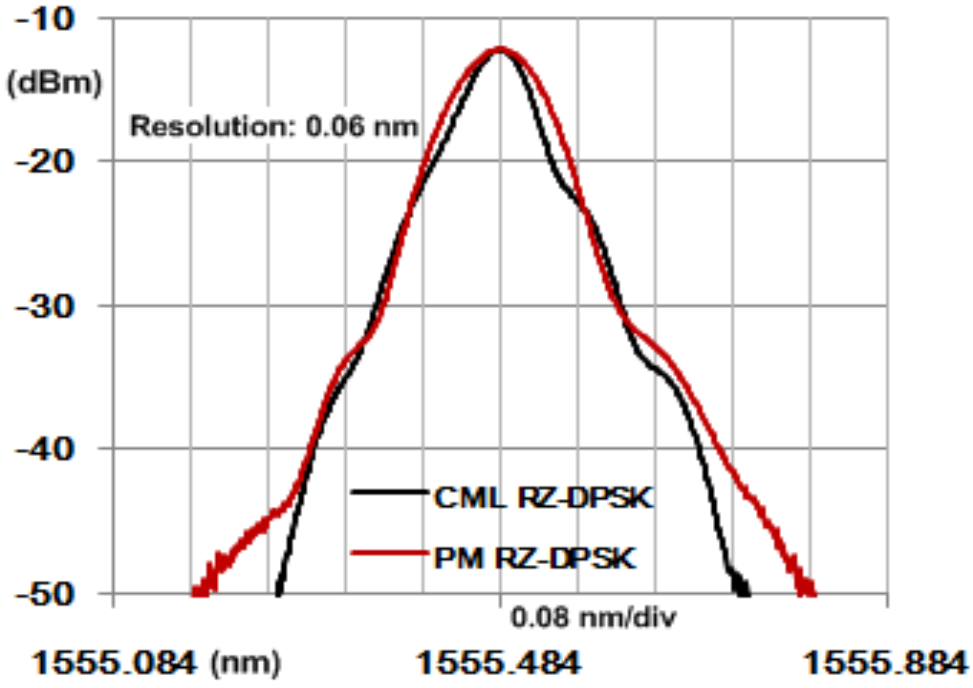

Fig. 4.5 Optical spectra of CML- and PM-based RZ-DPSK signals

Fig. 4.6 depicts the receiver sensitivities at BER of 10^{-9} measured after various lengths of SSMF transmission. The insets of Fig. 4.6 show that CML-based RZ-DPSK signal had much

clearer eye diagram than PM-based RZ-DPSK signal after 70-km SSMF transmission.

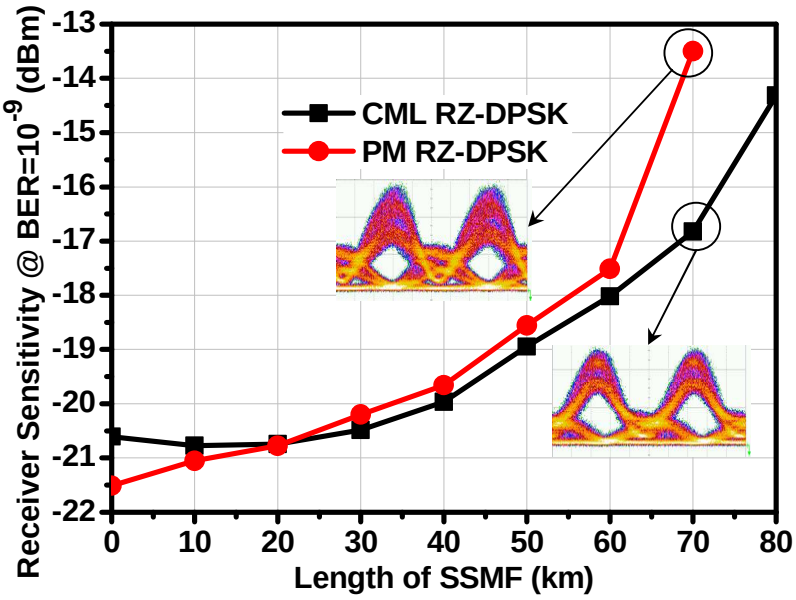

Fig. 4.6 Measured fiber CD tolerances for CML-based RZ-DPSK signal and PM-based RZ-DPSK signal. Insets show the respective eye diagrams after 70-km SSMF transmission. Time scale: 20 ps/div.

Fig. 4.7 shows the measured BER performances for the CML-based RZ-DPSK signal and PM- based RZ-DPSK signal. The BtB receiver sensitivities for the CML-based RZ-DSPK signal and the PM-based RZ-DSPK signal were -20.6 dBm and -21.5 dBm, respectively. The 0.9-dB difference in BtB receiver sensitivity was due to the asymmetric shape and noise of the driving signal and the limited bandwidth of the DFB laser and filter in the CML. 80-km error-free SSMF transmission was achieved for the CML-based 10-Gb/s RZ-DPSK signal, while the PM-based 10-Gb/s RZ-DPSK signal could only be transmitted up to 70 km with error-free performance. After 70-km SSMF transmission, their respective power penalties were 3.8 dB and 8.0 dB, with reference to their BtB receiver sensitivities.

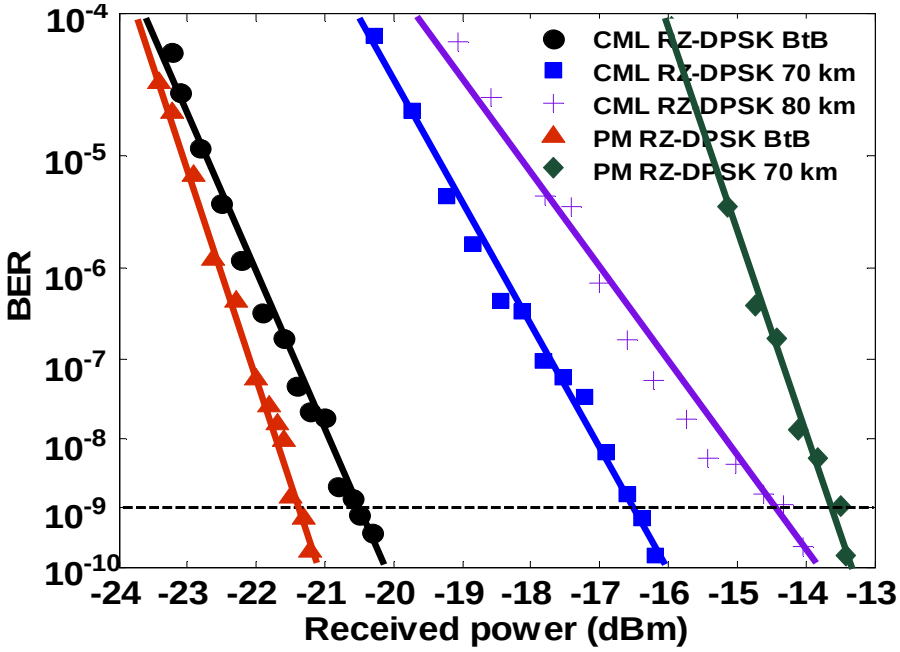

Fig. 4.7 BER measurements for the 10-Gb/s CML-based RZ-DPSK signal and PM-based RZ-DPSK signal.

We have further measured and compared the fiber nonlinearity tolerance of both CML-based RZ-DPSK signal and PM-based RZ-DPSK signal. One span of 80-km SSMF was used in this study. The fiber CD of the SSMF was compensated with DCM. The power launched into the SSMF was varied from 0 dBm to 16 dBm. The results of fiber nonlinearity tolerance for the two cases were shown in Fig. 4.8. The CML-based RZ-DPSK signal demonstrated comparable tolerance to high launch powers, compared with the PM-based RZ-DPSK signal. With reference to their respective receiver sensitivities at 0-dBm launch power, the CML-based RZ-DPSK signal and PM-based RZ-DPSK signal suffered from 1.1-dB and 1.3-dB power penalties, respectively, at launch power of 16 dBm. At launch power of 14 dBm, their respective power penalties were 0 and 0.6 dB. The insets of Fig. 4.8 show their corresponding eye diagrams at launch power of 16 dBm.

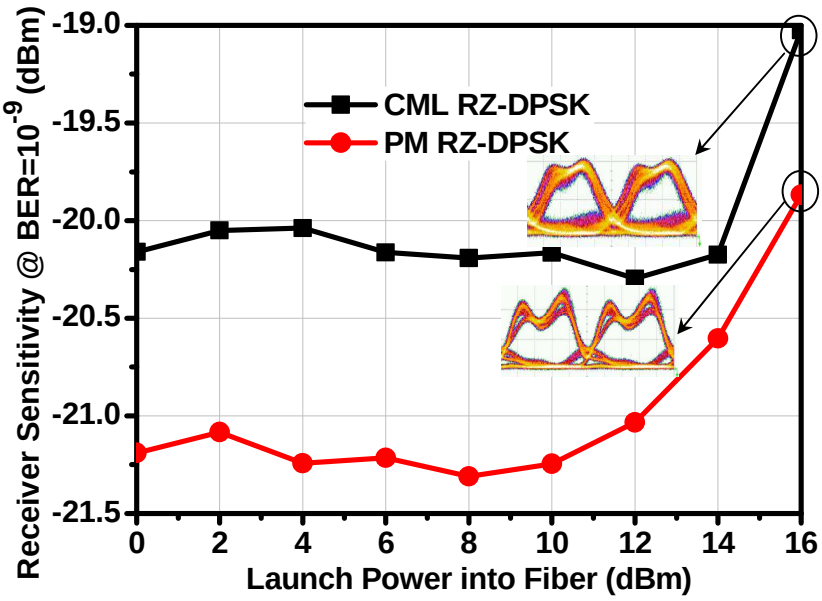

Fig. 4.8 Measured fiber nonlinearity tolerance for CML-based RZ-DPSK signal and PM-based RZ-DPSK signal. Insets show the respective eye diagrams at launch power of 16 dBm. Time scale: 20 ps/div.

4.1.4 Discussion

The CML-based RZ-DPSK transmitter has the merits of compact footprint, low cost, small power consumption, and excellent transmission performance. Here we have reported its transmission reach of 80-km SSMF for metropolitan network. Q. T. Le *et al.* have demonstrated the applications of CML-based DPSK signal with good optical power budget in WDM-PON [135]-[136]. The performance of CML-based RZ-DPSK signal in long-haul transmission system should be investigated using coherent detection in the future work. The other laser sources for direct modulation such as vertical-cavity surface-emitting laser (VCSEL) should also have the potential for similar application.

4.1.5 Summary

In this section, we have propose and experimentally demonstrated the generation of 10-Gb/s RZ-DPSK signal based on CML and pulse carver, without requiring any differential encoder or PM. The transmission performances of its tolerances in fiber CD and nonlinearity have been experimentally characterized and compared with that generated by $LiNbO_3$ PM. The applications of CML-based RZ-DPSK transmitter have also been discussed.

4.2 RZ-DQPSK signal generation using CML and pulse carver

4.2.1 Introduction

As reviewed in the chapter one, RZ-DQPSK modulation format has attracted much attention due to the advantages of high receiver sensitivity, increased spectral efficiency, and strong robustness towards fiber CD, PMD and nonlinearity impairments. Two parallel MZMs or PMs, a 90 degree phase shifter, and a pulse carver are the basis for the common RZ-DQPSK transmitter. Also, the conventional RZ-DQPSK transmitter requires complex electrical pre-coder for differential and gray coding. However, both the external modulators and electrical pre-coder make the RZ-DQPSK transmitter bulky and power hungry.

In the last section, we have generated the 10-Gb/s RZ-DPSK signal using CML and pulse carver with excellent transmission performance.

In this section, we extend to demonstrate a novel scheme to generate the 20-Gb/s RZ-

DQPSK signal using a commercially available 10-Gb/s CML. The two input data streams are firstly encoded in binary IRZ format with different driving voltages and then combined by a passive RF combiner to generate a four-level IRZ signal to directly drive the CML. The cost, footprint, and power consumption of RZ-DQPSK transmitter can be significantly reduced as no differential encoder or PM is required. This scheme could be generalized to generate the *M*-ary RZ-DPSK signal, where all the $\log_2 M$ data streams are in IRZ format with different driving voltages and combined to directly modulate the CML.

4.2.2 Operation principle

Fig. 4.9 depicts the proposed scheme of the 20-Gb/s RZ-DQPSK signal generation system using CML and pulse carver. The RZ-DQPSK transmitter consists of two IRZ encoders, a passive RF combiner, a CML, and a pulse carver.

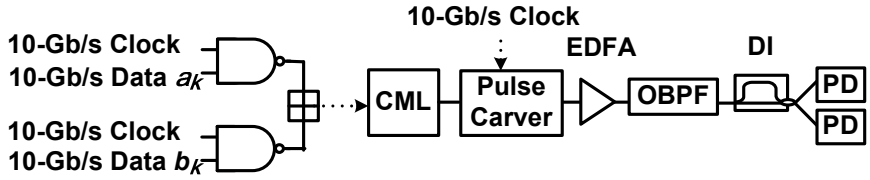

Fig. 4.9 Proposed scheme of RZ-DQPSK generation system using CML and pulse carver

Fig. 4.10 illustrates the operation principle through the intensity, chirp and phase characteristics of the output signals of the IRZ encoders, RF combiner, DFB laser (inside CML), and pulse carver.

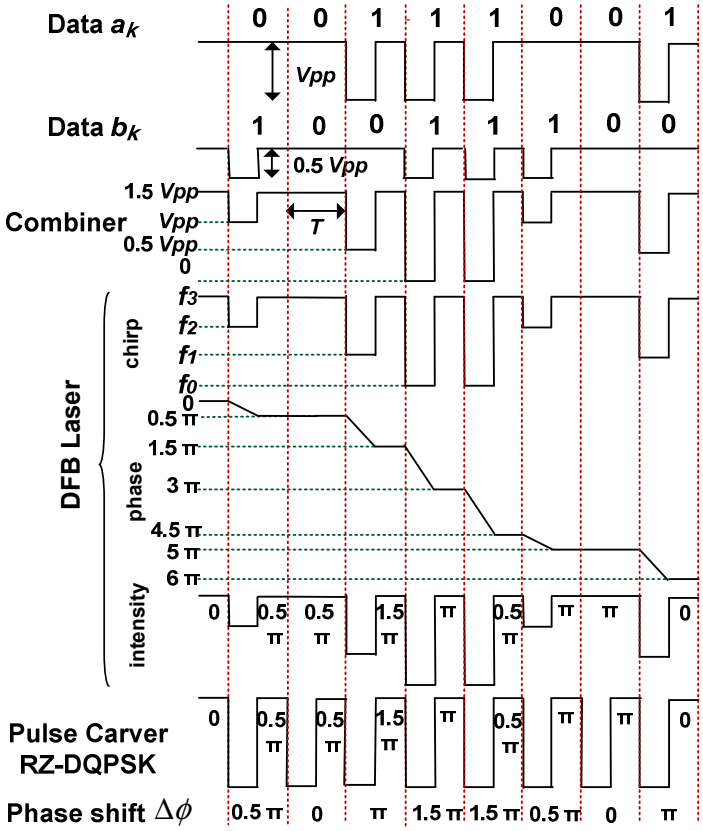

Fig. 4.10 Operation principle of RZ-DQPSK generation scheme using CML and pulse carver

Two IRZ-shaped data sequences a_k = 00111001 and b_k = 10011100 with duty cycles of 50% are generated, via two commercial logic NAND gates separately, before being combined to directly modulate the CML. The driving voltages of the two data sequences are V_{pp} and 0.5 V_{pp}, respectively. The laser is biased high above the threshold with the benefits of high output power, single mode operation, wide modulation bandwidth, and suppression of transient chirp. The driving voltage V_{pp} is adjusted to induce adiabatic chirp Δf, which is given by

$$\Delta f = 1/T \tag{4.3}$$

where T denotes the symbol period. The adiabatic chirp generates phase shift $\Delta\emptyset$, governed by

$$\Delta\emptyset = 2\pi \int_0^{\frac{T}{2}} \Delta f(t)dt$$

$$= 2\pi \times 1/T \times T/2$$

$$= \pi \tag{4.4}$$

during the first half-bit period of "10" symbol. Thus the phase shifts for the two-bit input a_k b_k of "00", "01", "10", and "11" are 0, 0.5 π, π, and 1.5 π, respectively. The maximum chirp value required for the CML to generate the 20-Gb/s RZ-DQPSK signal is 15 GHz. The relative spectral locations of the laser and filter are detuned to change the signal ER. The pulse carver with a duty cycle of 50% carves the second half-bit of the phase-modulated signal, thus generating the RZ-DQPSK signal.

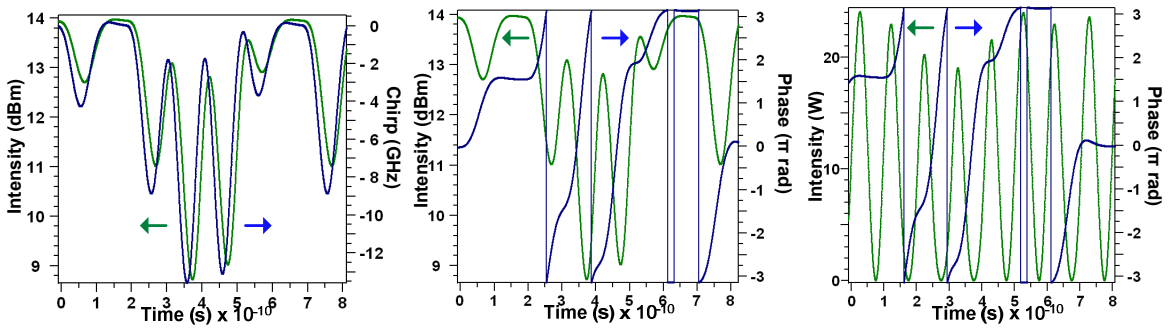

(a) (b) (c)

Fig. 4.11 Simulated (a) chirp profile of DFB laser output signal, (b) phase profile of DFB laser output signal, and (c) phase profile of pulse carver output signal for RZ-DQPSK generation using CML

Fig. 4.11 shows the simulated intensity, chirp and phase profiles of the DFB laser and pulse

carver output signals for RZ-DQPSK generation using CML. The phase modulation is intrinsically differentially encoded. Neither differential encoder nor PM is needed.

At the receiver, the phase differences of 0, 0.5 π, π, and 1.5 π corresponding to the two-bit input a_k b_k of “00”, “01”, “10”, and “11” are demodulated into two-bit output p_k q_k of “11”, “01”, “00”, and “10”, respectively, shown via simulation results in Fig. 4.12 (a) and (b).

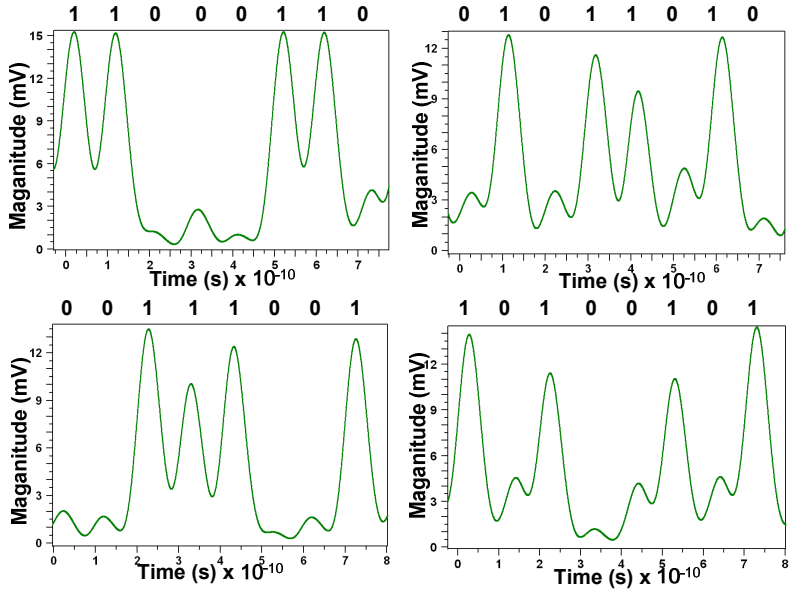

(a) (b)

Fig. 4.12 Simulation of (a) the demodulated output data p_k, and (b) the demodulated output data q_k at two output ports of the DI

Table 4.1(a) and (b) show that the relationships among input data, phase difference, and demodulated output data of CML-based RZ-DQPSK signal and PM-based RZ-DQPSK signal are different. Therefore, decoding processes of

$$a_k = \overline{q_k} \tag{4.5}$$

and

$$b_k = p_k \oplus q_k \tag{4.6}$$

are necessary to retrieve data a_k and data b_k correctly at the receiver for CML-based RZ-DQPSK signal. Table 4.1(c) shows that the complementary and XOR operations can also be implemented at the transmitter site instead of the receiver side for CML-based RZ-DQPSK.

Table 4.1 The relationships among input data, phase difference, and demodulated output data of (a) CML-based RZ-DQPSK signal, (b) PM-based RZ-DQPSK signal, and (c) precoding at the transmitter site instead of decoding at the receiver side for CML-based RZ-DQPSK.

Input Data $a_k b_k$	Phase Diff. $\Delta\phi$	Demodulated Output data $p_k q_k$
0 0	0	1 1
0 1	0.5 π	0 1
1 0	π	0 0
1 1	1.5 π	1 0

(a)

Input data $a_k b_k$	Phase Diff. $\Delta\phi$	Demodulated Output Data $p_k q_k$
0 0	π	0 0
0 1	0.5 π	0 1
1 0	1.5 π	1 0
1 1	0	1 1

(b)

Input Data $a_k b_k$	Precoding Operation	Precoded Data $a_k^* b_k^*$	Phase Diff. $\Delta\phi$	Demodulated Output data $p_k q_k$
0 0	$a_k^* = \overline{b_k}$	1 0	π	0 0
0 1		0 1	0.5 π	0 1
1 0	$b_k^* = a_k \oplus b_k$	1 1	1.5 π	1 0
1 1		0 0	0	1 1

(c)

4.2.3 Experiments and results

We have experimentally demonstrated the proposed 20-Gb/s RZ-DQPSK generation system using CML and pulse carver, as shown in Fig. 4.9. We used a standard CML module (Finisar DM80-01) in the experiment, which is the same as the one used in [128]. The input impedance, threshold current and FM efficiency of the DFB laser are 50 ohms, 25 mA and 0.24 GHz/mA, respectively. The filter in DM80-01 has a 3-dB bandwidth of 11 GHz and an average slope of 1.5 dB/GHz. Two 10-Gb/s IRZ data streams with respective driving voltages of 1.6 V and 0.8 V were combined by a passive RF combiner before directly modulating the DFB laser using 2^7-1 PRBS. The laser was biased at 85 mA. The central wavelength of signal after the filter was 1555.47 nm. A MZM driven by a 10-GHz clock was used as the pulse carver. The output power after the pulse carver was -0.5dBm. An EDFA was inserted at the receiver to boost optical signal power. A tunable OBPF with ~1 nm bandwidth was set after the EDFA to eliminate ASE noise. The generated RZ-DQPSK signal was demodulated by a 1-bit optical DI before being detected by a PD. The phase difference between the two arms of DI was adjusted by controlling temperature and bias to demodulate data a_k and data b_k, respectively.

Fig. 4.13 shows the experimental (upper) and corresponding simulated (lower) BtB eye diagrams of the signals after the RF combiner, CML, pulse carver, and demodulated data a_k signal at one port of the DI. The multiple lines of RZ-DQPSK signal shown in Fig. 4.13 (c) are due to the imperfect driving signal and limited modulation response of the DFB laser in CML, as shown in Fig. 4.13 (a) and (b), respectively.

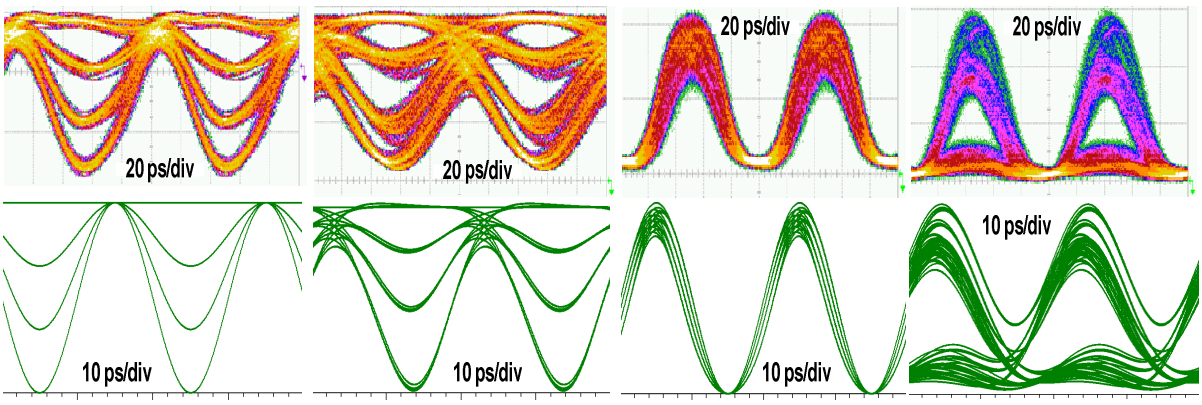

(a) (b) (c) (d)

Fig. 4.13 Experimental (upper) and corresponding simulated (lower) eye diagrams of (a) signal after the RF combiner, (b) signal after the CML, (c) RZ-DQPSK signal after the pulse carver, and (d) demodulated data a_k signal at one port of the DI

Fig. 4.14 shows the waveform traces measured by a real-time oscilloscope. Two data sequences a_k = 00111001 and b_k = 10011100 were applied to the transmitter. The subtraction of the bottom and top demodulated waveforms, as shown in Fig. 4.14 (c), would correctly regenerate the input bit sequence a_k. Decoding process of (4.6) would also regenerate the input bit sequence b_k, as shown in Fig. 4.14 (c) and (d). It illustrates that no differential encoding of the original data is required. The uneven marks and fluctuating spaces of demodulated signals shown in Figs. 4.14(c) and (d) are attributed to the imperfect driving signal shown in Fig. 4.13(a) and Fig. 4.14(b) and the limited modulation response and chirp value of the DFB laser. Since decoding process of (4.6) was not performed here, only the BtB BER performance of demodulated RZ-DQPSK data a_k signal at one port of the DI was measured. The BtB receiver sensitivity at BER of 10^{-9} for CML-based RZ-DQPSK signal was -15.31 dBm. The corresponding eye diagram is shown in Fig. 4.13 (d).

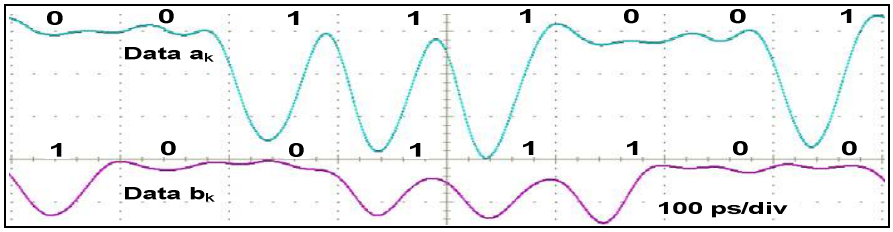

(a)

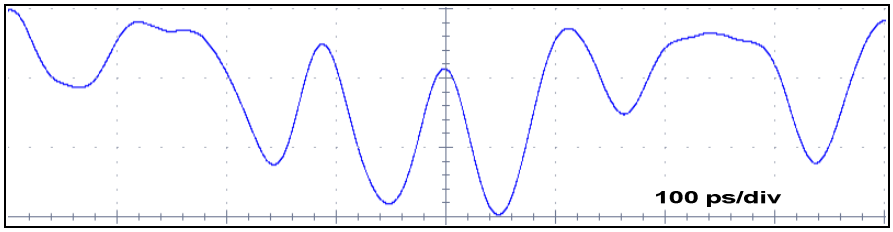

(b)

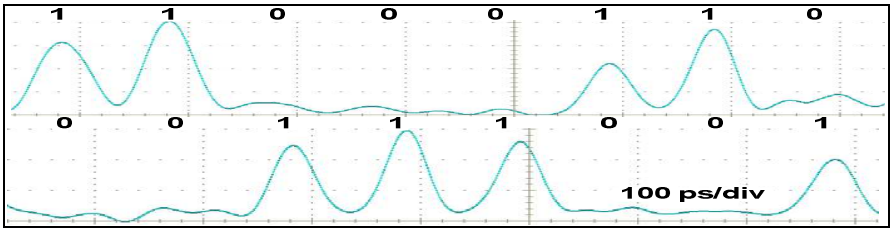

(c)

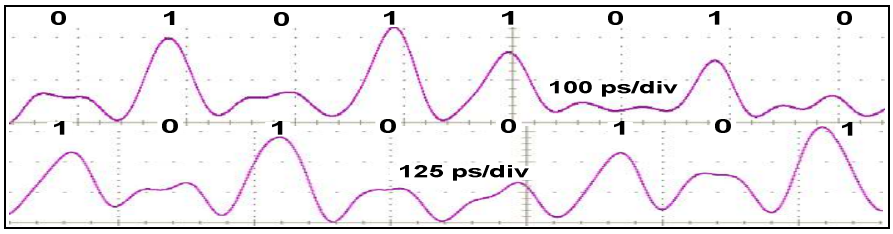

(d)

Fig. 4.14 Waveform traces for signals (a) of data a_k and b_k, (b) after the RF combiner, (c) of demodulated data p_k at the two output ports of DI, and (d) of demodulated data q_k at the two output ports of DI

4.2.4 Discussion

Fig. 4.15 shows the simulated constellation diagrams of CML-based RZ-DQPSK signals with different duty cycles of 50% and 33%. The duty cycles are changed by controlling the pulse carver. It denotes that the phase transitions between the different symbols in CML-based RZ-DQPSK signal become sharp with a smaller duty cycle.

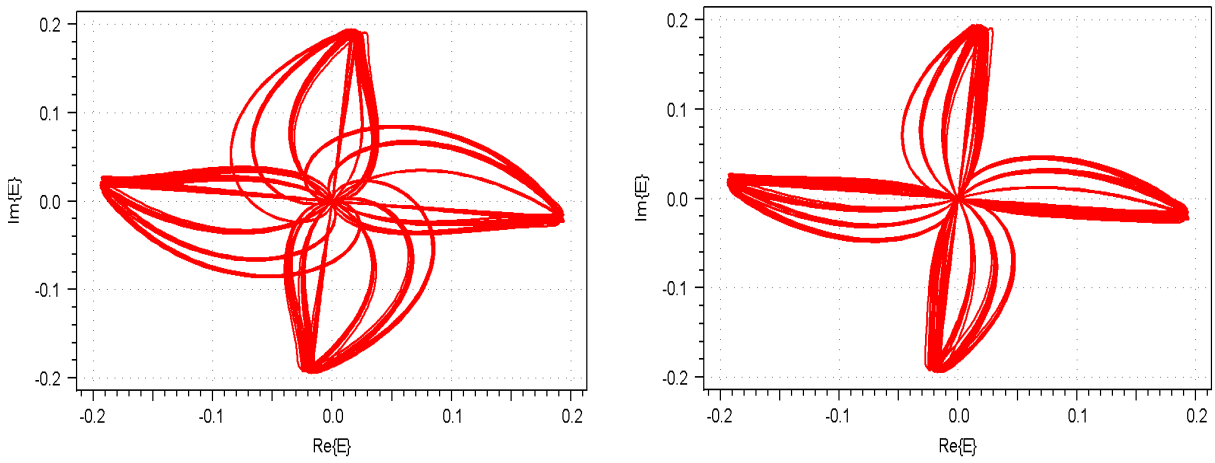

Fig. 4.15 Simulated constellation diagrams of CML-based RZ-DQPSK signals with different duty cycles of (a) 50% and (b) 33%

4.2.5 Summary

In this section, we have proposed and experimentally demonstrated a simple and cost-effective 20-Gb/s RZ-DQPSK transmitter using CML and pulse carver, without requiring any differential encoder or PM. This scheme could be generalized to generate *M*-ary RZ-DPSK signal. We have

also discussed the impact of different duty cycles on the phase shifts of the CML-based RZ-DQPSK signal.

4.3 ¾-RZ-DQPSK signal generation using single CML

4.3.1 Introduction

As described in chapter one, RZ-DQPSK is a promising signal modulation format in optical access, metropolitan, and long-haul WDM transmission systems, due to its advantages of high receiver sensitivity using balanced detection, high spectral efficiency, and large tolerance to fiber CD, PMD, and narrow optical filtering. However, a conventional optical RZ-DQPSK signal transmitter requires a complicated differential encoder, as well as several bulky and power-hungry external modulators.

In the last section, we have employed a 10-Gb/s DFB-laser based CML and an externally modulated pulse carver to generate the 10-Gbaud optical RZ-DQPSK signal, without the need of any differential encoder or PM. However, the BtB BER performance is poor, which may be attributed to the low bandwidth of the DFB laser, as well as the small value of available adiabatic chirp. The transmission performance is not yet extensively characterized. In addition, the use of an external pulse carver for RZ signal generation makes that scheme less attractive.

In this section, we propose and experimentally demonstrate the generation and transmission of 10-Gbaud optical ¾-RZ-DQPSK signal using single DBR-laser based CML, without the need for an external pulse carver. In this new signal format, the symbols with a differential phase shift of 0 remain NRZ, while those with differential phase shifts of 0.5 π, π, and 1.5 π are RZ; hence is

named as ¾- RZ-DQPSK. No differential encoding is needed. We have realized error-free transmission over 60-km SSMF without any dispersion compensation. Besides, no OSNR penalty is induced. We have also investigated the impact of different optical spectrum reshaper (OSR) filters in CML on the transmission performance, for instance, fiber CD tolerance. The impact of the amplitude fluctuation in the driving signal on the BER performance of the generated CML-based ¾-RZ-DQPSK signal is also characterized to be quite small. Only 1.17-dB OSNR penalty is induced for the BtB BER with +20.2% / -14.1% amplitude variations in the driving signal.

4.3.2 Operation principle

Fig. 4.16 depicts the proposed scheme for generation, transmission, and detection of CML-based optical ¾-RZ-DQPSK signal. The transmitter comprises a simple pre-coder, a 4-level driver, and a DBR-laser based CML.

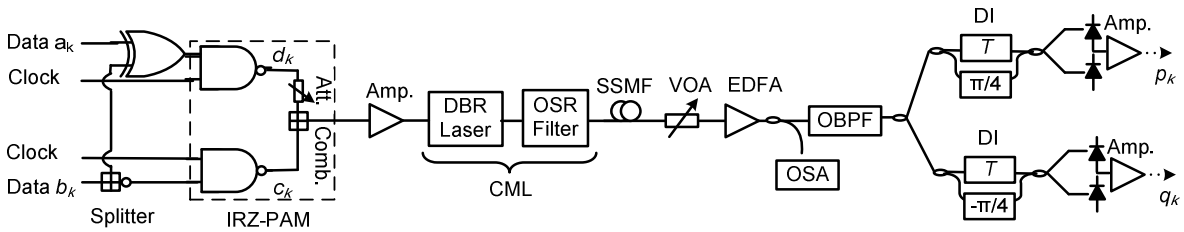

Fig. 4.16 Proposed scheme for CML-based ¾-DQPSK signal generation, transmission, and detection system.

Table 4.2 shows the values of the symbols in the two tributaries through the pre-coder, the driver, as well as after the demodulator. Given two 10-Gbaud tributaries with data a_k and b_k as inputs, the pre-coder generates the logical inverse of one tributary c_k, given by

$$c_k = \overline{b_k} \tag{4.7}$$

and the logic XOR of the two input tributaries d_k, given by

$$d_k = a_k \oplus b_k \tag{4.8}$$

as its two pre-coded outputs. These two pre-coded outputs, data c_k and d_k, are then converted into a four-level output using an IRZ pulse-amplitude-modulation (PAM) driver, emulated using two IRZ drivers, a RF attenuator (Att.), and a RF power combiner (Comb.). The driver generates the modulo-2 binary sum of the pre-coded input tributaries, which then is amplified to directly drive the laser. In a commercial implementation, the logic functions could be integrated on the same circuit with the IRZ-PAM driver, which comprises a so-called 'thermometer' architecture [137]. The PAM driver output is amplified to directly modulate the gain section of the DBR-laser based CML transmitter. Besides, the receiver is a standard optical DQPSK signal receiver including two sets of 1-bit DIs, balanced PDs, and electrical post amplifiers.

Table 4.2 The relationship among the input data, pre-coded data, phase shift, and demodulated output data for CML-based ¾-RZ-DQPSK generation and detection system.

Input Data $a_k b_k$	Pre-coding Operation	Pre-coded Data $c_k d_k$	Phase Shift $\Delta\phi$	Demodulated Output Data $p_k q_k$
0 0	$c_k=\overline{b}_k$	1 0	π	0 0
0 1		0 1	0.5 π	0 1
1 0	$d_k=a_k \oplus b_k$	1 1	1.5 π	1 0
1 1		0 0	0	1 1

Fig. 4.17 shows the operation principle of generation of CML-based optical ¾- RZ-DQPSK signal. Pre-coded data c_k and d_k are converted into IRZ-shaped signals with duty cycles of 50% via two NAND encoders and then combined and amplified to drive the DBR laser.

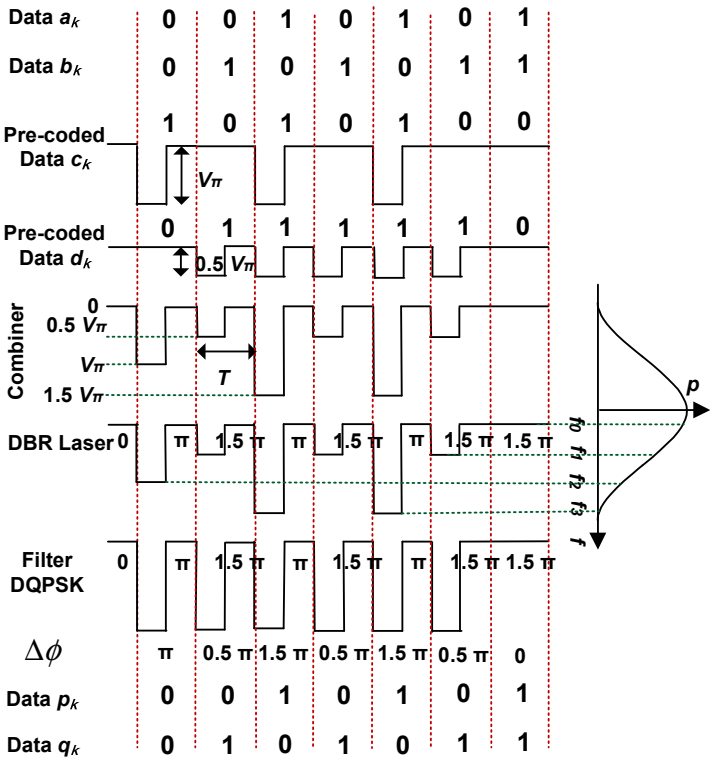

Fig. 4.17 Operation principle of generation of CML-based ¾-RZ-DQPSK signal

The 4-level PAM signal is generated by adjusting the relative driving amplitudes of the two data sequences to be in 2:1 ratio. The laser is biased high above threshold with the benefits of high output power, single mode operation, wide modulation bandwidth, and suppression of transient chirp. The driving voltage V_π is adjusted to induce adiabatic chirp Δf, given by

$$\Delta f = 1/T \tag{4.9}$$

where T denotes the symbol period. The adiabatic chirp in turn causes a phase shift $\Delta\emptyset$, calculated from

$$\Delta\emptyset = 2\pi \int_0^{\frac{T}{2}} \Delta f(t)dt$$

$$= 2\pi \times 1/T \times T/2$$

$$= \pi \tag{4.10}$$

which corresponds to the pre-coded 2-bit symbol of 10. The other levels of the 4-level PAM driver of 0, 0.5 V_π, and 1.5 V_π therefore generate phase shifts of 0, 0.5 π, and 1.5 π, which correspond to the pre-coded 2-bit symbols of 00, 01, and 11, respectively. The corresponding required chirp values for generation of phase shifts of 0, 0.5 π, π, and 1.5 π at the output of the DBR laser are 0, 5 GHz, 10 GHz, and 15 GHz. The wavelength of the laser is locked to the edge of the OSR filter to attenuate the first half-symbol signal levels with frequencies of f_1, f_2, and f_3, during which the laser power is low, and pass the second half-symbol signal level with frequency of f_0, during which the laser power is high and which contains the desired relative phase shift information, as shown in Fig. 4.17. For phase shifts of 0.5 π , π, and 1.5 π, the laser is chirped during the first half-symbol period to produce the phase shift for the second half-symbol period, generating RZ-shaped signal after the OSR filter. However, for the phase shift of 0, the laser is not chirped, and the output remains high. So the outputs are of RZ shape for three phase shifts and of NRZ shape for the other, generating what we call ¾-RZ-DQPSK. A full RZ-DQPSK signal can be generated if the laser is chirped to produce 2 π phase shift instead of 0 phase shift. However, this increases the required chirp value of the laser to two times the symbol rate, which makes the laser performance requirement more challenging. The proposed scheme could also be generalized to generate *M*-ary $\frac{M-1}{M}$ -RZ-DPSK, where all the $\log_2 M$ data streams in IRZ format with different driving amplitudes are combined to drive the CML.

The CML-based ¾-RZ-DQPSK signal requires a standard DQPSK receiver for demodulation and detection. However, the resulting eye diagrams are not standard, ¾ of the symbols being RZ and ¼ of the symbols being NRZ. Fig. 4.18(a) shows the simulated eye diagrams of the demodulated and balanced-detected CML-based ¾-RZ-DQPSK signal for the two outputs of the DQPSK receiver with phase differences $\Delta\theta = \frac{\pi}{4}$ and $\Delta\theta = -\frac{\pi}{4}$ between the two arms of the DI, respectively. The demodulated eye diagrams are of a combination of NRZ and RZ shapes. Fig. 4.18(b) shows the demodulation and detection of the pre-coded symbol *E(t-T)* of 00 upon interference with the adjacent pre-coded symbols *E(t)* of 00, 01, 10, and 11 in the DI, respectively, where *E* is the received electric field containing the relative phase shift information. The two balanced-detected outputs p_k and q_k of the standard DQPSK receiver are determined by

$$p_k \propto |E|^2 \times \cos\left(\frac{\pi}{4} + \Delta\emptyset\right) \tag{4.11}$$

and

$$q_k \propto |E|^2 \times \cos\left(-\frac{\pi}{4} + \Delta\emptyset\right) \tag{4.12}$$

where the sign of $\frac{\pi}{4}$ corresponds to the upper or lower branch of the DQPSK signal receiver. When the pre-coded symbol *E(t-T)* of 00 interferes with the adjacent pre-coded symbols *E(t)* of 01, 10, and 11, the energy of the first half-symbol signals at both the constructive output port and the destructive output port of the DI are non-zero and equal. However, they are eliminated after balanced-detection, resulting in balanced-detected RZ-DQPSK signal, as shown in Fig. 4.18(a). On the other hand, when the pre-coded symbol *E(t-T)* of 00 interferes with the adjacent pre-

coded symbol *E(t)* of 00, it will result in balanced-detected NRZ-DQPSK signal, as shown in Fig. 4.18(a). Therefore the flat lines on the top of the eye diagrams in Fig. 4.18(a) correspond to the demodulation and detection of the pre-coded symbol *E(t-T)* of 00, which are NRZ at the transmitter side, resulting in poorer receiver sensitivity than full RZ-shaped DQPSK.

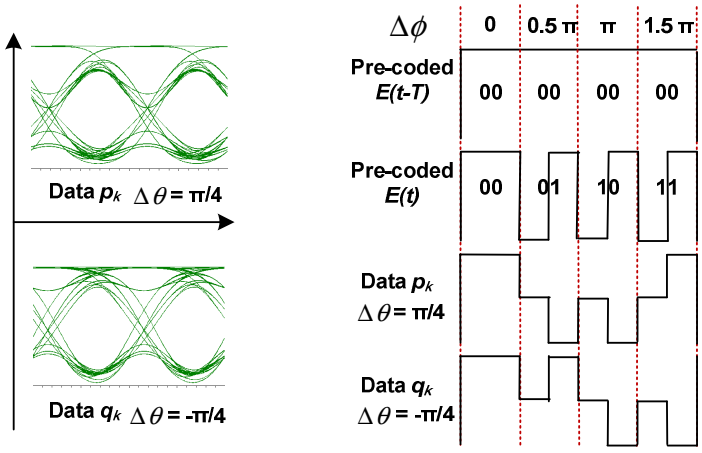

(a) (b)

Fig. 4.18 (a) The simulated eye diagrams of balance-detected CML-based ¾- RZ-DQPSK signal with different phase differences $\Delta\theta$ between the two arms of the DI. Time scale: 10 ps/div. (b) Demodulation and detection of the pre-coded symbol *E (t-T)* of 00 upon interference with the adjacent pre-coded symbols *E(t)* of 00, 01, 10, and 11 in the DI

4.3.3 Experiments and results

We constructed a CML transmitter using a DBR laser and one of three different OBPFs with respective 3-dB bandwidths of 50 GHz, 10 GHz and 7 GHz. The 50-GHz case was to simulate the CML without narrow filtering effect, while the 10-GHz and 7-GHz cases were to simulate the commercial available CML modules (Finsar DM 80-01 and Finsar DM 200-01) with narrow-

bandwidth OSR filters, respectively. A key element for the realization of the ¾-RZ-DQPSK signal is the high-speed DBR laser with high FM efficiency used in these experiments. The challenge in developing a high-speed directly modulated DBR laser with high FM efficiency is that the long passive sections used for tuning do not contribute to a round-trip differential gain or dynamic chirp, and therefore reduce the relaxation oscillation frequency f_r as well as the FM efficiency [138]. The DBR laser used here had a 3-dB bandwidth > 23 GHz up to 35 ^{o}C and a FM efficiency of 0.2 GHz/mA, which were maintained over a 13-nm tuning range. In this study, the DBR section was grounded, and the effect of tuning was not investigated. The corresponding side mode suppression ratio was 45 dB. Alternative for a full-C band tunable high-speed laser includes a Modulated Grating Y-branch (MG-Y) laser [138]. However, the 3-dB modulation bandwidth was reduced to 18 GHz, due to longer passive sections for a MG-Y laser.

Two 10.22-Gb/s tributaries with 2^7-1 PRBS were pre-coded using an XOR (Inphi 13611XR) and two NAND (Inphi 50712OR) logic gates and then combined and amplified to drive the DBR laser, as shown in Fig. 4.16. The amplitude of data d_k was attenuated to be half of the amplitude of the other data c_k. The peak-to-peak driving voltage V_{pp} was 4.1 V and was applied to the gain section of the DBR laser, which was in series with a 45-ohm matching resistor. This maximum swing generated a modulation current of 82 mA to generate adiabatic chirp of ~16 GHz, which nominally corresponded to a 1.5 π phase shift. The laser was biased at 110 mA using a bias tee. The center wavelength of the DBR laser was 1536.1 nm with an output power of 8.6 dBm.

The receiver comprised an EDFA, an OBPF with a 3-dB bandwidth of ~1 nm, a DI demodulator, and a balanced PD. We used an Optoplex DI with a FSR of 10.7 GHz. The balanced PD (U2T BPDV 2020R) had a 3-dB bandwidth of 42 GHz. The output of the balanced

PD was amplified by an electrical post amplifier with bandwidth of 50 GHz. The phase difference $\Delta\theta$ between the two arms of DI was adjusted to yield either the in-phase or quadrature-phase components of the incoming ¾-RZ-DQPSK. Fig. 4.19 shows the measured intensity and chirp waveforms of the generated CML-based DQPSK signal after the DBR laser. The measurement instrument converts the chirp and linewidth into power change using a DI. The chosen symbols showed four levels and correspond to chirp values of 0 GHz, 5 GHz, 10 GHz, and 15 GHz, hence generated the four phase values of 0, 0.5 π, π, and 1.5 π, respectively.

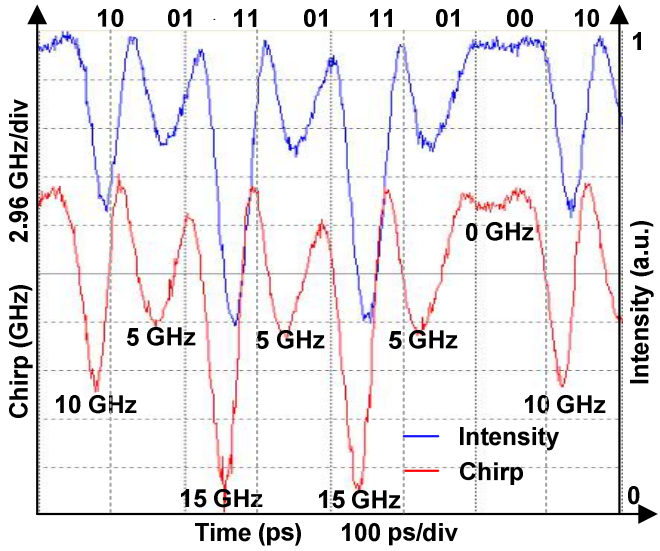

Fig. 4.19 Intensity and chirp waveforms of the CML-based DQPSK signal after DBR laser. Time scale: 200 ps/div.

We have evaluated the performance of the ¾-RZ-DQPSK signal for data tributary p_k using two different transmitter configurations having OSR filters with 3-dB bandwidths of 50 GHz and 10 GHz, respectively. To select data tributary p_k for demodulation, we adjusted the phase difference θ between the two arms of DI to $\frac{\pi}{4}$. Fig. 4.20 shows the BtB eye diagrams of the 4-level driving signal after the RF combiner, DBR laser output signal, ¾-RZ-DQPSK signals after

50-GHz OSR filter and 10-GHz OSR filter, and demodulated data tributary p_k after balanced-detection of ¾-RZ-DQPSK signals with 50-GHz OSR filter and 10-GHz OSR filter.

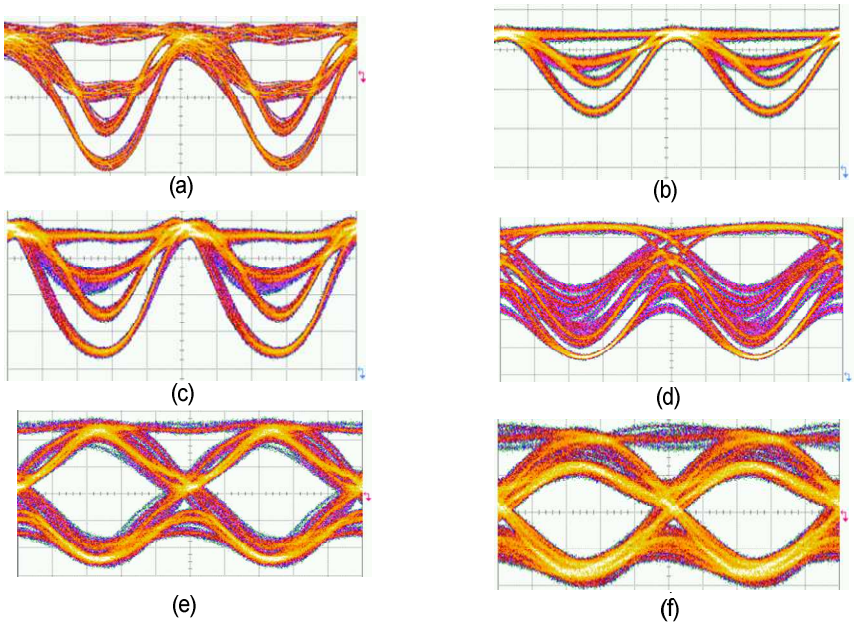

Fig. 4.20 BtB eye diagrams of (a) the 4-level driving signal after the RF combiner, (b) DBR laser output signal, (c) ¾-RZ-DQPSK signal after 50-GHz OSR filter, (d) ¾-RZ-DQPSK signal after 10-GHz OSR filter, (e) data p_k after balanced-detection of ¾-RZ-DQPSK signal using 50-GHz OSR filter, and (f) data p_k after balanced-detection of ¾-RZ-DQPSK signal using 10-GHz OSR filter. Time scale: 20 ps/div.

The OSR filter shapes were realized using a programmable WaveShaper (Finisar WaveShaper 4000S). In our experiment, the IRZ driver had no fine adjustment for output amplitude, so we optimized the phase shift $\Delta\emptyset$ between the adjacent pre-coded symbols by adjusting the duty cycles of the two IRZ data streams. Note that the phase shift $\Delta\emptyset$ is a function of the time duration T and the adiabatic chirp Δf denoted in (4.10). Fig. 4.20(b) shows that the DBR laser had fast modulation response and the output signal had low ER. Fig. 4.20(c) shows that the signal ER was enhanced and the first half-symbol signal levels with frequencies of f_1, f_2,

and f_3 were suppressed by tuning the spectral position of the 50-GHz OSR filter. Fig. 4.20(d) shows the first half-symbol signal levels with frequencies of f_1, f_2, and f_3 were suppressed further using the 10-GHz OSR filter. However, due to the narrower bandwidth of the 10-GHz OSR filter, the ¾-RZ-DQPSK signal became bandwidth-limited. Thus, the eye diagram of the balance-detected ¾-RZ-DQPSK signal using the 50-GHz OSR filter shown in Fig. 4.20(e) depicted a wider eye opening, compared with the one using the 10-GHz OSR filter shown in Fig. 4.20(f).

Fig. 4.21 shows the measured optical spectrum of the DQPSK signals after the DBR laser, 50-GHz OSR filter, and 10-GHz OSR filter. The respective 20-dB bandwidths of the ¾-RZ-DQPSK signals after the 50-GHz and 10-GHz OSR filters were 28.9 GHz and 18.6 GHz, respectively. With more compact spectrum, the ¾-RZ-DQPSK signal using the 10-GHz OSR filter should have better fiber CD tolerance, compared with the ¾-RZ-DQPSK signal using the 50-GHz OSR filter.

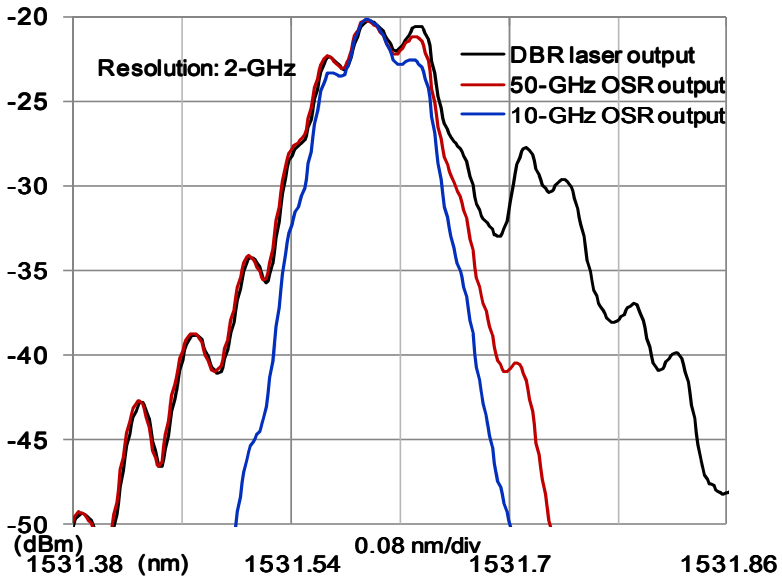

Fig. 4.21 Optical spectra of the DQPSK signals after the DBR laser, 50-GHz OSR filter, and 10-GHz OSR filter.

We have also evaluated a periodic three-cavity etalon filter with a 3-dB bandwidth of 7 GHz, a slope of 2.3 dB/GHz, and a FSR of 50 GHz as the OSR filter. The BtB eye diagrams of the ¾-RZ-DQPSK signal and the balanced-detected ¾-RZ-DQPSK signal at the receiver, using 7-GHz OSR filter, are shown in Fig. 4.22. Fig. 4.22(a) shows that the 7-GHz OSR filter brought larger ISI to the ¾-RZ-DQPSK signal and suppressed the first half-symbol signal levels with frequencies of f_1, f_2, and f_3 more completely due to its narrower bandwidth, compared with the 50-GHz and 10-GHz OSR filters. It also resulted in distortion to the balance-detected ¾-RZ-DQPSK signal, as shown in Fig. 4.22(b).

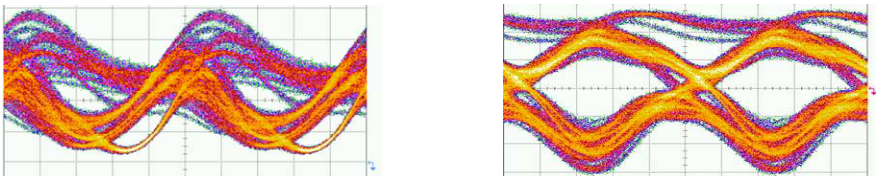

(a) (b)

Fig. 4.22 BtB eye diagrams of the (a) ¾-RZ-DQPSK signal, and (b) data p_k after balanced-detection of ¾-RZ-DQPSK signal using 7-GHz OSR filter. Time scale: 20 ps/div.

We compared the BtB OSNR performance and tolerance towards fiber CD for the CML-based ¾- RZ-DQPSK signals using the 50-GHz, 10-GHz, and 7-GHz OSR filters. The OSNR measurement setup was shown in Fig. 4.16. We placed a variable optical attenuator (VOA) before the EDFA to adjust the OSNR. A coupler with a 10:90 splitting ratio was placed after the EDFA to enable the OSNR to be monitored using an optical spectrum analyzer (OSA) with resolution of 0.1 nm. The power launched into the receiver was maintained at a constant value of 0.6 dBm by changing the gain of the EDFA. The amplitude of the balance-detected ¾-RZ-DQPSK signal after the 50-GHz electrical post amplifier was about 1.0 V. The maximum error-

free (no error within two minutes) SSMF transmission distances for the CML-based ¾-RZ-DQPSK signals using 50-GHz, 10-GHz and 7-GHz OSR filters were 40 km, 50 km, and 60 km, respectively. Fig. 4.23 shows the corresponding eye diagrams of the balanced-detected CML-based ¾-RZ-DQPSK signals using 50-GHz OSR filter after 40-km SSMF, 10-GHz OSR filter after 50-km SSMF, and 7-GHz OSR filter after 60-km SSMF. Fig. 4.23 shows that the balanced-detected CML-based ¾-RZ-DQPSK signal using 7-GHz OSR filter had a much wider eye opening than the other cases, even with longer transmission distance.

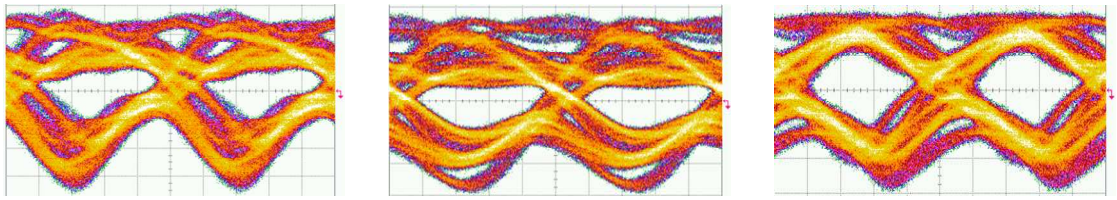

(a) (b) (c)

Fig. 4.23 Eye diagrams of the balanced-detected CML-based ¾-RZ-DQPSK signals using (a) 50-GHz filter after 40-km SSMF, (b) 10-GHz filter after 50-km SSMF, and (c) 7-GHz filter after 60-km SSMF. Time scale: 20 ps/div.

Fig. 4.24 depicts the measured BER versus required OSNR performances for the BtB and transmitted CML-based ¾-RZ-DQPSK signals using the three different OSR filters. The BtB required OSNR at BER of 10^{-13} (BER measured using the unlimited mode of the BERT for two minutes) for CML-based ¾-RZ-DQPSK signal using 50-GHz OSR filter was 14.65 dB. There was an OSNR penalty of 6.28 dB after 40-km SSMF transmission. The BtB required OSNR at BER of 10^{-13} for CML-based ¾-RZ-DQPSK signal using 10-GHz OSR filter was increased to 18.84 dB. The SSMF transmission distance was extended to 50 km with an OSNR penalty of 1.39 dB. The BtB required OSNR at BER of 10^{-13} for CML-based ¾-RZ-DQPSK signal using 7-GHz OSR filter was increased to 20.47 dB. However, it still realized 60-km SSMF transmission

with no OSNR penalty.

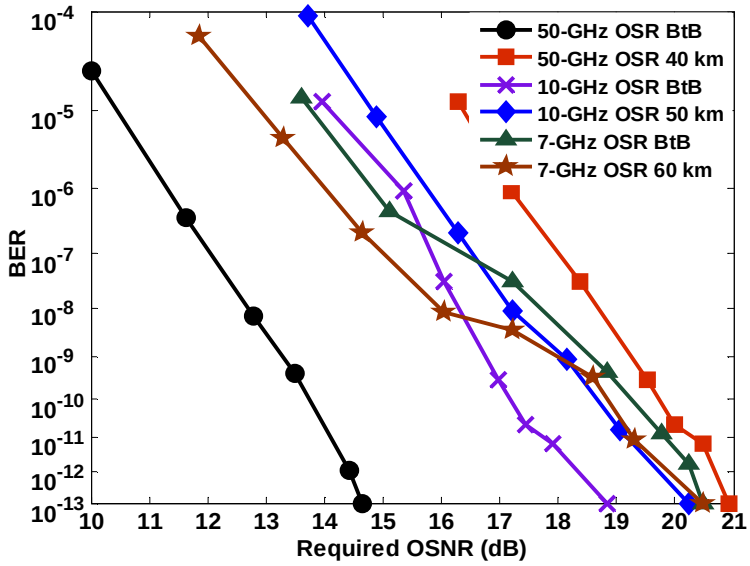

Fig. 4.24 Measured BER versus required OSNR performances for the BtB and transmitted CML-based ¾-RZ-DQPSK signals using three different OSR filters

Finally, the robustness of the amplitude variation in the driving signal was studied. The OSNR penalty of the BtB CML-based ¾-RZ-DQPSK signal using the 50-GHz OSR filter was measured, when the driving voltage was varied. When increasing the driving voltage, there was no need to change the spectral position of the OSR filter to get the best performance. However, the CML-based-¾-RZ-DQPSK signal was more susceptible to the negative amplitude change of the driving signal. When decreasing the driving voltage from 4.05 V to 3.48 V or 3.19 V, the spectral position of the OSR filter had to be detuned by 3 GHz or 6 GHz towards high frequency so as to enhance the ER of the ¾-RZ-DQPSK signal and get the widest eye opening of the balanced-detected signal. Thus there was a 0.9-dB OSNR difference between maintaining and tuning the spectral position of the OSR filter when the driving voltage was decreased from 4.05 V to 3.48 V. Their respective eye diagrams are shown in Fig. 4.25.

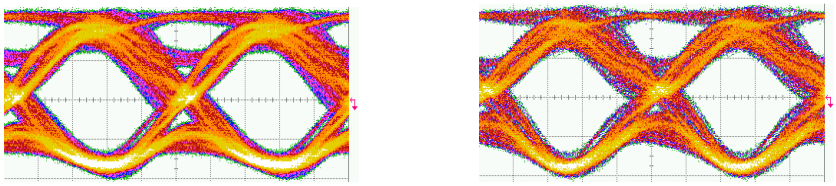

(a) (b)

Fig. 4.25 Eye diagrams of the balanced-detected CML-based ¾-RZ-DQPSK signal with the 50-GHz OSR filter spectral position (a) maintained, and (b) tuned by 3 GHz towards high frequency, when the driving voltage was decreased from 4.05 V to 3.48 V. Time scale: 20 ps/div.

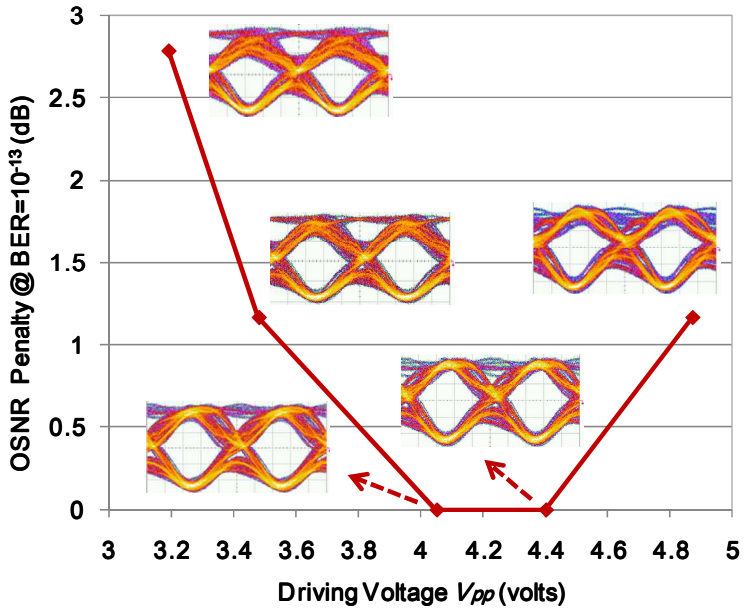

Fig. 4.26 Measured OSNR penalty of the CML-based ¾-RZ-DQPSK signal using the 50-GHz OSR filter when the amplitude of the driving signal was varied. Insets show the respective eye diagrams. Time scale: 20 ps/div.

Fig. 4.26 shows the measured OSNR penalty of the CML-based ¾-RZ-DQPSK signal at BER of 10^{-13} when the amplitude of the driving signal was varied. There was a 1.17-dB OSNR penalty when the driving voltage was increased from 4.05 V to 4.87 V, which corresponded to a change of +20.2%. There was a 1.17-dB OSNR penalty when the driving voltage was decreased

from 4.05 V to 3.48 V, which corresponded to a change of -14.1%. Insets show the respective eye diagrams.

Fig. 4.27 shows the measured optical spectra of the generated CML-based ¾-RZ-DQPSK signals using the 50-GHz OSR filter at different driving voltages V_{pp} of 3.19 V, 4.05 V, and 4.87 V. The respective 20-dB bandwidths were 20.5 GHz, 28.9 GHz, and 37.0 GHz. At a smaller driving signal, the spectrum of the CML-based ¾-RZ-DQPSK signal became more compact to suit WDM channels with flexible grids.

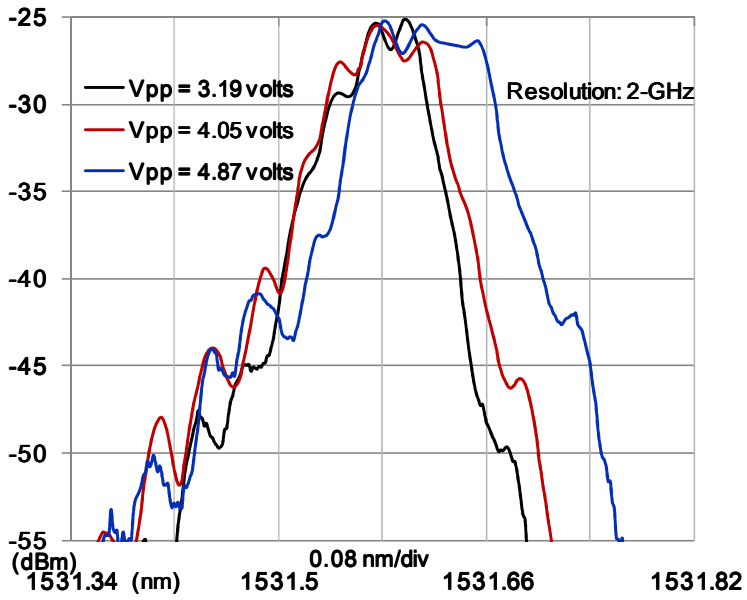

Fig. 4.27 Optical spectra of the CML-based ¾-RZ-DQPSK signals using the 50-GHz OSR filter at three different driving voltages

4.3.4 Summary

In this section, we have proposed and experimentally demonstrated the generation and transmission of 10-Gbaud optical ¾-RZ-DQPSK signals using single high-speed DBR-laser

based CML, without requiring any differential encoder or external modulator. Error-free transmission in 60-km SSMF without any dispersion compensation was realized. No OSNR penalty was induced. Besides, the transmission performances of fiber CD tolerance for the CML-based ¾-RZ-DQPSK signals with different OSR filters have been characterized. The robustness against possible amplitude variation of the driving signal was also investigated.

4.4 RZ-DQPSK signal generation using single CML

4.4.1 Introduction

As discussed in chapter one, RZ-DQPSK is an attractive modulation format for optical fiber transmission, owing to its increased spectral efficiency and high tolerances towards fiber CD, PMD, and nonlinearities. However, the conventional RZ-DQPSK transmitter requires a complex differential encoder and several bulky external modulators.

In the last section, we have used a DBR-laser based CML to generate 10-Gbaud ¾-RZ-DQPSK signal, without any differential encoder or external modulator. However, the full RZ-shaped DQPSK signal could not be obtained with this approach.

In this section, we demonstrate the generation of 10.709-Gbaud full RZ-shaped DQPSK signal using single CML without any differential encoder, external PM or pulse carver. 40-km SSMF transmission at BER of 10^{-9} is realized without any dispersion compensation for the 10.709-Gbaud CML-based RZ-DQPSK signal.

4.4.2 Operation principle

Fig. 4.28 shows the schematic of our proposed RZ-DQPSK signal transmitter, which comprises a CML driven by a simple designated electronic logic circuit.

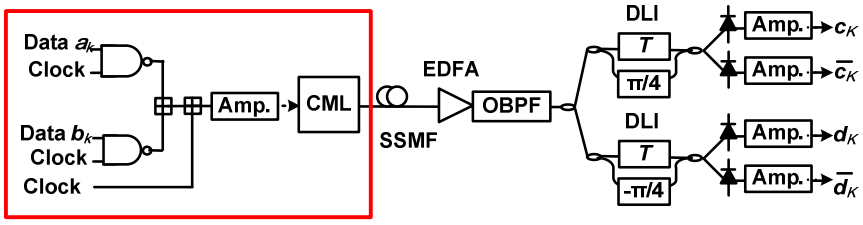

Fig. 4.28 optical RZ-DQPSK transmission system using our proposed CML-based RZ-DQPSK signal transmitter (denoted in red box)

The relations among the input data, phase shift, demodulated data, and output data after decoding are stated in Table 4.3.

Table 4.3 The relations among input data, phase shift, demodulated data, and output data

Input Data $a_k\, b_k$	Phase Shift $\Delta\phi$	Demodulated Data $c_k\ d_k$	Decoding Operation	Output Data $p_k\, q_k$
0 0	π	0 0	$p_k = d_k$	0 0
0 1	1.5 π	1 0		0 1
1 0	2 π	1 1	$q_k = c_k \oplus d_k$	1 0
1 1	2.5 π	0 1		1 1

Fig. 4.29 shows the operation principle of RZ-DQPSK signal generation using single CML through the intensity, chirp and phase characteristics of the output signals from the IRZ drivers, electrical combiner, DFB laser, and filter in CML. Two IRZ-shaped data sequences a_k = 01001101 and b_k = 10101001 with duty cycles of 50% generated by two NAND logic gates were combined together with a clock to drive the DFB laser.

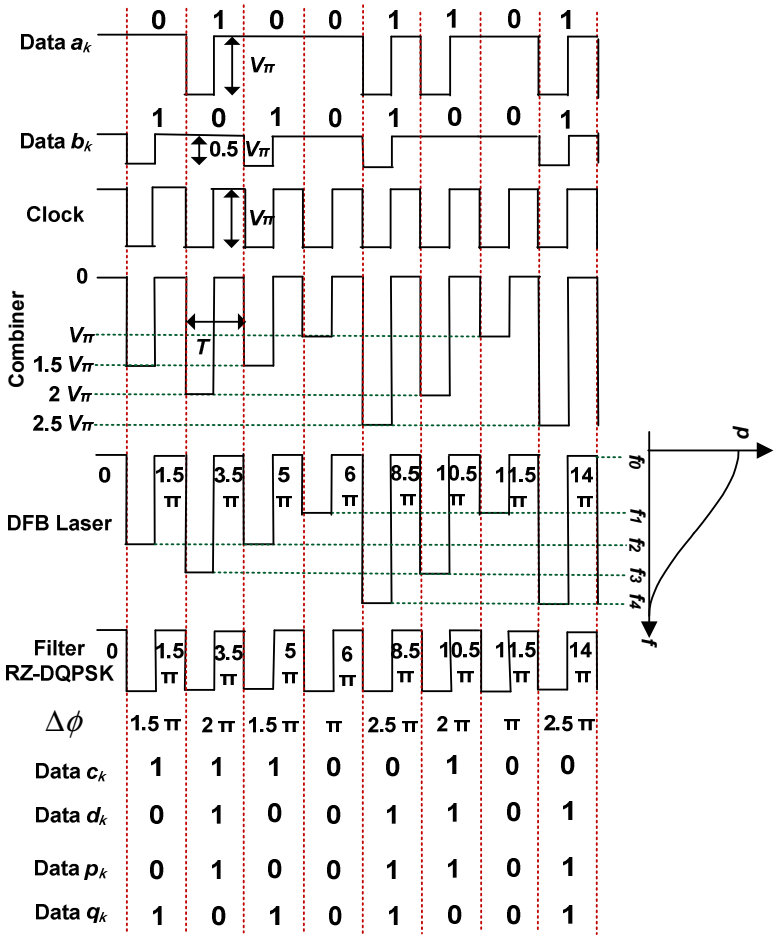

Fig. 4.29 Operation principle of CML-based RZ-DQPSK signal generation

The driving voltages of data a_k, data b_k, and clock are V_π, 0.5 V_π and V_π, respectively. The laser is biased high above the threshold with the benefits of high output power, single mode operation, wide modulation bandwidth, and suppression of the transient chirp. The driving voltage of V_π is adjusted to induce adiabatic chirp Δf, given by

$$\Delta f = 1/T \tag{4.13}$$

where T is the symbol period. The induced adiabatic chirp in turn causes a phase shift $\Delta\emptyset$,

calculated from

$$\Delta\emptyset = 2\pi \int_0^{\frac{T}{2}} \Delta f(t)dt$$

$$= 2\pi \times 1/T \times T/2$$

$$= \pi \tag{4.14}$$

during the first half-symbol period of 00 symbol. Thus the induced phase shifts of symbols of 00, 01, 10, and 11 for input a_k b_k are π, 1.5π, 2π, and 2.5π, respectively. Then, the spectral position of the filter integrated in the CML is tuned to suppress the first half-symbol signal with frequencies of f_1, f_2, f_3, and f_4 and pass through the second half-symbol signal with frequency of f_0, generating RZ-DQPSK. At the receiver, the symbols of 00, 01, 10, and 11 for input a_k b_k are demodulated into c_k d_k of 00, 10, 11, and 01 by a 1-bit optical DI. Finally, the decoding operations of

$$p_k = d_k \tag{4.15}$$

and

$$q_k = c_k \oplus d_k \tag{4.16}$$

are used to recover the input data a_k b_k., where data p_k q_k are the decoded output signal. The decoding operations at the receiver site could be replaced by the pre-coding operations at the transmitter side.

4.4.3 Experiments and results

We have experimentally demonstrated the system for generation and transmission of CML-based RZ-DQPSK signal, using the setup shown in Fig. 4.28. We employed a standard CML module (Finisar DM200-01) with input impedance of 50 ohms, threshold current of 25 mA, and FM efficiency of 0.24 GHz/mA. The filter in CML had a 3-dB bandwidth of 7 GHz and an average slope of 2.4 dB/GHz. Two 10.709-Gb/s IRZ data streams, generated by NAND logic gates, using 2^7-1 PRBS with driving voltages of 20 mV and 10 mV were combined together with a 20-mV clock. The peak-to-peak voltage V_{pp} of the driving signal was amplified to 4.2 V using an electrical amplifier. The DFB laser was biased at 110 mA. The central wavelength and the optical power of the generated optical RZ-DQPSK signal were 1555.69 nm and 1.4 dBm, respectively. The generated optical RZ-DQPSK signal was then transmitted over a piece of SSMF. The transmitted signal was received after being amplified via an EDFA, and filtered via a 1.0-nm OBPF for ASE noise elimination. The receiver was composed of two sets of DIs with FSRs of 10.664 GHz, PDs, and 10-GHz electrical amplifiers. We tuned the phase difference between the two arms of each DI to $\pi/4$ or $-\pi/4$, so as to demodulate the two data streams contained in the received optical RZ-DQPSK signal.

Fig. 4.30 shows the measured waveforms of the data a_k and data b_k after NAND logic gates, the input clock signal, the driving signal of the CML, and the demodulated data c_k and data d_k at the two output ports of the DIs. They verified that data a_k was recovered from data d_k and data b_k would be retrieved from XOR operation of data c_k and data d_k.

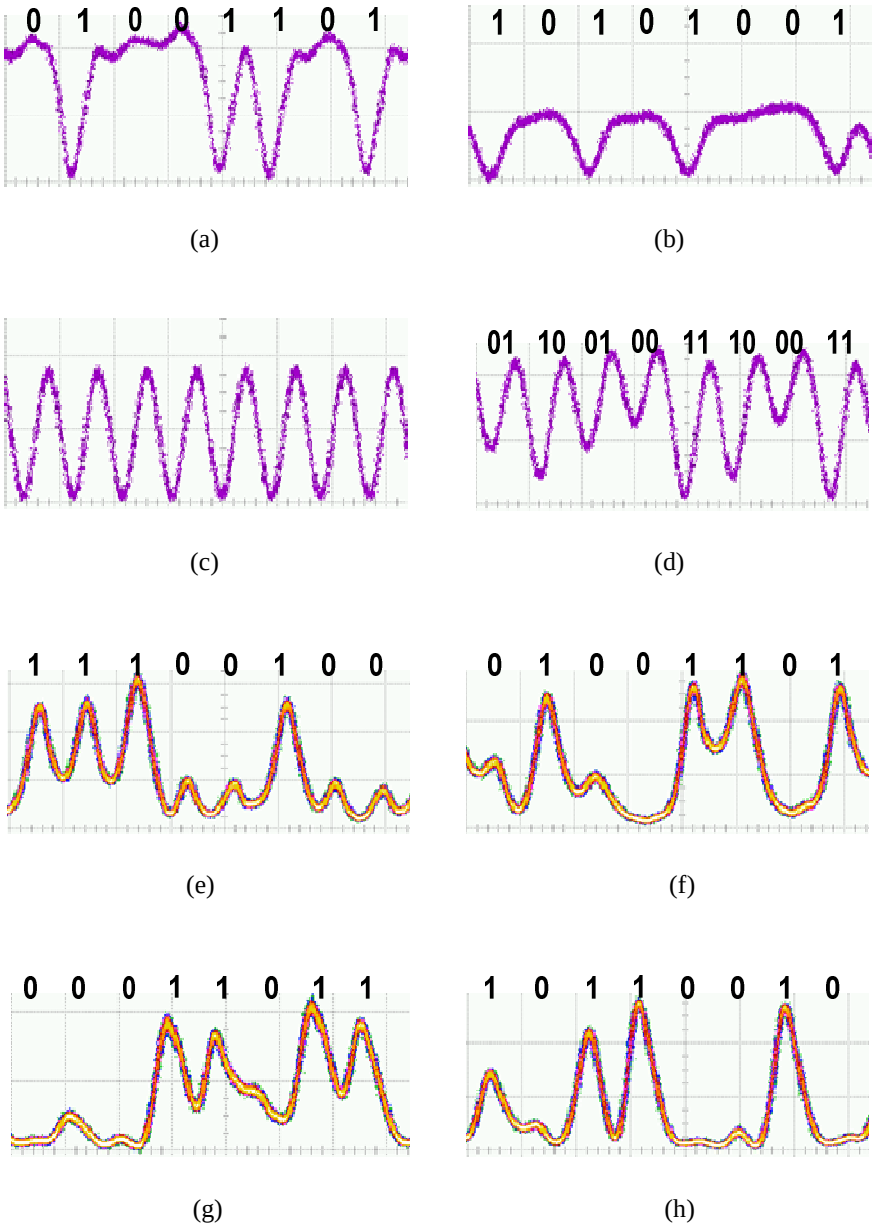

Fig. 4.30 Waveforms of (a) data a_k, (b) data b_k, (c) clock, (d) driving signal, (e) data c_k, (f) data d_k, (g) inverting data c_k, and (h) inverting data d_k. Time scale: 100 ps/div.

Fig. 4.31 shows the respective eye diagrams of the driving signal after electrical combiner, BtB RZ-DQPSK signal after CML, demodulated data c_k and data d_k at one output port of DI before and after the 40-km SSMF, using a 40-GHz PD.

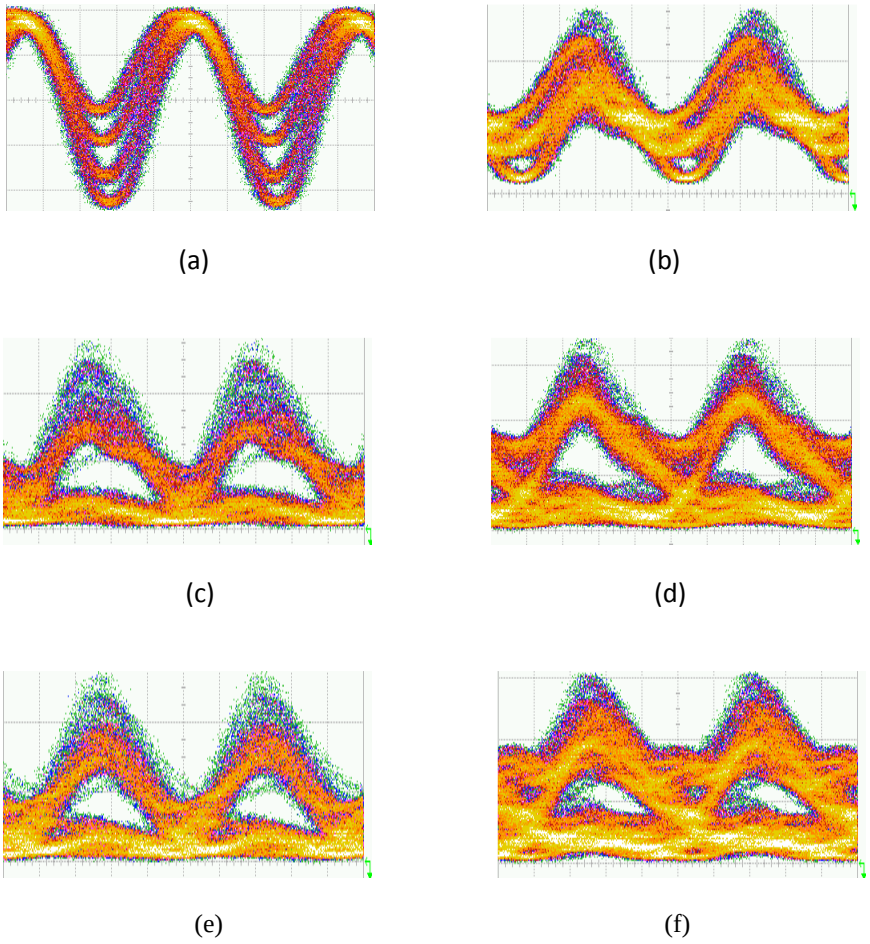

Fig. 4.31 Eye diagrams of (a) driving signal after electrical combiner, (b) RZ-DQPSK signal after CML, (c) BtB data c_k, (d) BtB data d_k, (e) data c_k after 40-km SSMF, and (f) data d_k after 40-km SSMF, using a 40-GHz PD. Time scale: 20 ps/div.

Fig. 4.32 shows the measured BER performance of the generated optical RZ-DQPSK signal using CML before and after 40-km SSMF transmission. Though the XOR decoding was not performed, we still could get the BER of data c_k to evaluate the signal quality, due to the pseudo-random property of PRBS. The power penalties at BER of 10^{-9} for data c_k and data d_k after 40-km SSMF were 0.95 dB and -0.41 dB, with reference to their BtB receiver sensitivities of -12.1 dBm and -13.9 dBm, respectively. The different performances for data c_k and data d_k might be

attributed to the un-optimized phase shifts between the symbols in the RZ-DQPSK signal. The insets show the eye diagrams of the detected signals fed into the BERT.

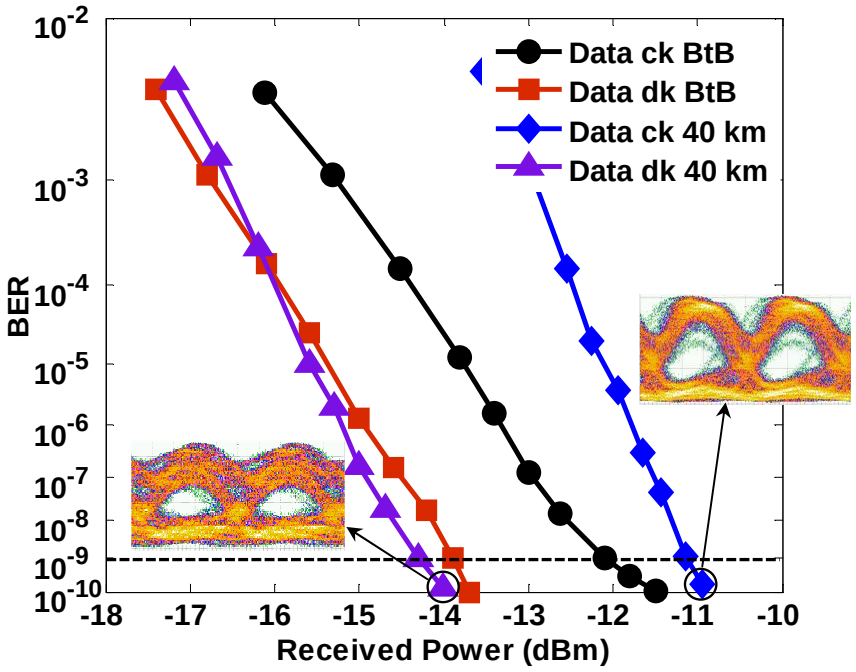

Fig. 4.32 Measured BER performance of CML-based RZ-DQPSK signal. Insets show the eye diagrams of detected signals fed into BERT. Time scale: 20 ps/div.

4.4.4 Summary

In this section, we have demonstrated the generation of 10.709-Gbaud RZ-DQPSK signal using single CML, without any differential encoder, external PM, or pulse carver. Optical transmission performance over 40-km SSMF without any dispersion compensation has been experimentally characterized for the two data tributaries in RZ-DQPSK signal.

4.5 Summary and discussion

In this chapter, step by step, we have proposed and experimentally demonstrated the generation of 10-Gb/s RZ-DPSK signal using CML and pulse carver, 20-Gb/s RZ-DQPSK signal using CML and pulse carver, 10-Gbaud ¾-RZ-DQPSK signal using single CML, and 10.709-Gbaud RZ-DQPSK signal using single CML. Actually, this scheme can be generalized to generate *M*-ary RZ-DPSK signal based on CML under the ideal conditions.

No external optical PM is needed, since these approaches make smart use of the adiabatic chirp in DML for phase modulation. Moreover, they do not need the complex electrical differential pre-coders in conventional *M*-ary RZ-DPSK transmitters using external modulators, for the natural differential encoding property of adiabatic chirp. The filter in CML or the following pulse carver contributes to convert the slow phase shifts into abrupt phase transitions for the DPSK and DQPSK signals generated by DML. With the elegant design of driving signal, the filter in CML can take the place of the pulse caver to generate full RZ-shaped DQPSK signal using only single CML. Therefore, the footprint, cost, and power consumption of CML-based RZ-DPSK and RZ-DQPSK transmitters are reduced significantly, compared with the equivalents using external modulators.

We have also investigated the transmission performances and robustness towards operation condition changes of the RZ-DPSK and RZ-DQPSK systems based on CML. The 10-Gb/s RZ-DPSK signal generated by 10-GHz standard CML and pulse carver shows better fiber CD tolerance and comparable fiber nonlinearity tolerance, in comparison with that generated using optical PM. Nevertheless, when this scheme upgrades to the 20-Gb/s RZ-DQPSK signal using the same CML, the performances degrade quickly. At the first glance, the evident reasons are

related with the limited modulation bandwidth and small adiabatic chirp value in commercial available CML. Hence, using a 23-GHz DBR-laser based CML together with high-speed electrical encoder, cable, combiner, and amplifier, the 10-Gbaud ¾-RZ-DQPSK demonstrates reasonable transmission performance and operation condition change robustness.

However, deep insight into the working principle of CML-based RZ-DQPSK transmitter may enable more impressive performance in the future work. The DML indeed functions as an optical PM with continuous phase change, instead of a MZM with accurate and instantaneous phase transition. If the relationship between adiabatic chirp change and symbol rate in (4.14) equation is not precisely maintained, the phase shifts between symbols will not be exact for DQPSK signal. Any intensity noise, over-shoot, and imperfection of the driving signal will transfer into the phase noise of the CML-based RZ-DQPSK signal. Since the distance between the constellations in RZ-DQPSK format is very close, the induced phase noise will result in severe impairments to the CML-based RZ-DQPSK signal. This becomes evident especially when the driving signal is complicated such as the five-level one. Though 40-km SSMF transmission is realized for the 10.709-Gaud RZ-DQPSK signal using single CML, it is clearly shown that the noisy driving signal in the experiment limits the potential of the system.

From a systemic viewpoint, if both the multi-level phase modulating function and pulse carving function are required to be realized by a single laser and an optical filter, it will put heavy burden on the laser. It is not easy to achieve both good performance and extreme simplicity at the same time. Therefore, the idea of several phase-locked lasers with independent direct modulations integrated in one transmitter is an attractive solution to further improve the performance of CML for generating advanced modulation formats.

Chapter 5 Enhanced CD Tolerance of CML with Pre-emphasis

5.1 Introduction

As reviewed in chapter two, CML is a promising transmitter in optical access and metropolitan networks due to its compact footprint, low cost, small power consumption, and high dispersion tolerance. The 10-Gb/s CML realized error-free 250-km SSMF transmission [62]. The EDC techniques help to further extend the reach of CML. Compared with post-EDC, pre-EDC takes the advantage of phase information in optical signal, which is more suitable for CML. With a 1-bit DSP driver for pulse shaping at the transmitter, the 10.709-Gb/s CML extended SSMF reach to 360 km at BER of 10^{-4} [124]. The 608-km SSMF transmission at BER of 10^{-3} was reported using a 10.709-Gb/s CML and a 6-bit 21.418-GSa/s DAC for electronic pre-distortion [125]. However, the DSP and DAC consume too much power and bring extra cost for CML, which are not desirable for access and metropolitan applications. Moreover, too heavy pre-distortion limits the dispersion tolerance of CML to 110 km for 1-dB penalty window [125].

In this section, we propose and experimentally demonstrate the 10-Gb/s 300-km SSMF transmission at BER of 10^{-9} using a commercial available CML with a simple and passive pre-emphasis driver at the transmitter. The 10-Gb/s standard CML signal without pre-emphasis could only be transmitted up to 220 km, in comparison. No expensive optical DCM or power-hungry EDC was used. The 20-Gb/s 100-km SSMF transmission at BER of 10^{-9} using CML with pre-emphasis driver was also reported.

5.2 Operation principle

Fig. 5.1 depicts the structure of the proposed pre-emphasis driver, which comprises the passive electrical splitter, inverter, attenuator, delay, and combiner.

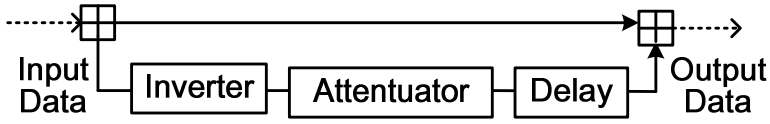

Fig. 5.1 Structure of the proposed pre-emphasis driver

Fig. 5.2 shows the simulated intensity and chirp characteristics for the 10-Gb/s standard CML signal without pre-emphasis and the CML signal with pre-emphasis before and after 300-km SSMF with an input bit sequence of “0011001001011100”. By tuning the spectral position of the narrow-bandwidth filter in the CML, high ER signal can be obtained. However, as shown in Fig. 5.2(a), it is observed that the intensity of the single “1” bit is slightly reduced, compared with the consecutive “1” bits, i.e., double “1” bits and triple “1” bits, caused by the narrow-bandwidth filtering or low laser modulation bandwidth. Fig. 5.1(b) shows that the main reason limiting the BER performance for the standard CML signal after 300-km SSMF is that the single “1” bit collapses quickly, while the consecutive “1” bits grow and become sharp, due to the interference among the adjacent bits, thus inducing severe intensity fluctuations. By employing the proposed pre-emphasis driver, the intensity of the single “1” bit is enhanced, compared with the main part of the consecutive “1” bits, as depicted in Fig. 5.2(c). Hence, the intensity differences between the single “1” bit and the consecutive “1” bits are reduced after SSMF, as shown in Fig. 5.2(d). Besides, a large red shifted transient chirp at the falling edge of bit

transition is generated, while the blue shifted transient chirp at the rising edge of bit transition is suppressed by tuning the spectral position of the filter in CML, as shown in Fig. 5.2(c). This uni-polar negative transient chirp also helps to increase the reach of CML [124].

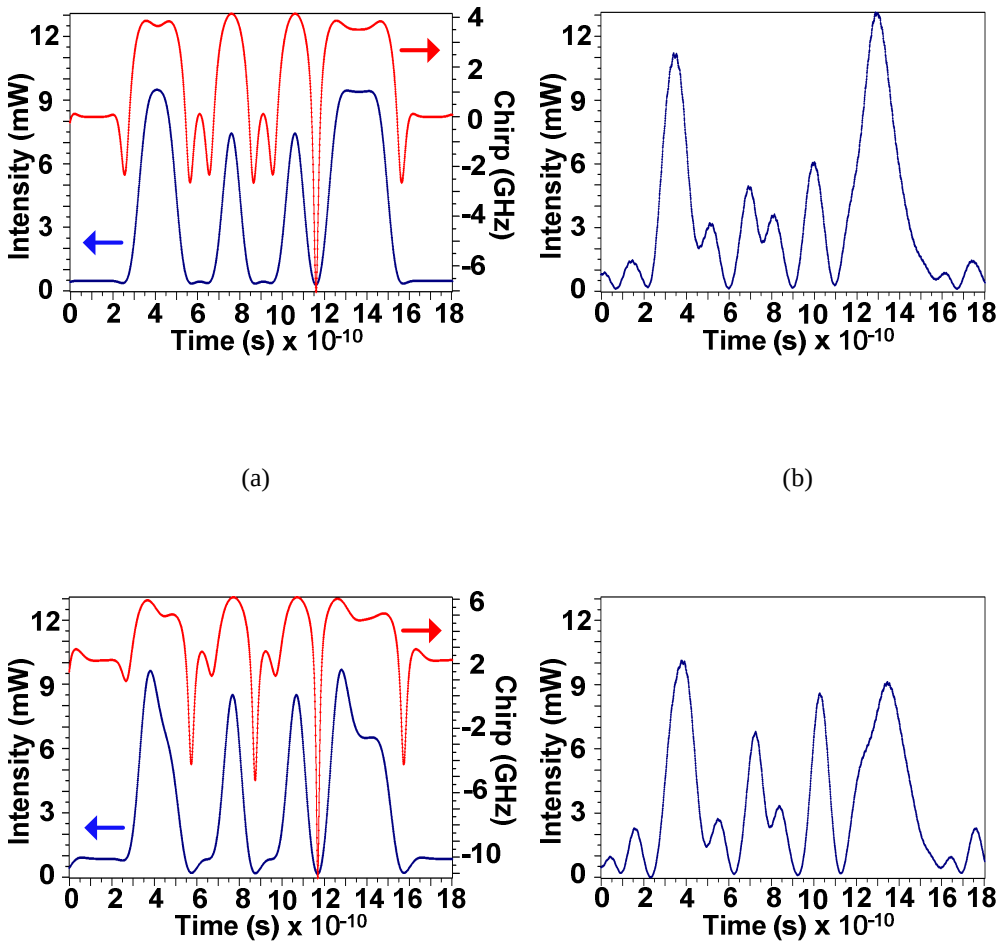

Fig. 5.2 Simulated intensity and chirp characteristics of (a) BtB standard CML signal, (b) standard CML signal after 300-km SSMF, (c) BtB CML signal with pre-emphasis, and (d) CML signal with pre-emphasis after 300-km SSMF with an input bit sequence of "0011001001011100"

5.3 Experiments and results

We have experimentally verified the proposed scheme at 10-Gb/s and 20-Gb/s. Fig. 5.3 shows the experimental setup for the transmission of CML signal with pre-emphasis.

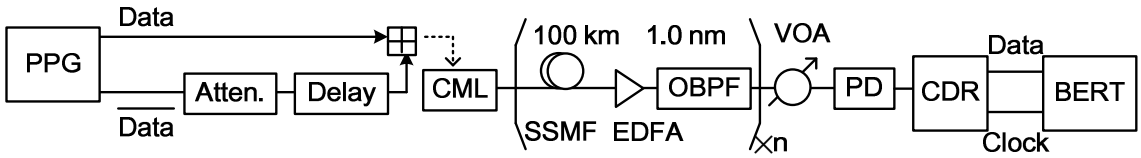

Fig. 5.3 Experimental setup for the transmission of CML signal with pre-emphasis

First, the 10-Gb/s experiment was performed using a standard CML module (Finisar DM200-01). The 9.953-Gb/s driving signal with pre-emphasis using 2^{31}-1 PRBS was generated by combining the non-inverting data and the inverting data from the pulse pattern generator (PPG), via a combiner. The inverting data was attenuated by 8 dB and delayed by 50 ps, compared with the non-inverting data. The peak-to-peak driving voltage V_{pp} was 0.9 V. The input impedance, threshold current, and FM efficiency of the DFB laser were 50 ohms, 25 mA, and 0.24 GHz/mA, respectively. The DFB laser was biased at 70 mA, high above the threshold to assure high output power, single mode operation, wide modulation bandwidth, and suppression of transient chirp. The filter in CML had a 3-dB bandwidth of 7 GHz and an average slope of 2.4 dB/GHz. The central wavelength, ER, and optical power of the CML signal were 1556.9 nm, 7.4 dB, and 0.95 dBm, respectively. The linear transmission line comprised three spans of 100-km SSMFs. An EDFA was inserted after every span to boost up the optical power to 2 dBm. A tunable OBPF with 1.0-nm bandwidth was placed after every EDFA to eliminate the ASE noise. A VOA was used to adjust the input power to the receiver composed of a PD and a 9.953-Gb/s

clock-data recovery (CDR) module. The recovered data and clock were sent to the BERT for BER measuring. In the control setup for the 9.953-Gb/s standard CML without pre-emphasis driver, the DFB laser was also biased at 70 mA. The peak-to-peak driving voltage V_{pp} was 0.7 V to generate an adiabatic chirp of 4 GHz. The bias, driving voltage, and spectral position of the filter in CML were optimized for maximum SSMF transmission at BER of 10^{-9}.

Fig. 5.4 shows the patterns of the 10-Gb/s driving signals and the CML signals after 300-km SSMF without and with pre-emphasis, using an input bit sequence of "0011001001011100". With pre-emphasis, intensity over-shoots at the rising and falling edges of the bit transitions of the driving signal were observed, as depicted in Fig. 5.4 (b). The intensity of the single "1" bit was improved, compared with the main part of the consecutive "1" bits. After 300-km SSMF, the single "1" bit of the standard CML signal collapsed quickly (see in Fig. 5.4 (c)), while that with pre-emphasis showed reduced intensity differences (see in Fig. 5.4 (d)), as compared with the consecutive "1" bits.

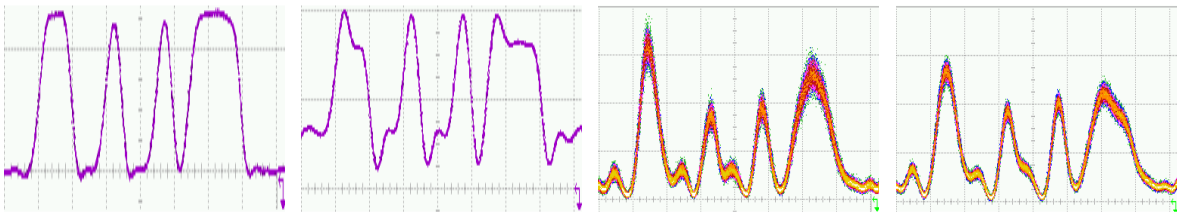

Fig. 5.4 Patterns of the 10-Gb/s (a) driving signal without pre-emphasis, (b) driving signal with pre-emphasis, (c) standard CML signal without pre-emphasis after 300-km SSMF, and (d) CML signal with pre-emphasis after 300-km SSMF. Time scale: 200 ps/div

Fig. 5.5 shows the eye diagrams of the 10-Gb/s driving signal, BtB CML signal, and CML signal after 220-km and 300-km SSMF before CDR, without and with pre-emphasis. Fig. 5 (g)-

(h) show that CML signal with pre-emphasis exhibited less mark noise and much wider eye opening, compared with standard CML signal in Fig. 5 (c)-(d), after 220-km and 300-km SSMF.

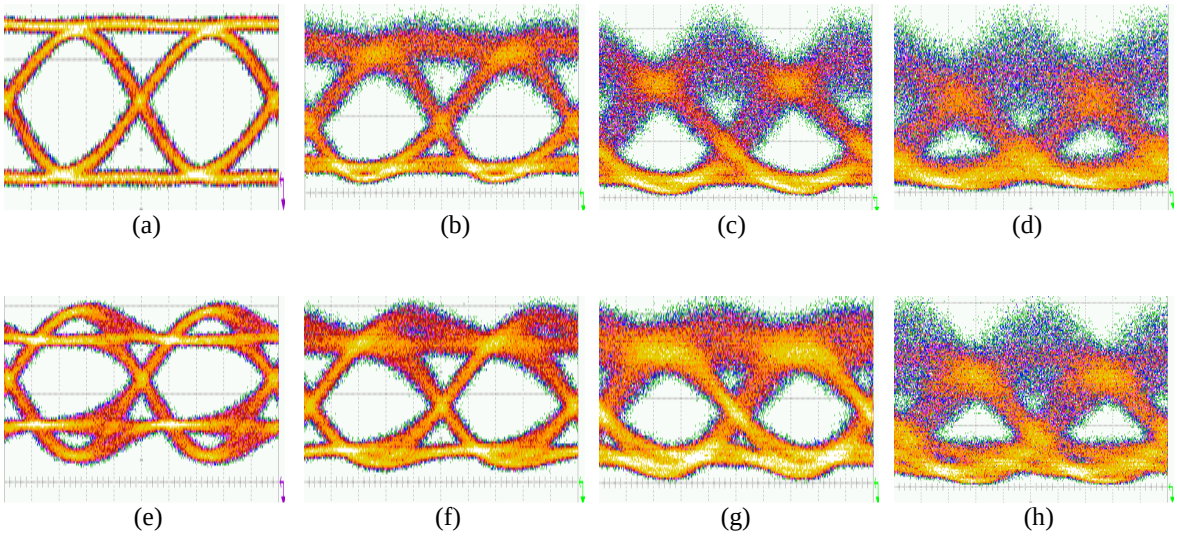

Fig. 5.5 Eye diagrams of the10-Gb/s (a)-(d) driving signal, BtB CML signal, CML signal after 220-km SSMF, and CML signal after 300-km SSMF without pre-emphasis, and (e)-(h) the ones with pre-emphasis. Time scale: 20 ps/div

We have also measured the transmission performances of fiber CD tolerance for the 10-Gb/s CML signals without and with pre-emphasis. Fig. 5.6 shows the receiver sensitivities at BER of 10^{-9} after various lengths of SSMF for the two different 10-Gb/s cases. The CML signal with pre-emphasis realized 300-km SSMF transmission, with a power penalty of 3.3 dB, compared with its BtB receiver sensitivity of -16.5 dBm. Its SSMF transmission reach at 1-dB power penalty was 290 km. It also showed a negative power penalty of -1.7 dB after 220-km SSMF. This was attributed to the mitigation of the over-shoots at the rising and falling edges of the bit transitions and the ER enhancement of the CML signal with pre-emphasis, after SSMF. The standard CML signal without pre-emphasis could only be transmitted up to 220 km with a power penalty of 5.1 dB, compared with its BtB receiver sensitivity of -16.1 dBm.

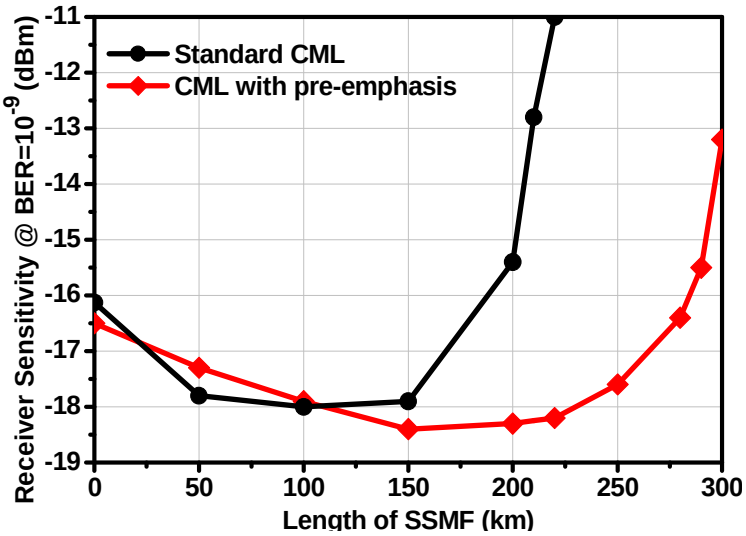

Fig. 5.6 Receiver sensitivities for the 10-Gb/s standard CML signal without pre-emphasis and CML signal with pre-emphasis after various lengths of SSMF

Fig. 5.7 shows the BER performances of the 10-Gb/s CML signals without and with pre-emphasis. The standard CML signal showed obvious error floor at BER of 10^{-10}, while the CML signal with pre-emphasis showed a straight BER curve, after 220-km SSMF transmission.

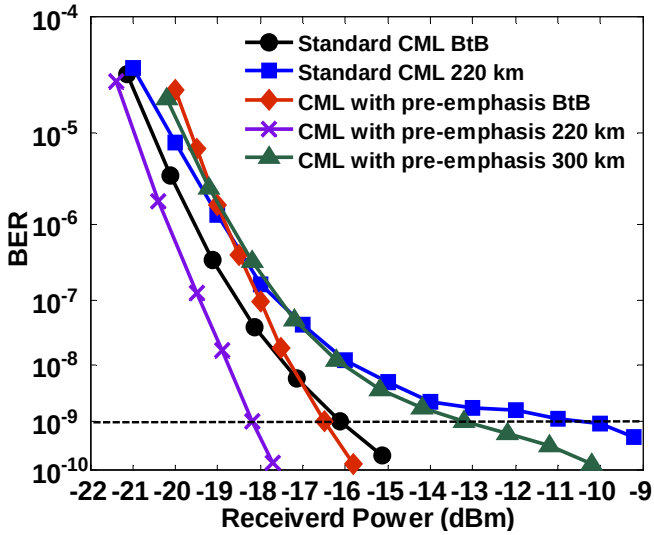

Fig. 5.7 BER performances for the 10-Gb/s CML signals without and with pre-emphasis

Later, the 20-Gb/s experiment with 2^{31}-1 PSBS was carried out using another standard 1555.5-nm CML module (Finisar DM80-01) with a built-in 11-GHz filter. The receiver had a 35-GHz PD and a 1:4 electrical DEMUX. However, a 20-Gb/s CDR was not available. The clock at the transmitter was sent to the DEMUX and BERT for timing decision. Fig. 5.8 shows the eye diagrams of the 20-Gb/s CML signals without and with pre-emphasis for 100-km and 120-km SSMF transmission. Fig. 5.8 (b)-(c) shows that the standard CML signals without pre-emphasis were nearly totally corrupted after 100-km and 120-km SSMF. No BER could be measured. However, there were still considerable eye openings for the CML signals with pre-emphasis after transmission.

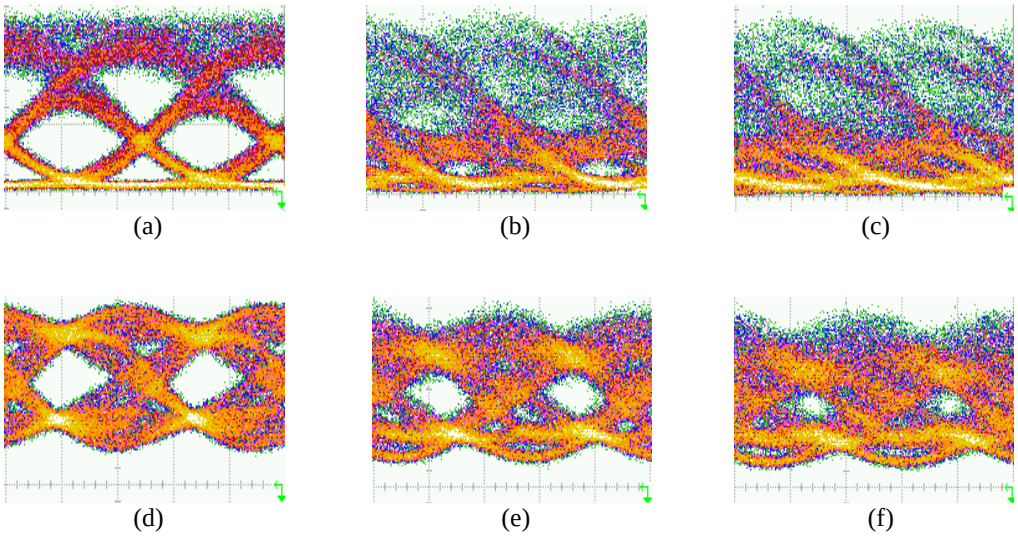

Fig. 5.8 Eye diagrams of the 20-Gb/s (a)-(c) BtB CML signal, CML signal after 100-km SSMF, and CML signal after 120-km SSMF without pre-emphasis, and (d)-(f) the ones with pre-emphasis. Time scale: 20 ps/div

Fig. 5.9 shows the 20-Gb/s BER performances for the CML signals without and with pre-emphasis. The CML signal with pre-emphasis realized 100-km SSMF transmission with a power penalty of 2.7 dB, with reference to its BtB receiver sensitivity of -4.9 dBm at BER of 10^{-9}. After

120-km SSMF, we still could measure its BER below 10^{-4}. In comparison, the ever reported transmission reach of the 20-Gb/s CML without ODC or EDC was 60-km SSMF [104]. As a reference, the BtB receiver sensitivity of the standard CML signal without pre-emphasis was -2.26 dBm at BER of 10^{-9}. The poor receiver sensitivity was caused by the decision timing jitter of BERT due to the lack of 20-Gb/s CDR module.

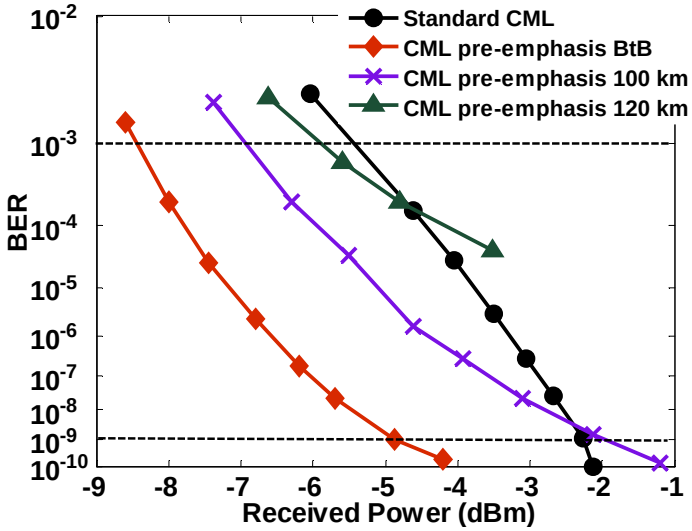

Fig. 5.9 BER performances for the 20-Gb/s CML signals without and with pre-emphasis

5.4 Summary

In this section, we have experimentally demonstrated the 10-Gb/s 300-km and 20-Gb/s 100-km SSMF transmissions at BER of 10^{-9} using the CMLs with pre-emphasis driver. The transmission performance of fiber CD tolerance was investigated and compared with the standard CML signals without pre-emphasis.

Chapter 6 Summary

6.1 Summary of this thesis

In this thesis, we have designed several novel optical transmitters based on CML, composed of a DML and an optical filter, by managing its adiabatic chirp. The applications include optical RZ pulse generation using CML, *M*-ary RZ-DPSK signals generation using CML, and enhanced CD tolerance of CML with pre-emphasis. We aim to achieve the simplicity while maintaining or improving the transmission performance of the transmitter in optical fiber communication systems.

In chapter one, firstly, we have talked about the history of optical fiber communication systems. The dynamic relationship between the system capacity and traffic need is analyzed. Transmission performance as well as footprint, cost, and power consumption are highlighted for transceiver design. Then, we have reviewed the transmission impairments of fiber CD, PMD, nonlinearities, and noises. The key role of advanced modulation formats such as duobinary, AMI, optical RZ pulses, RZ-DPSK, and RZ-DQPSK in reducing the signal distortions is discussed. The advantages and disadvantages of conventional transmitters based on DML, EAM, and MZM are presented. Finally, we have showed the common methods to generate advanced modulation formats using external modulators.

In chapter two, firstly, we have looked back the inventing process of CML. The device structure and control schematic of CML are presented. Then, we have analyzed the associated chirp origin and modulation bandwidth of DML. The potential laser design for CML is proposed. Finally, we have reviewed the previous works on CML including duobinary, AMI, and RZ-DPSK

signals generation and EDC for reach extension. The achievements and drawbacks of these schemes are also discussed.

In chapter three, firstly, we have proposed and experimentally demonstrated the generation of 10-Gb/s optical RZ pulses with duty cycles of 33% and 67% using CML driven at half pulse rate. The 10-Gb/s RZ-DPSK signals based on CML-RZ-pulses show comparable fiber CD and nonlinearity tolerance, compared with the equivalents based on pulse carver using MZM. Then, we have further experimentally demonstrated the generation of 20-Gb/s optical RZ pulses with 33%-duty-cycle and asymmetric-duty-cycle using CML driven at one-fourth pulse rate. We also characterize the transmission performance of 20-Gb/s RZ-OOK signals based CML-RZ-pulses.

In chapter four, firstly, we have proposed and experimentally demonstrated the generation of 10-Gb/s RZ-DPSK signal using CML and pulse carver. No differential pre-coder or PM is required. It realizes 80-km SSMF transmission and shows comparable fiber nonlinearity tolerance to RZ-DPSK signal based on PM. Then, we have proposed and experimentally demonstrated the generation of 20-Gb/s RZ-DQPSK signal using CML and pulse carver. No complex electrical pre-coding or PM is needed. Later, we have proposed and experimentally demonstrated the generation of 10-Gbaud ¾-RZ-DQPSK signal using single CML. It achieves 60-km SSMF error-free transmission without OSNR penalty. Finally, we have proposed and experimentally demonstrated the generation of 10.709-Gbaud RZ-DQPSK signal using single CML. It does not use any differential encoder, PM, or pulse carver. The generated RZ-DQPSK signal transmits over 40-km SSMF at BER of 10^{-9}.

In chapter five, we have proposed and experimentally demonstrated the 10-Gb/s 300-km and 20-Gb/s 100-km SSMF transmissions using commercial available CMLs and a passive pre-

emphasis driver, without any ODC or power-hungry EDC. Their CD tolerances are characterized and compared with the standard CMLs without pre-emphasis driver.

6.2 Future work

For all optical OFDM technique, either mode-locked laser or external modulator is required to generate the optical orthogonal subcarriers [139]-[140]. We propose to generate dual or more high-speed optical orthogonal subcarriers using the simultaneous AM and FM of the CML driven by sinusoidal signal to reduce the footprint, cost, and power consumption of all-optical-OFDM transmitter.

In chapter four, we have demonstrated the 80-km SSMF transmission of 10-Gb/s CML-based RZ-DPSK signal using direct detection. We propose to use the coherent receiver to characterize the affect of DML linewidth on the CML-based RZ-DPSK signal. Its long-haul transmission using coherent detection will also be investigated, where constellation diagrams can be obtained to calibrate the phase shifts in DPSK signal precisely.

In chapter four, we have analyzed the causes limiting the performances CML-based RZ-DQPSK signal. First, we propose to perform the laser design of short cavity with multiple QWs mentioned in chapter two to fabricate DML with high modulation bandwidth and large FM efficiency, as the laser candidate of CML-based DQPSK transmitter. Then, we propose to use an optical phase locked loop (OPLL) and a coupler to make two DMLs coherent and coupled together. The two DMLs will be modulated independently with two-level IRZ signals to generate DQPSK signal.

In chapter five, we have proposed to use a simple pre-emphasis driver to boost the intensity of the single “1” bit to improve the CD tolerance of CML. However, that pre-emphasis driver also adds over-shoots on the rising and falling edges of the consecutive “1” bits, which are not desirable. Therefore, a new way to only enhance the amplitude of the single “1” bit and not to affect the consecutive “1” bits is being considered in mind.

The tuning of laser bias, filter spectral position, and driving voltage have great impact on the proposed CML-based transmission systems in this thesis, which limit the practical utility. We will study the performance penalty due to the change of laser bias, filter spectral position, and driving voltage caused by unstable electrical current, temperature, pressure, and other environmental factors.

Reference

[1] Cisco Systems, “Fiber types in gigabit optical communications”, *White Paper*, April 2008.

[2] G. P. Agrawal, “Fiber-optic communication systems”, 3rd edition, John Wiley & Sons, 2002.

[3] R. W. Tkach, “Scaling optical communications for the next decade and beyond,” *Bell Labs Tech. J.*, vol. 14, no. 4, pp. 3-10, 2010.

[4] Cisco Systems, “Cisco visual networking index: forecast and methodology, 2012-2017,” *White Paper*, May 2013.

[5] A. H. Gnauck, A. R. Chraplyvy, R. W. Tkach, J. L. Zyskind, J. W. Sulhoff, A. J. Lucero, Y. Sun, R. M. Jopson, F. Forghieri, R. M. Derosier, C. Wolf, and A. R. McCormick, “ One terabit/s transmission experiment,” *IEEE/OSA Optical Fiber Communication Conference / National Fiber Optic Engineers Conference (OFC/NFOEC)*, Paper PD20, San Jose, California, USA, 1996.

[6] T. Morioka, H. Takara, S. Kawanishi, O. Kamatani, K. Takiguchi, K. Uchiyama, M. Saruwatari, H. Takahashi, M. Yamada, T. Kanamori, and H. Ono, “100 Gbit/s x 10 channel OTDM/WDM transmission using a single supercontinuum WDM source,” *IEEE/OSA Optical Fiber Communication Conference / National Fiber Optic Engineers Conference (OFC/NFOEC)*, Paper PD21, San Jose, California, USA, 1996.

[7] T. J. Xia, G. A. Wellbrock, A. Tanaka, M. F. Huang, E. Ip, D. Y. Qian, Y. K. Huang, S. L. Zhang, Y. Q. Zhang, P. N. Ji, Y. Aono, S. J. Murakami, and T. Tajima, “High capacity field trials of 40.5 Tb/s for LH distance of 1,822 km and 54.2 Tb/s for regional distance of 634 km,” *IEEE/OSA Optical Fiber Communication Conference / National Fiber Optic Engineers Conference (OFC/NFOEC)*, Paper PDP5A.4, Anaheim, California, USA, 2013.

[8] Binh, L. Nguyen, “Digital optical communications”, Taylor & Francis Group, 2009.

[9] C. Lin, H. Kogelnik, and L. G. Cohen, “Optical-pulse equalization of low-dispersion transmission in single-mode fibers in the 1.3-1.7-μm spectral region,” *OSA Opt. Lett*, vol. 5, no. 11 pp. 476-478, 1980.

[10] A. J. Antos and D. K. Smith, “Design and characterization of dispersion compensating fiber based on the LP_{01} mode”, *IEEE J. Lightw. Technol.*, vol. 12, no. 10, pp. 1739-1745, 1994.

[11] T. Ozeki, “Optical equalizers”, *OSA Opt. Lett.*, vol. 17, no. 5, pp. 375-377, 1992.

[12] R. I. Killey, P. M. Watts, V. Mikhailov, M. Glick, and P. Bayvel, “Electronic dispersion compensation by signal predistortion using digital processing and a dual-drive Mach-Zehnder modulator,” *IEEE Photon. Technol. Lett.*, vol. 17, no. 3, pp. 714-716, 2005.

[13] J. H. Winters and R. D. Gitlin, “Electrical signal processing techniques in long-haul fiber-optic systems,” *IEEE Transactions on Communications*, vol. 38, no. 9, pp. 1439-1453, 1990.

[14] S. J. Savory, “Digital filters for coherent optical receivers,” *OSA Opt. Express*, vol. 16, no. 2, pp. 804-817, 2008.

[15] L. Pierre, J. P. Thiery and D. Penninckx, “243, 10 Gbit/s transmission experiment through standard fibre and impact of self-phase modulation using partial response scheme,” *IEEE Electron. Lett.*, vol. 32, no. 7, pp. 673-674, 1996.

[16] W. Kaiser, T. Wuth, M. Wichers and W. Rosenkranz, “Reduced complexity optical duobinary 10-Gb/s transmitter setup resulting in an increased transmission distance,” *IEEE Photon. Technol. Lett.*, vol. 13, no. 8, pp. 884-886, 2001.

[17] R. A. Griffin and A. C. Carter, “Optical differential quadrature phase-shift key (oDQPSK) for high capacity optical transmission,” *IEEE/OSA Optical Fiber Communication Conference*

/ *National Fiber Optic Engineers Conference (OFC/NFOEC)*, Paper WX6, Anaheim, California, USA, 2002.

[18] M. Seimetz, "Performance of coherent optical square-16-QAM-systems based on IQ-transmitters and homodyne receivers with digital phase estimation," *IEEE/OSA Optical Fiber Communication Conference / National Fiber Optic Engineers Conference (OFC/NFOEC)*, Paper NWA4, Anaheim, California, USA, 2006.

[19] D. Mahgerefteh and C. R. Menyuk, "Effect of first-order PMD compensation on the statistics of pulse broadening in a fiber with randomly varying birefringence," *IEEE photon. Technol. Lett.*, vol.11, no. 3, pp. 340-342, 1999

[20] F. Buchali and H. Bülow, "Adaptive PMD compensation by electrical and optical techniques," *IEEE J. Lightw. Technol.*, vol. 22, no. 4, pp. 1116-1126, 2004.

[21] H. F. Haunstein, T. Schorr, A. Zottmann, W. Sauer-Greff, and R. Urbansky, "Performance comparison of MLSE and iterative equalization in FEC systems for PMD channels with respect to implementation complexity," *IEEE J. Lightw. Technol.*, vol. 24, no. 11, pp. 4047-4054, 2006.

[22] R. M. Jobson, L. E. Nelson, G. J. Pendock, and A. H. Gnauck, "Polarization-mode dispersion impairment in Return-to-Zero and Non-return-to-Zero systems," *IEEE/OSA Optical Fiber Communication Conference / National Fiber Optic Engineers Conference (OFC/NFOEC)*, Paper WE3, San Diego, California, USA, 1999.

[23] H. Sunnerud, M. Karlsson, and P. A. Andrekson, "A comparison between NRZ and RZ data formats with respect to PMD-induced system degradation," *IEEE Photon. Technol. Lett.*, vol. 13, no. 5, pp. 448-450, 2001.

[24] C. Xie, L. Moller, H. Haunstein and S. Hunsche, “Polarization mode dispersion induced impairments in different modulation format systems,” *IEEE/OSA Optical Fiber Communication Conference / National Fiber Optic Engineers Conference (OFC/NFOEC)*, Paper TuO1, Atlanta, Georgia, USA, 2003.

[25] P. Boffi, M. Ferrario, L. Marazzi, P. Martelli, P. Parolari, A. Righetti, R. Siano, and M. Martinelli, “Measurement of PMD tolerance in 40-Gb/s polarization-multiplexed RZ-DQPSK,” *OSA Opt. Express*, vol. 16, no. 17, pp.13398-13404, 2008.

[26] G. P. Agrawal, “Nonlinear fiber optics,” 4th edition, Elsevier Inc., 2007

[27] A. R. Chraplyvy, A. H. Gnauck, R. W. Tkach, and R. M. Derosier, “8 x 10 Gb/s transmission through 280 km of dispersion-managed fiber,” *IEEE Photon. Technol. Lett.*, vol. 5, no. 10, pp. 1233-1235, 1993.

[28] C. Kurtzke, “Suppression of fiber nonlinearities by appropriate dispersion management”, *IEEE Photon. Technol. Lett.*, vol. 5, no. 10, pp. 1250-1252, 1993.

[29] T. Naito, T. Terahara, T. Chikama, and M. Suyama, “Four 5-Gb/s WDM transmission over 4760-km straight-line using pre- and post-dispersion compensation and FWM cross talk reduction,” *IEEE/OSA Optical Fiber Communication Conference / National Fiber Optic Engineers Conference (OFC/NFOEC)*, Paper WM3, San Jose, California, USA, 1996,.

[30] K. Inoue, “Fiber four-wave mixing suppression using two incoherent polarized lights,” *IEEE J. Lightw. Technol.*, vol. 11, no. 12, pp. 2116-2122, 1993.

[31] D. van den Borne, S. L. Jansen, S. Calabro, N. E. Hecker-Denschlag, G. D. Khoe, and H. de Waardt, “Reduction of nonlinear penalties through polarization interleaving in 2 x 10 Gb/s polarization-multiplexed transmission,” *IEEE Photon. Technol. Lett.*, vol. 17, no. 6, pp. 1337-1339, 2005.

[32] S. Watanabe, T. Chikama, G. Ishikawa, T. Terahara, and H. Kuwahara, “Compensation of pulse shape distortion due to chromatic dispersion and Kerr effect by optical phase conjugation,” *IEEE Photon. Technol. Lett.*, vol. 5, no. 10, pp. 1241-1243, 1993.

[33] O. Kuzucu, Y. Okawachi, R. Salem, M. A. Foster, A. C. Turner-Foster, M. Lipson, and A. L. Gaeta, “Spectral phase conjugation via temporal imaging,” *OSA Opt. Express*, vol.17, no. 22, pp. 20605-20614, 2009.

[34] X. Liu, X. Wei, R. E. Slusher, and C. J. McKinstrie, “Improving transmission performance in different phase-shit-keyed systems by use of lumped nonlinear phase-shift compensation,” *OSA Opt. Lett.*, vol. 27, no. 18, pp. 1616-1618, 2002.

[35] C. Xu and X. Liu, “Postnonlinearity compensation with data-driven phase modulators in phase-shift keying transmission,” *OSA Opt. Lett.*, vol. 27, no. 18, pp. 1619-1621, 2002.

[36] K. -P. Ho and J. M. Kahn, “Electronic compensation technique to mitigate nonlinear phase noise,” *IEEE J. Lightw. Technol.*, vol. 22, no. 3, pp. 779-783, 2004.

[37] F. Yaman and G. F. Li, “Nonlinear Impairment compensation for polarization-division multiplexed WDM transmission using digital backward propagation,” *IEEE Photon. J.*, vol. 1, no. 2, pp. 144-152, 2009.

[38] M. Rohde, C. Caspar, N. Heimes, M. Konitzer, E.-J. Bachus, and N. Hanik, “Robustness of DPSK direct detection transmission format in standard fibre WDM systems,” *IEEE Electron. Lett.*, vol. 36, no. 17, pp. 1483-1484, 2000.

[39] A. H. Gnauck, G. Raybon, S. Chandrasekhar, J. Leuthold, C. Doerr, L. Stulz, A. Agarwal, S. Banerjee, D. Grosz, S. Hunsche, A. Kung, A. Marhelyuk, D. Maywar, M. Movassaghi, X. Liu, C. Xu, X. Wei, and D. M. Gill, “2.5 Tb/s (64 x 42.7 Gb/s) transmission over 40 x 100 km NZDSF using RZ-DPSK format and all-Raman-amplified spans,” *IEEE/OSA Optical*

Fiber Communication Conference / National Fiber Optic Engineers Conference (OFC/NFOEC), Paper FC2, Anaheim, California, USA, 2002.

[40] T. Mizuochi, K. Ishida, T. Kobayashi, J. Abe, K. Kinjo, K. Motoshima, and K. Kasahara, "A comparative study of DPSK and OOK WDM transmission over transoceanic distances and their performance degradations due to nonlinear phase noise," *IEEE J. Lightw. Technol.*, vol. 21, no. 9, pp. 1933-1943, 2003.

[41] P. J. Winzer, A. H. Gnauck, G. Raybon, S. Chandrasekhar, Y. K. Su and, and J. Leuthold, "40-Gb/s return-to-zero alternate-mark-inversion (RZ-AMI) transmission over 2000 km," *IEEE Photon. Technol. Lett.*, vol. 15, no. 5, pp. 766-768, 2003.

[42] Y. Miyamoto, A. Hirano, K. Yonenaga, A. Sano, H. Toba, K. Murata, and O. Mitomi, "320 Gbit/s (8x40 Gbit/s) WDM transmission over 367 km with 120 km repeater spacing using carrier-suppressed return-to-zero format," *IEEE Electron. Lett.*, vol. 35, no. 23, pp. 2041-2042, 1999.

[43] C. Behrens, R. I. Killey, S. J. Savory, M. Chen, and P. Bayvel, "Reducing the impact of intrachannel nonlinearities by pulse-width optimisation in multi-level phase-shift-keyed transmission," *European Conference on Optical Communication (ECOC)*, Paper 10.4.1, Vienna, Austria, 2009.

[44] T. Oyama, T. Hoshida, H. Nakashima, C. Ohshima, Z. Tao, and J. C. Rasmussen, "Impact of pulse shaping and transceiver electrical bandwidths on nonlinear compensated transmission," *IEEE/OSA Optical Fiber Communication Conference / National Fiber Optic Engineers Conference (OFC/NFOEC)*, Paper OTh3C.2, Anaheim, California, USA, 2013.

[45] L. Boivin and G. J. Pendock, “Receiver sensitivity for optically amplified RZ signals with arbitrary duty cycle,” in *Proc. Optical Amplifiers and Their Applications (OAA)*, Paper ThB4, 1999.

[46] P. J. Winzer and A. Kalmár, “Sensitivity enhancement of optical receivers by impulsive coding,” *IEEE J. Lightw. Technol.*, vol. 17, no. 2, pp. 171-177, 1999.

[47] W. Idler, A. Klekamp, R. Dischler, J. Lazaro, and A. Konczykowska, “System performance and tolerances of 43 Gb/s ASK and DPSK modulation formats,” *European Conference on Optical Communication (ECOC)*, Paper 2.6.3, Rimini, Italy, 2003.

[48] P. J. Winzer and R.-J. Essiambre, “Advanced optical modulation formats,” *IEEE Proceedings*, vol. 94, no. 5, pp. 952-985, 2006.

[49] T. Yamamoto, “High-speed directly modulated lasers,” *IEEE/OSA Optical Fiber Communication Conference / National Fiber Optic Engineers Conference (OFC/NFOEC)*, Paper OTh3F.5, Los Angeles, California, USA, 2012.

[50] B. W. Hakki, “Evaluation of transmission characteristics of chirped DFB lasers in dispersive optical fiber,” *IEEE J. Lightw. Technol.*, vol. 10, no. 7, pp. 964-970, 1992.

[51] M. Aoki, M. Suzuki, H. Sano, T. Kawano, T. Ido, T. Taniwatari, K. Uomi, and A. Takai, “InGaAS/InGaAsp MQW electroabsorption modulator integrated with a DFB laser fabricated by band-gap energy control selective area MOCVD,” *IEEE J. Quantum Electron.*, vol. 29, no. 6, pp. 2088-2096, 1993.

[52] Y. C. Yu, R. Lewen, S. Irmscher, U. Westergren, and L. Thylen, “80 Gb/s ETDM transmitter with a travelling-wave electroabsorption modulator,” *IEEE/OSA Optical Fiber Communication Conference / National Fiber Optic Engineers Conference (OFC/NFOEC)*, Paper OWE1, Anaheim, California, USA, 2005.

[53] X. Wei, J. Leuthold, and L. Zhang, “Delay-interferometer-based optical pulse generator,” *IEEE/OSA Optical Fiber Communication Conference / National Fiber Optic Engineers Conference (OFC/NFOEC),* Paper WL6, Los Angeles, California, USA, 2004.

[54] K. Sato, “Semiconductor light sources for 40-Gb/s transmission systems,” *IEEE/ OSA J. Lightw. Technol.*, vol. 20, no. 12, pp.2035-2043, 2002.

[55] K. Yonenaga, S. Kuwano, S. Norimatsu, and N. Shibata, “Optical duobinary transmission system with no receiver sensitivity degradation,” *IEEE Electron. Lett.*, vol. 31, no. 4, pp. 302-304, 1995.

[56] T. Ono, Y. Yano, K. Fukuchi, T. Ito, H. Yamazaki, M. Yamaguchi, and K. Emura, “Characteristics of optical duobinary signals in terabit/s high-spectral efficiency WDM systems,” *IEEE J. Lightw. Technol.*, vol. 16, no. 5, pp. 788-797, 1998.

[57] A. H. Gnauck and P. J. Winzer, “Optical phase-shift-keyed transmission,” *IEEE J. Lightw. Technol.*, vol. 23, no. 1, pp. 115 – 130, 2005.

[58] H. Kim and P. J. Winzer, “Robustness to laser frequency offset in direct-detection DPSK and DQPSK systems,” *IEEE J. Lightw. Technol.*, vol. 21, no. 9, pp. 1887-1891, 2003.

[59] K.-P. Ho, “Phase-modulated optical communication systems,” Springer Science + Business Media, 2005.

[60] I. Kang, “Phase-shift-keying and on-off-keying with improved performances using eletroabsorption modulators with interferometric effects,” *OSA Opt. Express*, vol.15, no. 4, pp. 1467-1473, 2007.

[61] C. R. Doerr, L. M. Zhang, A. L. Adamiecki, N. J. Sauer, J. H. Sinsky, and P. J. Winzer, “Compact EAM-based Inp DQPSK modulator and demonstration at 80 Gb/s,” *IEEE/OSA*

Optical Fiber Communication Conference / National Fiber Optic Engineers Conference (OFC/NFOEC), Paper PDP33, Anaheim, California, USA, 2007.

[62] D. Mahgerefteh, Y. Matsui, C. Liao, B. Johnson, D. Walker, X. Zheng, Z. F. Fan, K. McCallion, and P. Tayebati, "Error-free 250 km transmission in standard fibre using compact 10 Gbit/s chirp-managed laser directly modulated lasers (CML) at 1550 nm," *IEEE Electron. Lett.*, vol. 41, no. 9, pp. 543-544, 2005.

[63] Y. Matsui, D. Mahgerefteh, X. Zheng, C. Liao, Z. F. Fan, K. McCallion, and P. Tayebati, "Chirp-managed directly modulated laser (CML)," *IEEE Photon. Technol. Lett.*, vol. 18, no. 2, pp. 385-387, 2006.

[64] M. Blez, D. Mathoorasing, C. Kazmierski, M. Quillec, M. Gilleron, J. Landreau, and H. Nakajima, "Very low chirping of InGaAs-InGaAIAs MQW DFB BRS lasers under 10 Gbit/s modulation," *IEEE J. Quantum Electron.*, vol. 29, no. 6, pp. 1676-1681, 1993.

[65] J. Binder and U. Kohn, "10 Gbit/s-dispersion optimized transmission at 1.55 μm wavelength on standard single mode fiber," *IEEE Photon. Technol. Lett.*, vol. 6, no. 4, pp. 558-560, 1994.

[66] S. Mohrdiek, H. Burkhard, F. Steinhagen, H. Hillmer, R. Lösch, W. Schlapp, and R. Göbel, "10-Gb/s standard fiber transmission using directly modulated 1.55-μm quantum-well DFB lasers," *IEEE Photon. Technol. Lett.*, vol. 7, no. 11, pp. 1357-1359, 1995.

[67] B. Wedding, B. Franz, and B. Junginger, "10-Gb/s optical transmission up to 253 km via standard single-mode fiber using the method of dispersion-supported transmission," *IEEE J. Lightw. Technol.*, vol. 12, no. 10, pp. 1720 – 1727, 1994.

[68] C.-H. Lee, S.-S Lee, H.-K. Kim, J.-H. Han, and C.-S Shim, "Reduction of chirping penalty in directly modulated multigigabit transmission systems by spectral filtering," *Conf. Lasers Electro-Optics (CLEO),* Paper CTul10, Baltimore, MD, 1995.

[69] C.-H. Lee, S.-S Lee, H.-K. Kim, J.-H. Han, and C.-S Shim, “Transmission of directly modulated 2.5-Gb/s signals over 250-km of nondispersion-shifted fiber by using a spectral filtering method,” *IEEE Photon. Technol. Lett.*, vol. 8, no. 12, pp. 1725-1727, 1996.

[70] P. A. Morton, G. E. Shtengel, L. D. Tzeng, R. D. Yadvish, T. Tanbun-EK, and R. A. Logan, “38.5 km error free transmission at 10 Gbit/s in standard fibre using a low chirp, spectrally filtered, directly modulated 1.55μm DFB laser,” *IEEE Electron. Lett.*, vol. 33, no. 4, pp. 310-311, 1997.

[71] M. McAdams, E. Peral, D. Provenzano, W. K. Marshall, and A. Yariv, “Improved laser modulation response by frequency modulation to amplitude modulation conversion in transmission through a fiber grating,” *Appl. Phys. Lett.*, vol. 71, no. 7, pp. 879-881, 1997.

[72] D. Mahgerefteh, P. S. Cho, J. Goldhar, and H. I. Mandelberg, “Penalty-free propagation over 600 km of non-dispersion-shifted fiber at 2.5 Gb/s using a directly laser modulated transmitter,” *Conf. Lasers Electro-Optics (CLEO)*, Paper CTuQ2, Baltimore, MD, 1999.

[73] T. Niemi, M. Uusimaa, S. Tammela, P. Heimala, T. Kajava, M. Kaivola, and H. Ludvigsen, “Tunable silicon etalon for simultaneous spectral filtering and wavelength monitoring of a DWDM transmitter,” *IEEE Photon. Technol. Lett.*, vol. 13, no. 1, pp. 58-60, 2001.

[74] D. Mahgerefteh, A. M. Benzoni, P. S. Westbrook, K. S. Feder, P. I. Reyes, P. Steinvurzel, B. J. Eggleton, R. G. Ernst, L. A. Reith, and D. M. Gill, “DMRZ: a directly modulated 10-Gb/s RZ source for ultralong-haul WDM systems,” *IEEE Photon. Technol. Lett.*, vol. 14, no. 4, pp. 546-548, 2002.

[75] Finisar CML transmitter product specification, “http://zh.finisar.com/products/optical-components/CML-Transmitters/DM200-02” [on-line].

[76] G. P. Agrawal and N. K. Dutta, “Semiconductor lasers,” 2nd edition, Van Nostrand Reinhold, New York, 1993.

[77] C. H. Henry, R. A. Logan, and K. A. Bertness, “Spectral dependence of the change in refractive index due to carrier injection in GaAs lasers,” *J. Appl. Phys.*, vol. 52, no. 7, pp. 4457-4461, 1981.

[78] C. H. Henry, “Theory of the linewidth of semiconductor lasers,” *IEEE J. Quantum Electron.*, vol. 18, no. 2, pp. 259-264, 1982.

[79] T. L. Koch and J. E. Bowers, “Nature of wavelength chirping in directly modulated semiconductor lasers,” *IEEE Electron. Lett.*, vol. 20, no. 25/26, pp. 1038-1039, 1984.

[80] T. L. Koch and R. A. Linke, “Effect of nonlinear gain reduction on semiconductor laser wavelength chirping,” *Appl. Phys. Lett.*, vol. 48, no. 10, pp. 613-615, 1986.

[81] R. J. Corvini and T. L. Koch, “Computer simulation of high-bit-rate optical fiber transmission using single-frequency lasers,” *IEEE J. Lightw. Technol.*, vol. 5, no. 11, pp. 1591-1594, 1987.

[82] D. J. Channin, “Effect of gain saturation on injection laser switching,” *J. Appl. Phys.*, vol. 50, no. 6, pp. 3858-3860, 1979.

[83] M. J. Adams and M. Osinski, “Influence of spectral hole-burning on quaternary laser transients,” *IEEE Electron. Lett.*, vol. 19, no. 16, pp. 627-628, 1983.

[84] J. Manning, R. Olshansky, D. M. Fye, and W. Powazinik, “Strong influence of nonlinear gain on spectral and dynamic characteristics of InGaAsP lasers,” *IEEE Electron. Lett.*, vol. 21, no. 11, pp. 496-497, 1985.

[85] M. Asada and Y. Suematsu, “Density-matrix theory of semiconductor laser with relaxation broadening model-gain and gain-suppression in semiconductor lasers,” *IEEE J. Quantum Electron.*, vol. 21, no. 5, pp. 434-442, 1985.

[86] G. S. Pandian and S. Dilwali, “On the thermal FM response of a semiconductor laser diode,” *IEEE Photon. Technol. Lett.*, vol. 4, no. 2, pp. 130-133, 1992.

[87] B. Johnson, D. Mahgerefteh, K. McCallion, Z. Fan, D. Piede, and P. Tayebati, “Thermal chirp compensation systems for a chirp managed directly modulated laser (CML^{TM}) data link,” *U. S. Patent Application,* US 7505694B2, 2009.

[88] H. Shalom, A. Zadok, M. Tur, P. J. Legg, W. D. Cornwell, and I. Andonovic, “On the various time constants of wavelength changes of a DFB laser under direct modulation,” *IEEE J. Quantum Electron.*, vol. 34, no. 10, pp. 1816-1822, 1998.

[89] S. Kobayashi, Y. Yamamoto, M. Ito, and T. Kimura, “Direct frequency modulation in AlGaAs semiconductor lasers,” *IEEE J. Quantum Electron.*, vol. 18, no. 4, pp. 582-594, 1982.

[90] G. Jacobsen, K. Emura, T. Ono, and S. Yamazaki, “Requirements for LD FM characteristics in an optical CPFSK system,” *IEEE J. Lightw. Technol.*, vol. 9, no. 9, pp. 1113-1123, 1991.

[91] K. Iwashita, and T. Matsumoto, “Modulation and detection characteristics of optical continuous phase FSK transmission system,” *IEEE J. Lightw. Technol.*, vol. 5, no. 4, pp. 452-460, 1987.

[92] S. P. Mazumder, R. Gangopadhyay, E. Forestieri, and G. Prati, “Sensitivity penalty for AMI-coded CPFSK in heterodyne delay demodulation receiver,” *IEEE Photon. Technol. Lett.*, vol. 7, no. 10, pp. 1207-1209, 1995.

[93] E. Forestieri and G. Prati, “Analysis of delay-and-multiply optical FSK receivers with line coding and non-flat laser FM response,” *IEEE J. Sel. Areas Commun.*, vol. 13, no. 3, pp. 543-556, 1995.

[94] P. Baroni, V. Miot, A. Carena, and P. Poggiolini, “8B10B line coding to mitigate the non-uniform FM laser response of direct modulated CPFSK transmitter,” *OSA Opt. Express*, vol.16, no. 10, pp. 7279-7284, 2008.

[95] G. P. Agrawal, “Effect of gain and index nonlinearities on single-mode dynamics in semiconductor lasers,” *IEEE J. Quantum Electron.*, vol. 26, no. 11, pp. 1901-1909, 1990.

[96] R. Olshansky, P. Hill, V. Lanzisera, and W. Powazinik, “Frequency response of 1.3 μm InGaAsP high speed semiconductor lasers,” *IEEE J. Quantum Electron.*, vol. 23, no. 9, pp. 1410-1418, 1987.

[97] K. Uomi, M. Aoki, T. Tsuchiya, M. Suzuki, and N. Chinone, “Dependence of relaxation oscillation frequency and damping *K* factor on the number of quantum wells in 1.55 μm InGaAsP DFB lasers,” *IEEE Photon. Technol. Lett.*, vol. 3, no. 6, pp. 493-495, 1991.

[98] T. Takahashi and Y. Arakawa, “Nonlinear gain effects in quantum well, quantum well wire, and quantum well box lasers,” *IEEE J. Quantum Electron.*, vol. 27, no. 6, pp. 1824-1829, 1991.

[99] Y. Arakawa and T. Takahashi, “Effect of nonlinear gain on modulation dynamics in quantum-well lasers,” *IEEE Electron. Lett.*, vol. 25, no. 2, pp. 169-170, 1989.

[100] D. Mahgerefteh, Y. Matsui, X. Zheng, and K. McCallion, “Chirp managed laser and applications,” *IEEE J. Select. Topics Quantum Electron.*, vol. 16, no. 5, pp. 1126-1139, 2010.

[101] D. Mahgerefteh, Y. Matsui, X. Zheng, H. Chen, J. Zhou, M. Deutsch, G. Larosa, K.McCallion, Z. F. Fan, P. Tayebati, G. Yoffe, S. Zou, M. Emanuel, S. A. Rishton, X. Hong,

R. Narayan, and B. Pezeshki, “Tunable chirp managed laser,” *IEEE Photon. Technol. Lett.*, vol. 20, no. 2, pp. 108-110, 2008.

[102] Y. Yokoyama, T. Hatanaka, N. Oku, H. Tanaka, I. Kobayashi, H. Yamazaki, and A. Suzuki, “10.709-Gb/s-300-km transmission of PLC-based chirp managed laser packaged in pluggable transceiver without any optical or electrical dispersion compensation,” *European Conference on Optical Communication (ECOC)*, Paper We.1.C.4, Brussels, Belgium, 2008.

[103] S. Chandrasekhar, D. C. Kilper, X. Zheng, D. Mahgerefteh, Y. Matsui, K. McCallion, Z. Fan, and P. Tayebati, “Evaluation of chirp-managed lasers in a dispersion managed DWDM transmission over 24 spans,” *IEEE/OSA Optical Fiber Communication Conference / National Fiber Optic Engineers Conference (OFC/NFOEC)*, Paper OThL7, Anaheim, California, USA, 2007.

[104] S. Matsuo, T. Kakitsuka, T. Segawa, N. Fujiwara, Y. Shibata, H. Oohashi, H. Yasaka, and H. Suzuki, “Extended transmission reach using optical filtering of frequency-modulated widely tunable SSG-DBR laser,” *IEEE Photon. Technol. Lett.*, vol. 20, no. 4, pp. 294-296, 2008.

[105] S. Matsuo, T. Kakitsuka, T. Segawa, R. Sato, Y. Shibata, R. Takahashi, H. Oohashi, and H. Yasaka, “4 x 25 Gb/s frequency-modulated DBR laser array for 100-GbE 40-km reach application,” *IEEE Photon. Technol. Lett.*, vol. 20, no. 17, pp. 1494-1496, 2008.

[106] T. Kakitsuka, S. Matsuo, T. Segawa, Y. Shibata, Y. Kawaguchi, and R. Takahashi, “20-km transmission of 40-Gb/s signal using frequency modulated DBR laser,” *IEEE/OSA Optical Fiber Communication Conference / National Fiber Optic Engineers Conference (OFC/NFOEC)*, Paper OThG4, San Diego, California, USA, 2009.

[107] J. Yu, P. N. Ji, Z. Jia, T. Wang, X. Zheng, Y. Matsui, D. Mahgerefteh, K. McCallion, Z. F. Fan, and P. Tayebati, "42.8 Gbit/s chirp-managed signal transmission over 20 km standard SMF at 1550 nm without DCF," *IEEE Electron. Lett.*, vol. 43, no. 23, 2007.

[108] J. Yu, M.-F. Huang, P. N. Ji, and T. Wang, "42.8 Gb/s chirp-managed signal transmission over 100 m graded-index plastic optical fiber," *IEEE/OSA Optical Fiber Communication Conference / National Fiber Optic Engineers Conference (OFC/NFOEC)*, Paper PDP28, San Diego, California, USA, 2008.

[109] J. Yu, Z. Jia, M.-F. Huang, M. Haris, P. N. Ji, T. Wang, and G.-K. Chang, "Applications of 40-Gb/s chirp-managed laser in access and metro networks," *IEEE J. Lightw. Technol.*, vol. 27, no. 3, pp. 253-265, 2009.

[110] M.-F. Huang, J. Yu, M. Haris, P. N. Ji, T. Wang, and G.-K. Chang, "42.8-Gb/s chirp-managed signal transmission over 640-km SSMF with large dispersion tolerance," *IEEE/OSA Optical Fiber Communication Conference / National Fiber Optic Engineers Conference (OFC/NFOEC)*, Paper OThG5, San Diego, California, USA, 2009.

[111] H. Kim, S. K. Kim, H. Lee, S. Hwang, and Y. Oh, "A novel way to improve the dispersion-limited transmission distance of electroabsorption modulated lasers," *IEEE Photon. Technol. Lett.*, vol. 18, no. 8, pp. 947-949, 2006.

[112] K. Hasebe, S. Matsuo, H. Sanjoh, A. Ohki, T. Kakitsuka and Y. Shibata, "Directly frequency modulated DFB laser integrated with EA modulator for extended transmission reach," *European Conference on Optical Communication (ECOC)*, Paper Th.9.D.5, Torino, Italy, 2010.

[113] K. Kechaou, T. Anfray, K. Merghem, C. Aupetit-Berthelemot, G. Aubin, C. Kazmierski, C. Jany, P. Chanclou, and D. Erasme, "First demonstration of dispersion limit improvement at

20 Gb/s with a dual electroabsorption modulated laser," *IEEE/OSA Optical Fiber Communication Conference / National Fiber Optic Engineers Conference (OFC/NFOEC)*, Paper OTh3F.1, Los Angeles, California, USA, 2012.

[114] K. Kechaou, T. Anfray, K. Merghem, C. Aupetit-Berthelemot, G. Aubin, C. Kazmierski, C. Jany, P. Chanclou, and D. Erasme, "NRZ transmission range record at 40-Gb/s in standard fiber using a dual electro-absorption modulated laser," *European Conference on Optical Communication (ECOC)*, Paper Mo.1.E.2, Amsterdam, Netherlands, 2012.

[115] J. L. Wei, C. Sánchez, R. P. Giddings, E. Hugues-Salas, and J. M. Tang, "Significant improvements in optical power budgets of real-time optical OFDM PON systems," *OSA Opt. Express*, vol.18, no. 20, pp. 20732-20745, 2010.

[116] Z. X. Liu and C.-K. Chan, "Generation of dispersion tolerant Manchester-duobinary signal using directly modulated chirp managed laser," *IEEE Photon. Technol. Lett.*, vol. 23, no. 15, pp. 1043-1045, 2011.

[117] Z. X. Liu, J. Xu, Q. K. Wang, and C.-K. Chan, "Rayleigh noise mitigated 70-km-reach bi-directional WDM-PON with 10-Gb/s directly modulated Manchester-duobinary as downstream signal," *IEEE/OSA Optical Fiber Communication Conference / National Fiber Optic Engineers Conference (OFC/NFOEC)*, Paper OW1B.2, Los Angeles, California, USA, 2012.

[118] S. Chandrasekhar, C. R. Doerr, L. L. Buhl, D. Mahgerefteh, Y. Matsui, B. Johnson, C. Liao, X. Zheng, K. McCallion, Z. Fan, and P. Tayebati, "Flexible transport at 10-Gb/s from 0 to 675 km (11,500 ps/nm) using a chirp-managed laser, no DCF, and a dynamically adjustable dispersion-compensating receiver," *IEEE/OSA Optical Fiber Communication*

Conference / National Fiber Optic Engineers Conference (OFC/NFOEC), Paper PDP30, Anaheim, California, USA, 2005.

[119] C. R. Doerr, M. Cappuzzo, A. Wong-Foy, L. Gomez, E. Laskowski, and E. Chen, "Potentially inexpensive 10-Gb/s tunable dispersion compensator with low polarization sensitivity," *IEEE Photon. Technol. Lett.*, vol. 16, no. 5, pp. 1340-1342, 2004.

[120] P. J. Winzer, F. Fidler, M. J. Matthews, L. E. Nelson, S. Chandrasekhar, L. L. Buhl, M. Winter, and D. Castagnozzi, "Electronic equalization and FEC enable bidirectional CWDM capacities of 9.6 Tb/s-km," *IEEE/OSA Optical Fiber Communication Conference / National Fiber Optic Engineers Conference (OFC/NFOEC),* Paper PDP7, Los Angeles, California, USA, 2004.

[121] S. Chandrasekhar, C. R. Doerr, L. L. Buhl, Y. Matsui, D. Mahgerefteh, X. Zheng, K. McCallion, Z. Fan, and P. Tayebati, "Repeaterless transmission with negative penalty over 285 km at 10 Gb/s using a chirp managed laser," *IEEE Photon. Technol. Lett.*, vol. 17, no. 11, pp. 2454-2456, 2005.

[122] S. Chandrasekhar, A. H. Gnauck, G. Raybon, L. L. Buhl, D. Mahgerefteh, X. Zheng, Y. Matsui, K. McCallion, Z. Fan, and P. Tayebati, "Chirp-managed laser and MLXE-RX enables transmission over 1200 km at 1550 nm in a DWDM environment in NZDSF at 10 Gb/s without any optical dispersion compensation," *IEEE Photon. Technol. Lett.*, vol. 18, no. 14, pp. 1560-1562, 2006.

[123] X. Zheng, K. McCallion, D. Mahgerefteh, Y. Matsui, Z. F. Fan, J. Zhou, and M. Deutsch, "Performance demonstration of 300-km dispersion uncompensated transmission using tunable chirp-managed laser and EDC integratable into small-form-factor XFP," *IEEE/LEOS Summer Topical Meetings*, Paper TuD2.2, Acapulco, 2008.

[124] X. Zheng, S. Priyadarshi, D. Mahgerefteh, Y. Matsui, T. Nguyen, J. Zhou, M. Deutsch, V. Bu, K. McCallion, J. Zhang, and P. Kiely, "Transmission from 0-360 km (6120 ps/nm) at 10 Gb/s without optical or electrical dispersion compensation using digital pulse shaping of a chirp managed laser," *IEEE/OSA Optical Fiber Communication Conference / National Fiber Optic Engineers Conference (OFC/NFOEC)*, Paper OThE5, San Diego, California, USA, 2009.

[125] A. S. Karar, J. C. Cartledge, and K. Roberts, "Transmission over 608 km of standard single-mode fiber using a 10.709-Gb/s chirp managed laser and electronic dispersion precompensation," *IEEE Photon. Technol. Lett.*, vol. 24, no. 9, pp. 760-762, 2012.

[126] S. Chandrasekhar, A. H. Gnauck, L. L. Buhl, X. Zheng, D. Mahgerefteh, Y. Matsui, K. McCallion, Z. F. Fan, and P. Tayebati, "Single channel transmission over 9280 km at 10-Gb/s using small form factor chirp managed laser generating RZ AMI modulation format," *European Conference on Optical Communication (ECOC)*, PD Paper Th 4.2.5, Glasgow, Scotland, 2005.

[127] S. Chandrasekhar, A. H. Gnauck, D. Mahgerefteh, X. Zheng, Y. Matsui, K. McCallion, Z. Fan, and P. Tayebati, "Experimental study comparing characteristics of 10-Gb/s RZ-AMI formats generated by CML and MZM-DI transmitters," *IEEE/OSA Optical Fiber Communication Conference / National Fiber Optic Engineers Conference (OFC/NFOEC)*, Paper OThI4, Anaheim, California, USA, 2006.

[128] J. Franklin, L. Kil, D. Mooney, D. Mahgerefteh, X. Zheng, Y. Matsui, K. McCallion, F. Fan, and P. Tayebati, "Generation of RZ-DPSK using a chirp-managed laser (CML)," *IEEE/OSA Optical Fiber Communication Conference / National Fiber Optic Engineers Conference (OFC/NFOEC)*, Paper JWA67, San Diego, California, USA, 2008.

[129] R. S. Vodhanel, “5 Gbit/s direct optical DPSK modulation of a 1530-nm DFB laser,” *IEEE Photon. Technol. Lett.*, vol. 1, no. 8, pp. 218-220, 1989.

[130] X. Zheng, D. Mahgerefteh, Y. Matsui, X. Ye, V. Bu, K. McCallion, H. Xu, M. Deutsch, H. Ereifej, R. Lewén, J.-O. Wesström, R. Schatz, and P.-J. Rigole, “Generation of RZ-AMI using a widely tuneable modulated grating Y-branch chirp managed laser,” *IEEE/OSA Optical Fiber Communication Conference / National Fiber Optic Engineers Conference (OFC/NFOEC)*, Paper OThE5, San Diego, California, USA, 2010.

[131] M. Radziunas, U. Bandelow, M. Wolfrum, U. Troppenz, J. Kreissl, A. Glitzky, and R. Hünlich, “Design of multisection semiconductor laser for 40 Gb/s direct modulation,” *European Conference on Optical Communication (ECOC)*, Paper We4. P. 088, Glasgow, Scotland, 2005.

[132] C. Yu, Z. Pan. T. Luo, S. Kumar, L.-S. Yan, B. Zhang, L. Zhang, Y. Wang, M. Adler, and A. E. Willner, “160-GHz pulse generator using a 40-GHz phase modulator and PM fiber,” *IEEE/OSA Optical Fiber Communication Conference / National Fiber Optic Engineers Conference (OFC/NFOEC)*, Paper OThR5, Anaheim, California, USA, 2005.

[133] A. J. Torregrosa, H. Maestre, J. Capmany, and C. R. Fernández-Pousa, “Return-to-zero pulse generators using overdriven amplitude modulators at one fourth of the data rate,” *Photon. Technol. Lett.*, vol. 19, no. 22, pp. 1837-1839, 2007.

[134] R. S. Vodhanel, A. F. Elrefaie, R. E. Wagner, M. Z. Iqbal, J. L. Gimlett, and S. Tsuji, “Ten-to-twenty gigabit-per-second modulation performance of 1.5-μm distributed feedback lasers for frequency-shift-keying systems,” *IEEE J. Lightw. Technol.*, vol. 7, no. 10, pp. 1454-1460, 1989.

[135] Q. T. Le, K. Zogal, T. von Lerber, C. Gierl, A. Emsia, D. Briggmann, and F. Kueppers, "Direct DPSK modulation of chirp managed lasers for symmetrical 10-Gbit/s WDM-PONs," *European Conference on Optical Communication (ECOC)*, Paper P6.14, Amsterdam, The Netherlands, 2012.

[136] Q. T. Le, A. Emsia, D. Briggmann, and F. Küppers, "Direct DPSK modulation of chirp-managed laser as cost-effective downstream transmitter for symmetrical 10-Gbit/s WDM PONs," *OSA Opt. Express*, vol.20, no. 26, pp. B470-B478, 2012.

[137] D. Mahgerefteh, K. McCallion, The'Linh Nguyen, and D. Alluche, "Chirped laser with passive filter element for differential phase shift keying generation," *US Patent Application*, US0003842 A1, 2009.

[138] Y. Matsui, D. Mahgerefteh, X. Zheng, X. Ye, K. McCallion, H. Xu, M. Deutsch, R. Lewén, J. O. Wesström, R. Schatz, and P. J. Rigole, "Widely tunable modulated grating Y-branch chirp managed laser," *European Conference on Optical Communication (ECOC)*, Paper PD1.5, Vienna, Austria, 2009

[139] H. Yamazaki, T. Saida, T. Goh, A. Mori, and S. Mino, "Dual-carrier IQ modulator using a complementary frequency shifter," *European Conference on Optical Communication (ECOC)*, Paper Mo.1.LeSaleve.5, Geneva, Switzerland, 2011.

[140] L. B. Du, J. Schröder, J. Carpenter, B. J. Eggleton, and A. J. Lowery, "Flexible all-optical OFDM using WSSs," *IEEE/OSA Optical Fiber Communication Conference / National Fiber Optic Engineers Conference (OFC/NFOEC)*, Paper PDP5B.9, Anaheim, California, USA, 2013.

Appendix

A. List of abbreviations

AMI: alternate-mark inversion

AM: amplitude modulation

Amp.: amplifier

ASE: amplified spontaneous emission

Att.: attenuator

BER: bit-error-rate

BERT: BER-tester

BtB: back-to-back

CD: chromatic dispersion

CDR: clock-data recovery

CML: chirp managed laser

Comb.: combiner

CSRZ: carrier-suppressed RZ

CW: continuous-wave

DAC: digital-to-analog converter

DBPSK: differential binary phase-shift-keying

DBR: distributed-Bragg-reflector

DCF: dispersion compensating fiber

DCM: dispersion compensating module

D-EML: dual-modulated EML

DEMUX: demultiplexer

DFB: distributed-feedback

DFE: detection feedback equalization

DGD: differential group delay

DI: delay interferometer

DML: directly modulated laser

DQPSK: differential quadrature phase-shift-keying

DSP: digital signal processing

EAM: electro-absorption modulator

EDC: electronic dispersion compensation

EDFA: erbium-doped fiber amplifier

EML: electro-absorption modulated laser

ER: extinction ratio

FBG: fiber Bragg grating

FFE: feedforward equalization

FM: frequency modulation

FM-DBR: frequency-modulated DBR

FP: Fabry-Perot

FSR: free-spectral-range

FWM: four-wave mixing

GI-POF: graded index plastic optical fiber

GVD: group velocity dispersion

IM: intensity modulator

IM-DD: intensity-modulation and direct-detection

IRZ: Inverse-RZ

ISI: inter symbol interference

ITU: International Telecommunication Union

LO: local-oscillator

MG-Y: Modulated Grating Y-branch

MLSE: maximum likelihood sequence estimation

MZM: Mach-Zehnder modulator

NDSF: non-dispersion-shifted fiber

NRZ: non-return-to-zero

NZDSF: nonzero dispersion-shifted fiber

OBPF: optical band pass filter

ODC: optical dispersion compensation

OOK: on-off-keying

OPLL: optical phase locked loop

OSA: optical spectrum analyzer

OSNR: optical signal-to-noise ratio

OSR: optical spectrum reshaper

PAM: pulse-amplitude-modulation

PC: polarization controller

PD: photo-detector

PLC: planer lightwave circuit

PM: phase modulator

PMD: polarization mode dispersion

PMF: polarization-maintaining fiber

Pol-SK: polarization shift keying

PON: passive optical network

PPG: pulse pattern generator

PRBS: pseudo-random binary sequence

PSP: principal orthogonal state of polarization

QAM: quadrature amplitude modulation

QW: quantum-well

RMS: root-mean-square

RZ: return-to-zero

SBS: stimulated Brillouin scattering

SHB: spectral hole-burning

SMF: single mode fiber

SPM: self-phase modulation

SRS: stimulated Raman scattering

SSMF: standard single mode fiber

TDM: time division multiplexing

TEC: thermoelectric cooler

TIA: transimpedance amplifier

TOSA: transmitter optical sub-assembly

VCSEL: vertical-cavity surface-emitting laser

VOA: variable optical attenuator

WDM: wavelength division multiplexing

XFP: small form factor pluggable

XOR: exclusive-or

XPM: cross-phase modulation

B. List of publications

Journal

[1] **Wei Jia**, Jing Xu, Zhixin Liu, Kam-Hon Tse, and Chun-Kit Chan, "Generation and transmission of 10-Gb/s RZ-DPSK signals using a directly modulated chirp managed laser," *IEEE Photon. Technol. Lett.*, vol. 23, no. 3, pp. 173-175, 2011.

[2] **Wei Jia** and Chun-Kit Chan, "Generation of return-to-zero optical pulses using directly modulated chirp managed laser," *IEEE Photon. Technol. Lett.*, vol. 24, no. 14, pp. 1227-1229, 2012.

[3] **Wei Jia**, Yasuhiro Matsui, Daniel Mahgerefteh, Ilya Lyubomirsky, and Chun-Kit Chan, "Generation and transmission of 10-Gbaud optical ¾-RZ-DQPSK signals using a chirp managed DBR laser," *IEEE J. Lightw. Technol.*, vol. 30, no. 21, pp. 3299-3305, 2012.

Conference

[1] **Wei Jia,** Dong Shen, Kam-Hon Tse, Jing Xu, Ming Li, and Chun-Kit Chan, "A novel scheme to realize a power-efficient WDM passive optical network ," *OptoElectronics and Communications Conference (OECC)*, Paper 8A3-4, Sapporo, Hokkaido, Japan, 2010.

[2] **Wei Jia**, Jing Xu, Zhixin Liu, Chun-Kit Chan, and Lian-Kuan Chen, "Generation of 20-Gb/s RZ-DQPSK signal using a directly modulated chirp managed laser," *IEEE/OSA Optical Fiber Communication Conference / National Fiber Optic Engineers Conference (OFC/NFOEC)*, Paper OThE4, Los Angeles, California, USA, 2011.

[3] **Wei Jia**, Zhixin Liu, and Chun-Kit Chan, "Generation and transmission of 10.709-Gbaud RZ-DQPSK using a chirp managed laser" *OptoElectronics and Communications Conference (OECC)*, Paper 4B4-1, Busan, Korea, 2012.

[4] **Wei Jia** and Chun-Kit Chan, "300-km SSMF transmission of 10-Gb/s chirp managed laser signal with pre-emphasis," *OptoElectronics and Communications Conference (OECC)*, Paper TuPR-3, Kyoto, Japan, 2013.

[5] Jing Xu, Zhixin Liu, **Wei Jia**, and Lian-Kuan Chen, "A novel chirp-free optical Manchester signal transmitter with enhanced dispersion tolerance," *Asia Communications and Photonics Conference and Exhibition (ACP)*, Paper SA2, Shanghai, China, 2010.

[6] Chun-Kit Chan, Zhixin Liu, and **Wei Jia**, "Optical Inverse-RZ duobinary format for high-speed optical transmission," *International Conference on Optical Communications and networks (ICOCN)*, **Invited Paper**, Nanjing, China, 2010.

[7] Kam-Hon Tse, **Wei Jia**, and Chun-Kit Chan, "A cost-effective pilot-pone-based monitoring technique for power saving in RSOA-based WDM-PON," *IEEE/OSA Optical Fiber Communication Conference / National Fiber Optic Engineers Conference (OFC/NFOEC)*, Paper OThB6, Los Angeles, California, USA, 2011.

[8] Chun-Kit Chan, **Wei Jia**, and Zhixin Liu, "Advanced modulation format generation using high-speed directly modulated lasers for optical metro/access systems," *Asia Communications and Photonics Conference and Exhibition (ACP)*, **Invited Paper** 8309-32, Shanghai, China, 2011.